# Development and Improvement of Active Vehicle Safety Systems by Means of Smart Tire Technology

Mustafa Ali Arat

Dissertation submitted to the Faculty of the
Virginia Polytechnic Institute and State University
in partial fulfillment of the requirements for the degree of

Doctor of Philosophy
in
Mechanical Engineering

Saied Taheri, Chair
Mehdi Ahmadian
John Ferris
Robert West
Hesham Rakha

August 15th, 2013
Blacksburg, Virginia

Keywords: Active Vehicle Safety Systems, Smart/Intelligent Tire, Adaptive Control, Optimization, Nonlinear Systems

# Development and Improvement of Active Vehicle Safety Systems by Means of Smart Tire Technology

Mustafa Ali Arat

## ABSTRACT

The dynamic behavior of a vehicle is predominantly controlled by the forces and moments generated at the contact patch between the tire and the road surface. As a result, tire characteristics can dramatically change vehicle response, especially during maneuvers that yields the tires to reach to the limits of its adhesion capacity. To assist the driver in such cases and to prevent other possible instability scenarios, various vehicle control systems e.g. anti-lock brakes (ABS), stability controllers (ESP, ESC) or rollover mitigation schemes are introduced, which are generally known as active vehicle safety systems. Based on the above facts, one can easily come to the conclusion that to improve upon the current control algorithms developed for the technology in use; a vehicle control system design requires accurate knowledge of the tire states. This study proposes the use of a smart tire system that can provide information on momentary variation of tire features through the sensor units attached directly on the tire and develops control algorithms based on this information to assure the match-up between tire and controller dynamics. A prototype smart tire system was developed for field testing and for detailed analysis of its potential. Based on the collected prototype data, novel observer and controller schemes were developed to obtain dynamic tire state information and to improve vehicle handling performance. The proposed algorithms were implemented and evaluated using numerical analysis in MATLAB/Simulink® environment. For a more realistic simulation environment, vehicle models were integrated from Mechanical Simulations CarSim® software suite.

This work was supported in part by the Turkish National Ministry of Education and the NSF I/UCRC Center for Tire Research.

# Acknowledgments

I am infinitely grateful to many individuals for their support, collaboration, and friendship that inspired and bolstered me through this journey. The demanding route through the doctorate would have never come to an end without their contributions. First and foremost I would like to thank to my advisor, Prof. Saied Taheri, for his constant presence and continuous encouragement. He has always been there for guidance as well as for motivation to keep me moving forward. I would also like to sincerely thank Prof. Mehdi Ahmadian, Prof. John Ferris, Prof. Robert West and Prof. Hesham Rakha for their invaluable support and feedback on my studies and for all their help while serving in my doctorate committee.

Special thanks go to all of my colleagues at CenTire and CVeSS for the academic and non-academic discussions we shared. I want to especially thank Mr. Bharat Singh, Dr. Nenggen Ding, Dr. Jian Zhao, Dr. Clement Nagode and Mr. Micheal Craft who have not hesitated to spare their time on all the tedious questions I kept coming up with. I also owe many thanks to my dear friends, Dr. Onur Bilgen, Mr. Matt Oremland, Dr. Kyonghoon Cho, Mr. Umut Atalay and many others I could not list here, who always kept my spirits up whenever the pressure peaked. Of course, none of these would have been possible without the unconditional love and infinite support of my parents, and without my teacher-mother Mrs. Serpil Arat. Finally, I would like to thank to my wife Seda for her care, her endless love and for being there at every step.

# Dedication

*...to my beloved Grandfather, my lifelong mentor,*
*Mustafa Ali Altıntaş*

# Contents

# List of Figures

# List of Tables

# Chapter 1

# Introduction

Vehicle active chassis safety systems, which are designed to help the driver especially during emergency maneuvers, have been the topic of considerable research over the past three decades. These systems are tuned based on the vehicle dynamic characteristics and its interaction with the road surface which is initiated at the contact patch of the tires. This small patch dictates the resulting motion of the vehicle and is a major governing factor of the vehicle's stability and control, especially under severe maneuvers. This relationship makes it very desirable to track the interaction between the tire and the road surface and use the information to enhance the performance of the active safety systems. Furthermore, these dynamics are not intuitive for the daily driver and are not perceivable as long as the vehicle progresses in the intended path. On the other hand, for an average driver, it becomes too difficult to stabilize a vehicle that is not responding to his/her commands leading to an unstable vehicle.

To improve vehicle stability during such events, active safety systems (Figure 1.1) have been introduced which will intervene once certain thresholds are reached. A considerable number of studies have been conducted on the effects of such systems on highway safety and majority of them have concluded positively. A highly referred study which was completed at the National Highway Transportation Safety Administration (NHTSA) in 2007 indicates 14% to 28% reduction in overall fatal crash involvements in passenger cars and Light Trucks [2]. In [3], Farmer reports the results of a risk analysis study completed in seven states in the U.S. over two years. The study is carried out using otherwise identical vehicles with and without stability controllers and concludes that the availability of stability controller yields to a 34%

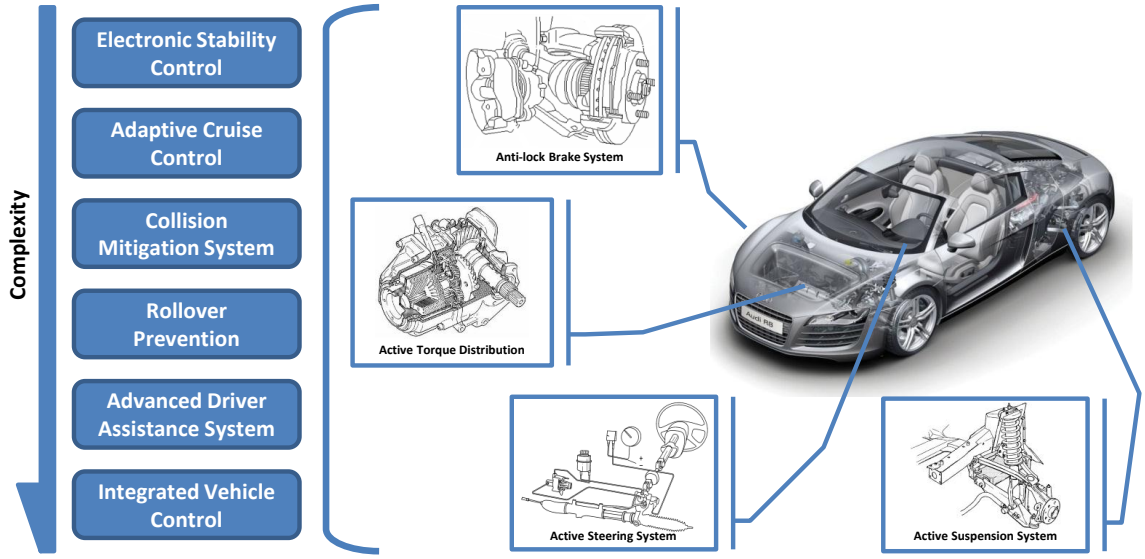


Figure 1.1: Common vehicle chassis control systems available in modern vehicles

reduction on the overall fatal crash involvement risk. Another similar study was conducted by Lie et.al. [4], this time in Sweden where the authors analyzed crash data from 1998 to 2004 on various surface conditions and concluded that stability control systems show around 13 overall effectiveness and a 35% effectiveness on low friction surfaces. A more recent study by Ferguson [5] shows results from investigations conducted world-wide with the conclusions similar to the ones mentioned above. As a consequence of these and many other similar studies, the European Union decided in 2009 to make stability control systems mandatory so that all new models will be equipped with a stability control system starting November 1 of 2011 and old models without a controller will have to be withdrawn from traffic by the end of 2013 [6]. A similar act also took place in the U.S. via NHTSA requiring all vehicles carrying passengers with a gross vehicle weight rating of $4,536$ $Kg$ $(10,000$ $pounds)$ or less to be equipped with a stability control system by 2012. By this act, NHTSA estimates $5,300$ to $9,600$ fatalities to be prevented once all passenger vehicles are instrumented with the stability control system [7].

These reports underline the fact that the current safety systems have undoubtedly become a life-saving technology. Nevertheless; although these systems have advanced in many aspects, there are still many areas that they can be improved. As mentioned above, the tire-road

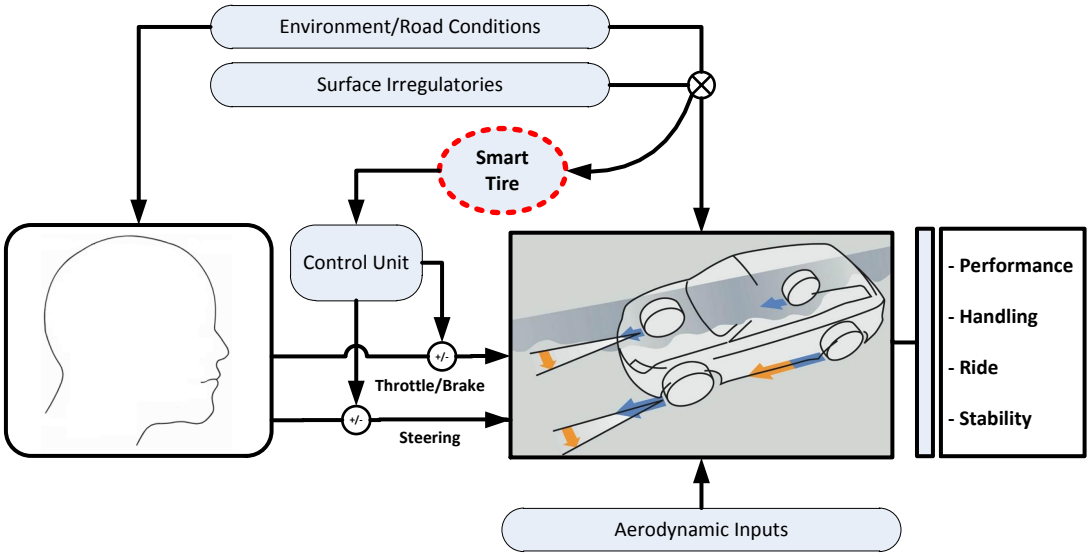


Figure 1.2: Proposed role of the smart tire in active safety systems

contact conceals very valuable information about vehicle's momentary action on the road. Regarding their positions, it is easy to imagine possible improvements for vehicle handling and comfort characteristics that could be achieved by receiving information directly from the tires [8]. Present methods for estimating tire-road parameters make use of information from chassis based sensor systems and highly rely on vehicle kinematic relations. In addition, this indirect approach introduces additional uncertainties to the control procedure and may result in inaccuracies such as integration errors or time lags which might be crucial for the driver and driver assist systems to react to an emergency. The advances in on-board electronics and sensor technology have given rise to a new concept, namely smart tire or intelligent tire technology, as a potential solution to this problem (Figure 1.2). Smart tire technology basically proposes instrumenting the tire and monitoring its momentary conditions, which provides important information about the tire-road contact (Figure 1.3). Furthermore it has the potential to significantly reduce or completely remove the aforementioned inaccuracies by reducing the need for indirect means.

This potential forms the basis and the motivation behind this research for exploring the development and implementation of new active safety systems based on smart tire concept. In the light of the above arguments, the main goal of this study is to develop control algorithms

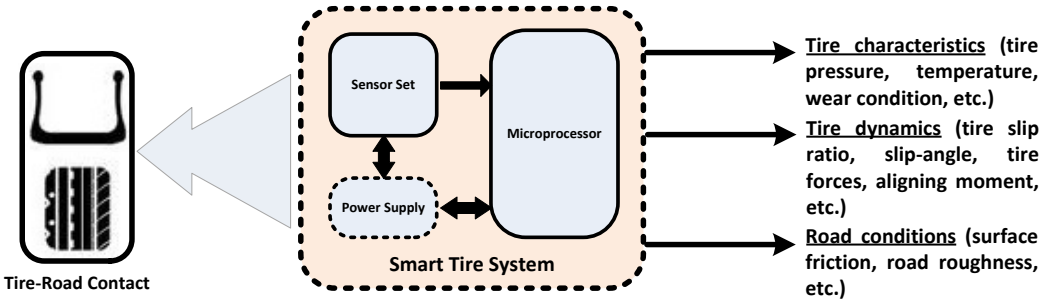


Figure 1.3: Diagram for the potential instrumentation and outputs of the smart tire

based on the information made available by smart tire for further improvements of vehicle and highway safety. A strong background on the state of the art of smart tire technology is an important prerequisite before promoting to the development stage. For that purpose, the rest of this chapter provides a summary of the advances in the smart tire technology along with the initial studies completed on a prototype system developed in the Intelligent Transportation Laboratory (ITL). Following that the objectives and contributions of this study are provided and an outline of this documentation is given.

## 1.1 Smart Tire Technology

### 1.1.1 State of the Art

The potential of the smart tire technology in the development and improvement of safety systems can be better judged by the possible amount of information that can be obtained about the tire in terms of the sensor outputs. With this concept, the tire will not only be responsible for generating the forces and moments to drive and steer the vehicle, but also for supplying the control/safety systems with valuable information regarding the tire-road contact characteristics (Figure 1.4). From the application perspective, the range of possible solutions and products comprises various direct and indirect systems as well as simple and/or complex means for the relevant driver information systems. Some of the proposed automotive applications of a smart tire system can be listed as follows:

- providing real time information about the tire condition to the driver [9],

- providing existing electronic control units (ECUs) with load, friction and slip angle information [10],
- using this information for providing services for external users (e.g. vehicle-to-vehicle (V2V) communication or vehicle-to-infrastructure (V2I) communication) [11].

A standardized technology found in almost every vehicle today, the Tire Pressure Monitoring Systems (TPMS) are considered to be the first smart tire product introduced into the market. Today, with the advances in sensor technology, the interest has also spread into tire temperature monitoring [12], which is also highly related to and therefore can be utilized in observing tire wear. Furthermore, the effects of such features on tire-road dynamics (tire forces, tire-road friction, etc.) are expected to help promoting the studies in the development of smart tire based active safety systems.

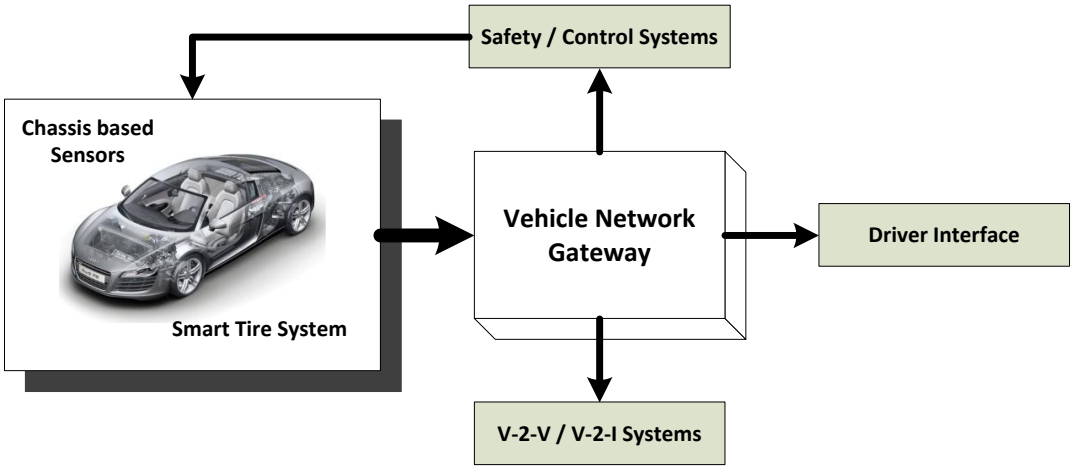


Figure 1.4: Interaction of the smart tire with the vehicle and highway infrastructure

The first patent for the TPMS appeared in 1985 [13] which has been followed by many others along with a slight shift in the development activities towards new aspects such as self-sufficient power supply or wireless means for data transmission/handling. As such, these technologies are also very important for an advanced smart tire system. Nonetheless, despite the new level of safety TPMS provide, they lack essential information regarding the state of the tire road contact characteristics. With the aim of obtaining more information for further optimization of vehicle and highway safety, research in this field has focused on developing

more sophisticated and competent intelligent tire systems. One of the earliest studies for a prototype system was carried out in the Darsmstadt University of Technology in Germany. The resulting system used a magnet placed inside a single tire tread block and the movements of this magnet was monitored by a Hall-effect sensor which allowed the tire deformation to be measured [14]. Another innovative application in the field was the system developed by the Continental Tire, namely the Side Wall Torsion (SWT) sensor, in 1999 [15]. The SWT sensor allowed measurement of the tire side wall deformation and thereby estimation of the forces acting at the tire-road contact. Another mainstream in this initial phase of research was using acoustic wave based systems (*i.e.* Surface Acoustic Wave Sensors) [9], which was very advantageous in terms of power requirements as the sensor system did not require an additional power source.

The success of these pioneering studies triggered the Apollo and Friction programs [16, 17], a collaboration of several Europe based research institutes and private companies. The Apollo program started in 2002 in the lead of VTT (Technical Research Center of Finland) and concluded in 2005 with quite valuable results for the intelligent tire research in general. A thorough feasibility analysis had been conducted and different approaches apart from hall-effect sensors had been tested. Basically a 3-in-1 approach was employed where three different sensor systems (a strain sensor, an optical based sensor and an accelerometer) were placed inside a single tire. Out of these three major sensor systems, accelerometers came out to be the most viable solution due to their durability and ease of utilization inside the tire. The results stated a firm proof for that the possibility exists to predict tire characteristics based on sensors embedded in the tire and solidified the possibility of the benefits of an intelligent tire concept.

The Apollo program was followed by the Friction project to complete the task of measuring the surface friction condition. The project was majorly aimed at proving the possibility of quantifying the friction condition by using a sensor fusion approach that integrates tire based sensors with currently available cost-effective chassis based systems. A specific subtitle of the project was dedicated to further analysis of the optical based sensor developed in the Apollo program. The potential of the approach was studied by employing a detailed finite elements analysis (FEA) and simulations. The optical sensor was reported to provide quite accurate information about tire's momentary deflection which was utilized to estimate the

generated tire forces and eventually the surface friction [18].

The results of these initial studies have made a substantial headway in the field, but also yielded to a number of other key issues waiting to be resolved such as the signal-to-noise ratio in sensor readings, difficulties in decomposition of coupled deflections and measurements or transmission rate of the collected information for real-time active safety control systems. A number of individual studies attempted to come up with feasible solutions to these problems. In [19] Umeno studied vibrations of a free-rolling tire and proposed an algorithm to estimate tire friction and detect hydroplaning. In another study, Zhang et.al. [20], investigated design considerations for a sensor system to be implemented inside the tire, specifically a SAW based sensor, and commented on the required environment and signal conditions. Seki et.al. in [21] introduced a new approach by using tire sound to analyze tire characteristics via wavelet analysis which yields to the estimation of tire tread patterns. Matsuzaki et.al. proposed the use of strain sensors in smart tire systems in [22] and further investigated the potential of such system in [23, 24]. In [25], Ohori et.al. introduced another approach to the smart tire concept by instrumenting the rim and investigated measurement of tire forces and moments by means of this new system. Another exciting study was carried out by Braghin et.al. [26] where the authors investigated the use of accelerometer inside the tire as well as its advantages in the development of vehicle control systems. This approach has been adopted by many others including Brusarosco et.al. [27] and Savaresi et.al. [28], who further investigated the use of acceleration based sensors inside tire; and has become a mainstream in smart tire research per se. Upon the advances in the sensor research in the subject, recent studies focus more on its implementation. Audisio et.al. [29] reports the initial studies and introduces their road-map about a commercial product based on smart tire technology specifically designed for use in safety systems. Ergen et.al. [30] investigates a top-down design procedure for the circuitry to be implemented inside the tire along with an application specific wireless transmission protocol. Another investigation on the application of smart tire systems in vehicle control is done by Cheli et.al. [31] where the authors specifically review possible improvements on the anti-lock brake systems (ABSs) by assuming wheel loads and frictions are available through smart tires. Next, Erdogan et.al. [32] proposed a method to estimate tire-road friction through a smart tire based mechanism. Finally, in [33] and [34] same authors investigate further use of smart tires in ABS and stability control systems. As for the industrial interest about this technology, many private companies already exposed their

initial prototypes in various events, such as the Intelligent Tire by Continental, CyberTire® by Pirelli and Contact Area Information Sensor (CAIS) by Bridgestone, and a commercial product is expected to be released in a near future.

### 1.1.2 Studies at the Intelligent Transportation Laboratory (ITL)

Perceiving the soaring interest in the subject, an industrial partner has approached ITL to collaborate in the development of a prototype smart tire system and to further study possible benefits of it. Initial studies have been carried out on the details of the mechanisms through which tires generate forces and moments. These studies helped with determining the intended tire and surface characteristics using the sensory outputs. In what follows, various sensor candidates were reviewed to be implemented inside the tire and regarding the results of the studies summarized above, micro tri-axial accelerometers were selected for instrumentation (Figure 1.5).

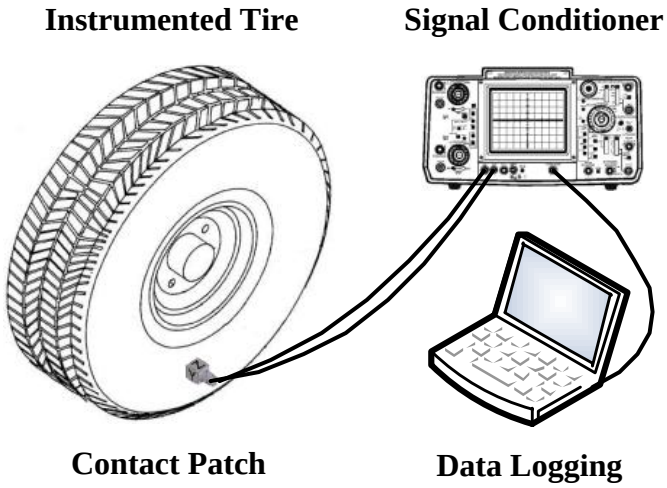


Figure 1.5: The prototype smart tire system developed at the ITL

Testing with multiple sensors inside the tire proved to be impractical due to wiring issues in the rapid rotating frame of the tire. As a result, a single micro tri-axial accelerometer was mounted on the center of the innerliner of the tire. For the prototype system all data and power transmission were managed via wiring inside the tire through a high-speed rated slip ring. A signal conditioner powered the accelerometer and the data was logged on a PC for further analysis. After proper instrumentation of the tire, the system was taken out for

testing using the in-house tire testing trailer (Figure 1.6).

(a) Prototype mounted on the testing trailer (b) The in-house tire testing trailer at ITL

Figure 1.6: Testing of the developed smart tire prototype

The collected data indicated that as a tire rolls and deforms during operation under load, the tire produces a signature waveform that can be interpreted into information regarding the tire and road surface conditions. Basically the four major zones of curvature within an inflated tire, as shown in Figure 1.7a, shape the waveform per revolution. These four zones include the contact patch which varies with braking and acceleration, the zones just before and just after the contact patch relating to the leading and trailing edges, respectively, and finally the area of the tire that is largely unaffected by loading. Through implementation of a multi-axis accelerometer, it was possible to measure the acceleration and deformation of the tire in the longitudinal, lateral and vertical directions (Figure 1.7b). The data collected from the accelerometer was processed using various methods including neural networks and power spectrum densities (PSD).

The prototype was extensively tested on different surface conditions to collect sufficient amount of data for further analysis. Finally, the studies were concluded by the development of two novel signal processing algorithms [35] that can compute the dynamic wheel load (Figure 1.8a) and tire slip-angle (Figure 1.8b) variations. Furthermore, based on the wheel load information, a surface condition classification method has been developed and implemented for the development of a new ABS control algorithm [36].

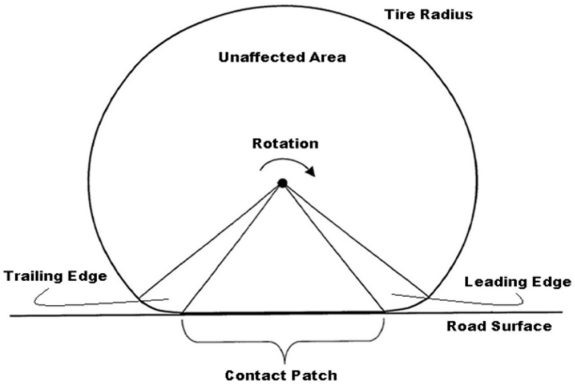


(a) The four zones of curvature within an inflated tire

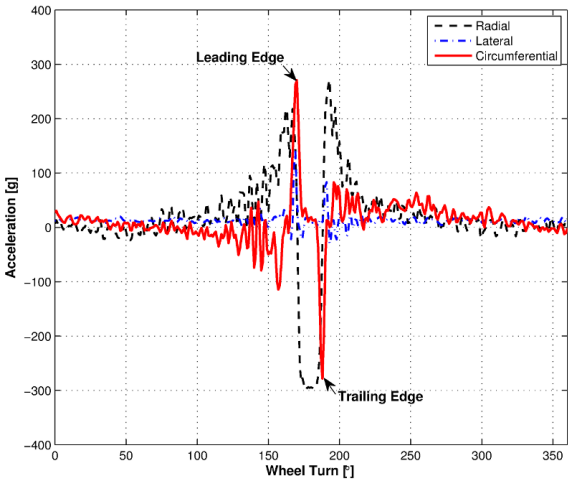


(b) Sample vibration data logged for a full revolution

Figure 1.7: Tire vibration waveform generation.

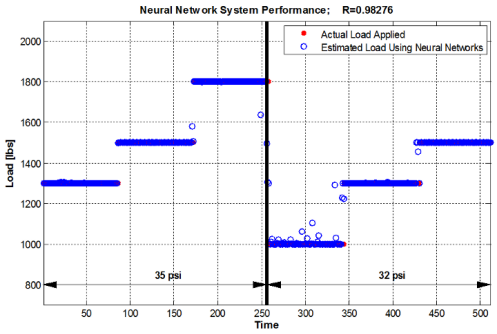


(a) The wheel load algorithm is based on contact patch characteristics.

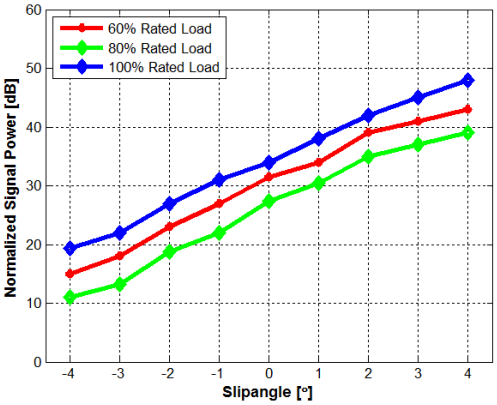


(b) Tire slip-angle estimation is based on lateral acceleration signals.

Figure 1.8: Results of the signal processing algorithms using the smart tire prototype developed in ITL

## 1.2 Objectives & Contributions

As summarized above, the tire-road characteristic plays a vital role in the development and performance of the vehicle control systems. The current methods for obtaining information on tire-road characteristics heavily rely on indirect estimation mechanisms and are quite

open for improvements. The literature proves that smart tire technology is a promising path for reducing the dependency on indirect estimation and for attaining considerable improvements in the estimation of dynamic tire states. The initial studies completed at the ITL also concluded with very encouraging results including a prototype system and algorithms to obtain valuable information from the data collected by an accelerometer mounted inside the tire. In addition, various discussions between the ITL and our industry partner during the development of the prototype system indicated that there is a considerable interest in the market for such a technology, which proclaimed its implementation as an open field to explore. Based on these arguments, this study aims to develop novel vehicle control systems that can make efficient use of the smart tire technology and takes full advantage of being able to obtain information about tire-road characteristics.

The active safety systems available on vehicles today are based on the longitudinal and lateral stability of the vehicle chassis as well as its rolling stability. Regarding these groundwork on the subject, the objectives of this study can be expanded as follows:

- Investigating points in vehicle stability and control where the smart tire becomes most beneficial.
- Developing algorithms for primary vehicle chassis control systems (e.g. ABS, stability control, active steering, and torque distribution) with additional information from the smart tire
- Developing novel control algorithms that can coordinate various primary chassis control systems to achieve better vehicle stability and handling performance.
- Finally, developing integrated vehicle control algorithms that can inherently account for the actuation dynamics as well as adapting to possible variations in environmental conditions, aiming to compute a set of control laws guaranteeing optimal actuator coordination and performance.

The study was initiated by conducting a brief parametric study based on mathematical vehicle models, which revealed the points where the smart tire will be most useful in vehicle control systems. The results were then utilized to channel the information from the smart tire into novel control algorithms for improved vehicle safety and performance. Based on these endeavors, the major contributions of this research can be listed as follows:

- Contributed in the development of a prototype smart tire system that is capable of providing dynamic wheel load and tire slip-angle information in addition to classifying current road surface condition, and developed novel signal processing algorithms to estimate corresponding tire-road states.
- Developed two adaptive stability control algorithms primarily based on the tire slip-angle and force information provided by smart tire, which integrates active steering and yaw control schemes to improve vehicle safety and performance.
- Developed a self-tuning ABS algorithm based on contemporary rule-based commercial systems that can update the pre-defined rule set to provide best possible braking performance irrespective of the surface conditions.
- An Integrated Chassis Control scheme is introduced to accommodate the previously developed stability and braking control algorithms. A dynamic control allocation strategy is implemented that can optimally distribute wheel brake forces while successfully avoiding actuator saturation or over-rating conditions.
- Finally, evaluated the effectiveness of the developed control algorithms using validated nonlinear vehicle models and a commercial software (CarSim) under various surface and driving conditions.

Regarding these outcomes, this study is a frontier in a new phase of developments on vehicle control systems by allowing effective use of information about the tire-road interaction. The smart tire technology brings in the possibility of acquiring very detailed and accurate knowledge of the dynamical variations of the tire as well as the contact patch between the tire and the road, which in return opens up a new lane for advancements in the field. In what follows, the results of this research set down a strong foundation in terms of the integration of this novel technology in vehicle controls and to extend it to further advance in vehicle safety and performance.

## 1.3 Document Outline

The rest of this document is organized as follows:

*Chapter 2: Mathematical Modeling & Simulation* details the vehicle dynamics and related mathematical models utilized in the development of the control algorithms as well as in their simulations. Also a brief analysis of system stability is conducted to figure out which parameters might impel most the improvement of vehicle control systems.

*Chapter 3: Adaptive Vehicle Stability Control* first briefly reports the studies on the development of vehicle stability systems so far. Next, the sensor fusion approach to estimate the tire slip-angle is outlined. Finally the work on a new adaptive control algorithm for vehicle stability is introduced, which utilizes the sensor fusion concept to obtain dynamic information about tire slip angle and provides assistance to the driver to maintain stability of the vehicle.

*Chapter 4: Advanced Anti-lock Braking* briefly summarizes the literature on handling and braking studies based on ABS algorithms up to dat. In what follows the integrated estimation scheme for obtaining surface friction condition with the use of the smart tire and a model based observer is explained. Finally, the chapter introduces an ABS algorithm integrated with the surface friction estimation to improve performance. Based on the estimated friction condition, the algorithm is capable of updating the predefined limit criteria for applying/releasing the brakes, thereby providing best performance irrespective of any variations on the surface conditions.

*Chapter 5: Integrated Vehicle Control Systems* introduces the notion of integrated chassis control and a dynamic control allocation strategy. The control allocation strategy implements optimal tire force distribution to articulate the stability and braking control schemes. The resulting lower level controller aims to signal the brakes for the optimum brake forces with respect to the yaw moment requirement to maintain vehicle stability. In what follows, a new adaptive control strategy, namely the $\mathcal{L}_1$ adaptive control method, is presented that proposes improved adaptation capabilities.

*Chapter 6: Conclusion* shortly summarizes the outcomes of the above studies based on the results and the current state-of-the-art. Finally, the chapter reflects on possible extensions of this research for further development.

## 1.4 List of Publications

This research so far has led to a series of peer-reviewed conference and journal publications as listed below:
*Peer Reviewed Abstracts:*

- **Arat, M.A.**, Taheri, S., "*Application of Smart Tire Technology in Vehicle Chassis Control Systems*", $17^{th}$ International Conference of ISTVS, Blacksburg, VA, 2011
- **Arat, M.A.**, Singh, K.B., Taheri, S., "*Application of a Smart Tire System in Improving the Performance of Advanced Vehicle Control Systems*", $31^{st}$ Annual Meeting and Conference on Tire Science and Technology, Cleveland, Ohio, 2012
- **Arat, M.A.**, Taheri, S., "*Development and Improvement of Active Vehicle Safety Systems by Means of Smart Tire Technology*", SIAM Conference on Control and Its Applications, San Diego, CA, 2013

*Peer Reviewed Conference Papers:*

- **Arat, M.A.**, Singh, K.B., Taheri, S., "*An Intelligent Tire based Adaptive Vehicle Stability Control System*", International Conference on Advanced Vehicle Technologies and Integration (AVTI), Changchun, China, 2012
- **Arat, M.A.**, Singh, K.B., Taheri, S., "*An Adaptive Vehicle Stability Control Algorithm based on Tire Slip-Angle Estimation*", SAE Commercial Vehicle Engineering Congress, Rosemont, Illinois, 2012
- **Arat, M.A.**, Singh, K.B., Taheri, S., "*Adaptive Vehicle Stability Control with Optimal Tire Force Allocation*", ASME 2012 International Mechanical Engineering Congress and Exposition, Houston, Texas, 2012
- Singh, K. B., **Arat, M. A.**, and Taheri, S., "*Adaptive Control of Antilock Braking System Using an Intelligent Tire Based Tire-Vehicle State Estimator*", FISITA 2012 World Automotive Congress, Beijing, China, 2012
- Singh, K. B., **Arat, M. A.**, and Taheri, S., "*Enhancement of Collision Mitigation Braking System Performance Through Real-Time Estimation of Tire-Road Friction*

*Coefficient by Means of Smart Tires*", SAE Commercial Vehicle Engineering Congress, Rosemont, Illinois, 2012

- Singh, K. B., **Arat, M. A.**, and Taheri, S., "*Development of a Smart Tire System and its use in Improving the Performance of a Collision Mitigation Braking System*", ASME 2012 International Mechanical Engineering Congress and Exposition, Houston, Texas, 2012

*Peer Reviewed Journal Papers:*

- **Arat, M.A.**, Singh, K.B., Taheri, S., "*An Intelligent Tire based Adaptive Vehicle Stability Controller*", International Journal of Vehicle Design - Special Issue on Advanced Developments in Tire Modeling, Analysis and Dynamics (in print)
- **Arat, M.A.**, Singh, K.B., Taheri, S., "*Optimal Tire Force Allocation by Means of Smart Tire Technology*", SAE Int. J. Passeng. Cars - Mech. Syst. 6(1):2013.
- Singh, K., **Arat, M.A.**, and Taheri, S.,"*Enhancement of Collision Mitigation Braking System Performance Through Real-Time Estimation of Tire-road Friction Coefficient by Means of Smart Tires*", SAE Int. J. Passeng. Cars - Electron. Electr. Syst. 5(2):607-624, 2012
- Singh, K.B., **Arat, M.A.**, Taheri, S., "*An Intelligent Tire Based Tire-Road Friction Estimation Technique and Adaptive Wheel Slip Controller for Anti-lock Brake System*", Journal of Dynamic Systems, Measurement and Control, **135**, 0310032, 2013.

# Chapter 2

# Mathematical Modeling and Simulations

## 2.1 Introduction

To be able to analyze the interplay of forces and motions acting on the vehicle, one needs an integrated treatment of all system components interacting with each other. The basis of such a theoretical analysis of vehicle systems is an appropriate mathematical model adapted to the given task. This underlying model has to be sufficiently detailed to represent the essential properties of the vehicle system and, at the same time, as simple as possible to allow for reasonable simulation capabilities. Obtaining a balance between the reality and abstraction of the model is most important as it dictates the quality of the results achievable on a system's dynamical behavior. These conflicting requirements depict the challenge in selecting the appropriate model for different engineering tasks.

In this study, linearized vehicle models are utilized for control system development and their evaluations are done on more realistic non-linear models. The following subsections detail these models. The handling and braking studies are based on a two-degrees-of-freedom quarter car model. Another linearized two-degrees-of-freedom model (bicycle model) is used in stability studies to represent the vehicle lateral dynamics. The initial evaluations of the developed control algorithms are executed using an eight-degrees-of-freedom nonlinear vehicle model which represents the lateral, longitudinal, roll and yaw dynamics as well as the

rotational dynamics of each of the four wheels on the vehicle. Finally CarSim® commercial software is utilized as a more realistic test bed.

## 2.2 Vehicle Models used in Control System Development

### 2.2.1 Quarter Car Model

The most simplistic yet very useful model in vehicle dynamics analysis is the quarter-car model (a.k.a. single corner model) which as its name implies is derived by taking only a single wheel of the vehicle into account. This model, despite its simplicity, can quite successfully represent the longitudinal and vertical dynamics on a single wheel with the proper selection of required parameters. Although based on a single wheel, a quarter car model can also be developed in a non-linear fashion and with higher degrees of freedom by including suspension dynamics and/or road profile variations if needed. Therefore it is a widely used and accepted model in suspension as well as braking studies. In this study, the quarter car model is utilized to define the vehicle longitudinal dynamics in the development of a new anti-lock braking system (ABS) algorithm (4).

Considering the essential features for brake dynamics (e.g. wheel angular speed, vehicle speed, wheel load and the net torque acting on the wheel), Figure 2.1 represents the free body diagram of the single wheel which is the basis for the model.

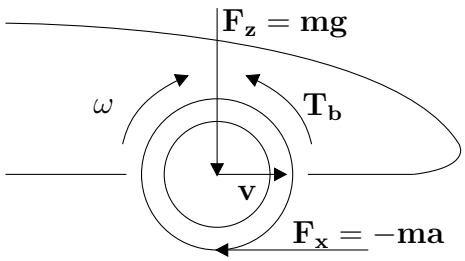


Figure 2.1: The quarter-car model illustration

The model basically consists of a single wheel attached to the quarter vehicle with mass ($m$).

The respective equations of motion for this system are given as below:

$$ma = -F_x \tag{2.1}$$

$$J\dot{\omega} = F_x R_w - T_b \tag{2.2}$$

For a quarter car system, the longitudinal tire force ($F_x$) is the key variable that dominates the wheel dynamics. It can be defined as a non-linear function of wheel load ($F_z$), tire longitudinal slip ($\lambda$), tire slip angle ($\alpha$) and the maximum tire-road friction coefficient ($\mu_{max}$):

$$F_x = F_z \mu(\alpha, \lambda, \mu_{max})$$

When studying the straight line braking, the tire slip angle ($\alpha$), is generally omitted assuming negligible steering activity. As for the tire slip ratio (wheel slip), it can be defined by the ratio of the relative velocity between the tire and the road to the maximum of the two, which is mathematically defined as below:

$$\lambda = \frac{v - R_w\omega}{max(v, R_w\omega)} \tag{2.3}$$

It is worth to note that zero slip characterizes the free rolling when no friction force applies ($F_x = 0$) on the wheel, and unit slip ($\lambda = 1$) indicates complete wheel lock-up. The quarter car model can reveal very valuable details about the vehicle's stability characteristics during braking. The rest of this section aims to provide a brief analysis to underline the important parameters in the development of a successful ABS algorithm. The key element in such an analysis is the accuracy of the selected friction or tire model. The Burckhardt model is one of the most widely used models as it defines the utilized friction ($\mu$) in terms of wheel slip and constant coefficients ($C_1$, $C_2$ and $C_3$) that are pre-defined w.r.t. maximum surface friction:

$$\mu(\lambda) = C_1(1 - e^{1-C_2\lambda}) - C_3\lambda \tag{2.4}$$

The constant coefficients help to adjust the model for different surface conditions. In what follows, the wheel slip ($\lambda$) dynamics can be determined by taking the time derivative of equation 2.3 and substituting equations 2.1, 2.2 and 2.4 for the appropriate terms, which yields to the below differential equation:

$$\dot{\lambda} = \frac{R_w(T_b - T_e)}{Jv} \tag{2.5}$$

where

$$T_e = R_w \mu(\lambda) F_z \left(1 + \frac{(1-\lambda)J}{mR_w^2}\right)$$

is the equilibrium torque. It is important to note that the rate of change of slip drops to zero when equilibrium torque equals to the brake torque. Next equation 2.5 is augmented with the brake torque dynamics by assuming a constant brake torque rate:

$$\dot{T}_b = U \tag{2.6}$$

The phase plane of the resulting system can provide an insight on the stability characteristics of a braking vehicle as depicted in Figure 2.2a. This simple analysis shows the relation between the applied brake torque, or brake pressure as they can be assumed linearly proportional, and the wheel lock-up condition which defines the stability of the vehicle.

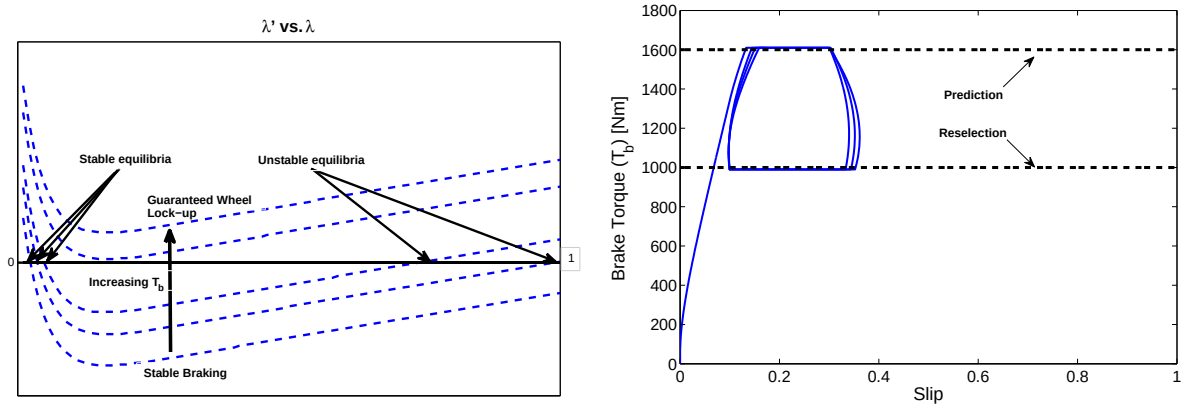


(a) Phase-plane for the wheel slip dynamics with constant brake torque rate

(b) System trajectory for the quarter-car with simple rule-based ABS algorithm implemented

Figure 2.2: Stability analysis for a quarter car model

As these results indicate, heedlessly increasing the brake torque results in wheel lock-up which dramatically reduces the braking performance and even worse drives the vehicle unstable. To avert such failure scenarios, ABS algorithms are proposed that allows brakes to be applied in a cyclic way to adjust the applied brake torque/pressure. Figure 2.2b illustrates the system trajectory ($T_b$ vs. $\lambda$) of the system defined in eq. 2.5 and 2.6 with a simple rule-based ABS algorithm at work. The algorithm basically prevents constant increase in the applied brake torque by releasing and reapplying the brakes w.r.t. specified limits, namely the Prediction and Reselection rules. Equation 2.5 suggests that, aside from the applied brake torque, the behavior of the system trajectory also highly depends on the surface friction condition, which

defines the tire force characteristics and thereby also the equilibrium points. Therefore a set of Prediction and Reselection rules defined for a certain surface condition will not yield to the same performance, or will not even guarantee averting wheel lock-up on a different surface. A viable solution is adapting the specified rule-set to the varying surface conditions where the involvement of a smart tire would be essential for dynamically observing the tire-road conditions. These results motivated the development of a smart tire based ABS algorithm detailed in Chapter 4.

### 2.2.2 Bicycle (Linear 2 DoF) Model

The vehicle bicycle model is a linearized model basically for vehicle's lateral dynamics. It provides a mathematical description of the vehicle motion without considering the forces that affect the pitch and roll motion assuming that these forces are canceled due to symmetry w.r.t. the imaginary single track passing through the middle of the vehicle, hence the other name for the model as single track. The equations for steering and turning motions are based purely on geometric relationships governing the system.

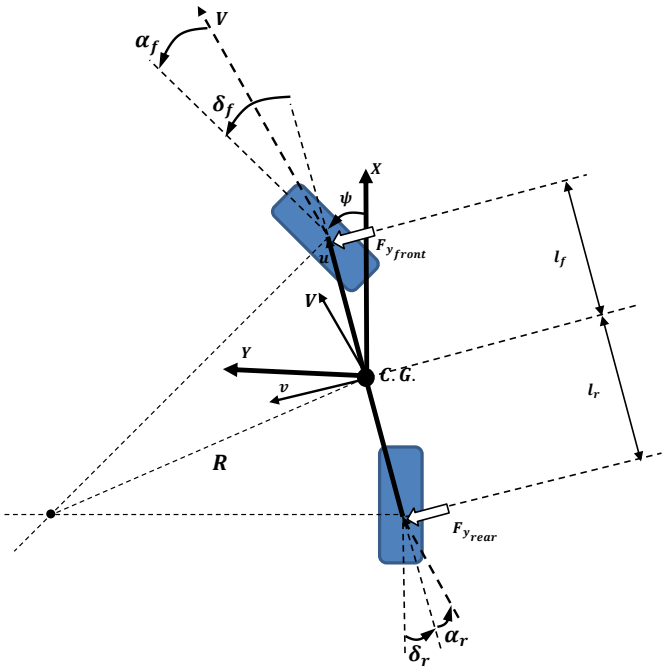


Figure 2.3: Single track vehicle model

Figure 2.3 shows the free body diagram for the bicycle model. As mentioned above the

left and right side wheels are represented on a single track with front and rear wheels only. Furthermore in this study the rear steer ($\delta_r$) is neglected assuming a front-steer vehicle. In its simplest form the lateral dynamics of the vehicle chassis can be defined using Newton's law. The sum of the lateral forces acting on the vehicle chassis defines the lateral acceleration and the total moment acting at the vehicle c.g. is defined by the lateral forces at the front and rear axles:

$$m\dot{v} = F_{y_{front}} + F_{y_{rear}} \tag{2.7}$$

$$I_z\dot{r} = l_f F_{y_{front}} - l_r F_{y_{rear}} \tag{2.8}$$

where $I_z$ is the vehicle chassis' moment of inertia w.r.t. the $Z$ axis, $r$ stands for the rate of change of the yaw angle and $F_{y_{front}}$ and $F_{y_{rear}}$ represent the sum of the lateral tire forces at the front and rear axles. Tires have intrinsic nonlinear characteristics (Section 2.3), including the relation between the generated tire forces and the excitation parameters (*e.g.* tire slip ratio and slip angle); however a linear approximation is acceptable at lower excitation rates (*i.e.* $|\alpha| \leq \pm 10^\circ$) [37]. Assuming small tire slip-angles, the tire forces can be defined by the following linear relations:

$$F_{y_{front}} = 2C_{\alpha f}\alpha_f \tag{2.9}$$

$$F_{y_{rear}} = 2C_{\alpha r}\alpha_r \tag{2.10}$$

where $C_{\alpha f}$ and $C_{\alpha r}$ are the front and rear tire cornering stiffness values. The same small angle approach allows defining the front and rear tire slip-angles as below by utilizing kinematic relations from the model geometry depicted in Figure 2.3.

$$\alpha_f = \delta - \frac{v - l_f r}{u} \tag{2.11}$$

$$\alpha_r = -\frac{v - l_r r}{u} \tag{2.12}$$

In what follows, equations 2.9-2.12 are substituted back into equation 2.7 and 2.8 which yields to define what is generally known as the vehicle bicycle model:

$$\dot{v} = -\frac{2C_f + 2C_r}{mu}v - \left(\frac{2C_f l_f - 2C_r l_r}{mu} + u\right) r + \frac{C_f}{m}\delta \tag{2.13}$$

$$\dot{r} = -\frac{2C_f l_f - 2C_r l_r}{I_z u}v - \frac{2C_f l_f^2 + 2C_r l_r^2}{I_z u}r + \frac{C_f l_f}{I_z}\delta \tag{2.14}$$

Chassis side-slip angle ($\beta$) is considered as another important indicator for vehicle lateral performance and can be defined as the proportion between lateral and longitudinal vehicle speeds:

$$\beta = \frac{v}{u} \tag{2.15}$$

Derivating equation 2.15 w.r.t. time and substituting for $\dot{v}$ in equation 2.13 yields to another common representation used in vehicle stability studies:

$$\dot{\beta} = -\frac{2C_f + 2C_r}{mu}\beta - \left(\frac{2C_f l_f - 2C_r l_r}{mu^2} + 1\right) r + \frac{C_f}{mu}\delta \tag{2.16}$$

Equations 2.13 and 2.16 can be used in place of each other depending on the purpose of the analysis or control strategy to be accomplished. The bicycle (single-track) model provides an invaluable tool for vehicle lateral stability analysis and control design. A very important performance metric in lateral stability analysis is the understeer gradient of a vehicle which basically indicates the responsiveness of the vehicle to the given steering inputs. Assuming the single-track model undergoing a constant radius ($R$) turn, the understeer gradient can be derived as follows. First the steering angle during a constant radius turn is approximated as:

$$\delta = \frac{L}{R} + \alpha_f - \alpha_r \tag{2.17}$$

Next, using the linear tire model in equations 2.9 and 2.10 and the approximation for lateral acceleration as $a_y = V^2/R$, equation 2.17 is rewritten as:

$$\delta = \frac{L}{R} + \left(\frac{m_f}{C_{\alpha f}} - \frac{m_r}{C_{\alpha r}}\right)\frac{a_y}{2} = \frac{L}{R} + K a_y \tag{2.18}$$

where $m_f = m(l_r/L)$ and $m_r = m(l_f/L)$ and $K$ stands for the understeer gradient. A significant point for this study is found by comparing equation 2.17 and 2.18 which demonstrates the direct relation between the understeer gradient and tire slip-angles. As mentioned before, this metric defines the vehicle's dynamic behavior for a given steering input, and due to the direct relation, same interpretation can be made using the tire slip-angles as well. Using equation 2.17 and 2.18 one can validate the relation of the difference between the front and rear slip-angles and the vehicle's understeer (steering angle needs to be increased to negotiate a turn of constant radius), neutralsteer (steering angle should remain constant) and oversteer (steering angle needs to be decreased) behavior. Furthermore, equations 2.13, 2.14 and 2.16 can be solved under steady-state conditions ($\dot{r} = 0$, $\dot{v} = 0$, $\dot{\beta} = 0$) to observe

the variation of these characteristics w.r.t. tire slip-angles.

$$r = \frac{V/R}{\frac{L}{R} - \frac{m}{2LR}\frac{C_{\alpha f}l_f - C_{\alpha r}l_r}{C_{\alpha f}C_{\alpha r}}V^2}\delta \tag{2.19}$$

$$v = \frac{\left(2l_r - \frac{l_f}{L}\frac{mu^2}{C_{\alpha r}}\right)V/R}{\frac{L}{R} - \frac{m}{2LR}\frac{C_{\alpha f}l_f - C_{\alpha r}l_r}{C_{\alpha f}C_{\alpha r}}V^2} \tag{2.20}$$

It is important to note that in these definitions:

$$\frac{m}{2LR}\frac{C_{\alpha f}l_f - C_{\alpha r}l_r}{C_{\alpha f}C_{\alpha r}}V^2 = \left(\frac{m_f}{C_{\alpha f}} - \frac{m_r}{C_{\alpha r}}\right)\frac{V^2}{2R} = \alpha_f - \alpha_r \tag{2.21}$$

Figure 2.4 depicts the variation of the turning radius, vehicle yaw rate and lateral speed w.r.t. the vehicle speed for the oversteer (OS), neutralsteer (NS) and understeer (US) vehicle, which are basically defined by the difference between the tire slip-angles.

The transient response of the single-track model can be studied using the characteristics equation of the system defined by eq. 2.14 and 2.16:

$$s^2 + \left(\frac{2m(C_{\alpha f}l_f^2 + C_{\alpha r}l_r^2) + 2I_z(C_{\alpha f} + C_{\alpha r})}{mI_zV}\right)s + \left(\frac{4C_{\alpha f}C_{\alpha r}l^2}{mI_zV^2} - \frac{2(C_{\alpha f}l_f - C_{\alpha r}l_r)}{I_z}\right) = 0 \tag{2.22}$$

the roots of which are given as:

$$\lambda_{1,2} = -\frac{(C_{\alpha f}l_f^2 + C_{\alpha r}l_r^2) \pm 2\sigma}{I_zV} \tag{2.23}$$

where

$$\sigma = \left((C_{\alpha f}l_f^2 + C_{\alpha r}l_r^2)^2 - \frac{I_zuC_{\alpha f}C_{\alpha r}L}{m}\left[L - \frac{m}{2L}\frac{C_{\alpha f}l_f - C_{\alpha r}l_r}{C_{\alpha f}C_{\alpha r}}V^2\right]\right)^{\frac{1}{2}}$$

and where the understeer gradient appears inside the square root as in the form given in eq. 2.21. The qualitative evaluation of this analysis is done by brief simulations, results of which are shown in Figure 2.5. Similar to the steady-state case, the results show the distinct characteristics of an US, NS and OS vehicle under the same steering input.

This brief analysis summarizes some fundamental results about vehicle stability and also

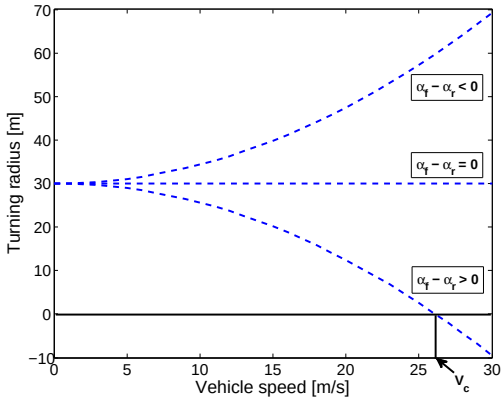


(a) Position response

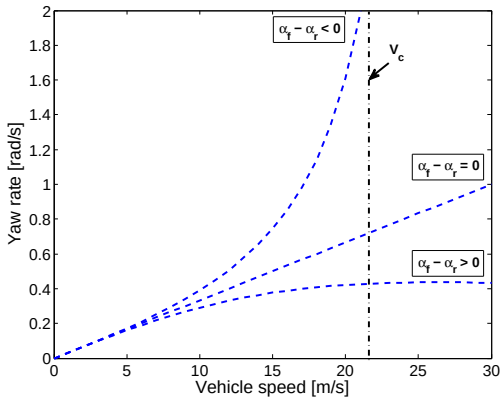


(b) Yaw-rate response

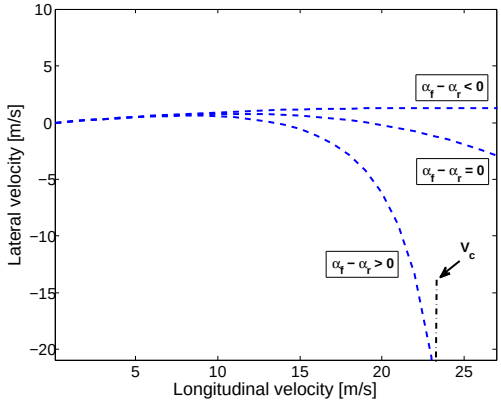


(c) Lateral velocity response

Figure 2.4: Vehicle steady-state response under US, NS and OS characteristics

reveals the importance of tire parameters such as cornering stiffness or slip-angle in defining a vehicles stability characteristics. Furthermore, the results suggest that observing the tire slip-angles allows one to comment on the momentary lateral chassis dynamics. Based on

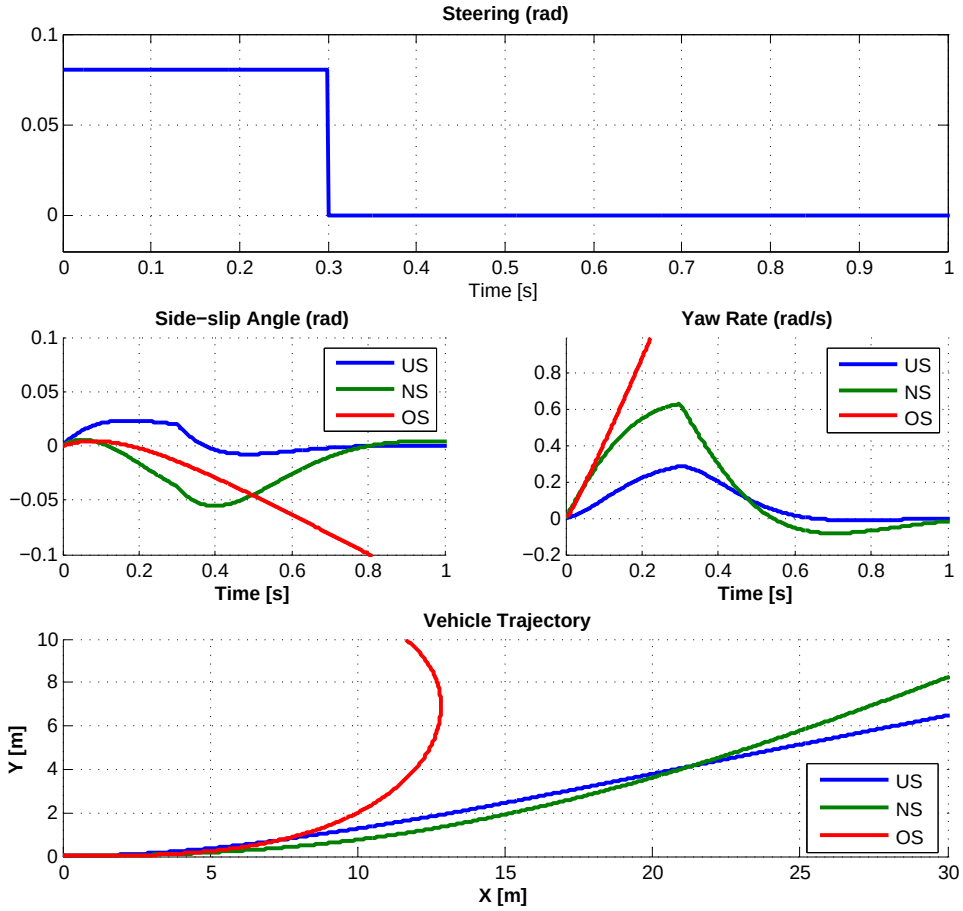


Figure 2.5: Vehicle transient response to the given pulse steering input

these deductions, the stability control investigations focus on the estimation and use of tire slip-angle in control algorithms.

## 2.3 Models used in Simulation Studies

### 2.3.1 Nonlinear Vehicle Model

A four degree-of-freedom (DoF) chassis model is adopted from [38], that accounts for vehicle's longitudinal, lateral, yaw and roll dynamics, and is integrated with rotational dynamics for each of the four wheels. The resulting model is a nonlinear eight DoF vehicle model that also utilizes combined slip tire model to compute tire forces. The chassis dynamics are derived

using Lagrange's method based on the principle of conservation of energy:

$$\frac{d}{dt}\frac{\partial T}{\partial \dot{q}_i} - \frac{\partial T}{\partial q_i} + \frac{\partial U}{\partial q_i} = Q_i \tag{2.24}$$

where $T$ stands for system's kinetic energy, $U$ for potential, $Q_i$ refers to the external generalized forces and moments acting on the system and $q_i$ represents the generalized coordinates to describe system motion. The longitudinal ($u$), lateral ($v$) and yaw ($r$) velocities and the roll angle ($\phi$) of the chassis are taken as the generalized coordinates. Following from [**?**], the generalized forces and moments are found to be:

$$\begin{aligned} Q_u &= F_{x_{fl}} cos\delta - F_{y_{fl}} sin\delta + F_{x_{fr}} \\ Q_v &= F_{x_{fl}} sin\delta + F_{y_{fl}} cos\delta + F_{y_{fr}} \\ Q_r &= l_f F_{x_{fl}} sin\delta + l_f F_{y_{fl}} cos\delta + M_{z_{fl}} - bF_{y_{fr}} + M_{z_{fr}} \\ Q_\phi &= -(k_{\phi_{fl}} + k_{\phi_{fr}})\dot{\phi} \end{aligned} \tag{2.25}$$

where $Q_u$ is the sum of the forces in longitudinal direction, $Q_v$ is the sum of forces in lateral direction, $Q_r$ is the sum of the moments in yaw direction and $Q_\phi$ is the sum if the moments in roll direction. Defining the kinetic and potential energy of the system as:

$$\begin{aligned} T &= 1/2m\left[(u - h'\phi r)^2 + (v + h'\dot{\phi})^2\right] + 1/2I_x\dot{\phi}^2 + 1/2I_y(\phi r)^2 \\ &\quad +1/2I_z(r^2 - \phi^2 r^2 + 2\theta_r r\dot{\phi}) - I_{xz} r\dot{\phi} \end{aligned} \tag{2.26}$$

$$U = 1/2(C_{\phi_{fl}} + C_{\phi_{fr}})\phi^2 - 1/2mgh'\phi^2 \tag{2.27}$$

yields to the equations of motion for chassis as below:

$$\begin{aligned} m(\dot{u} - rv - h'\phi\dot{r} - 2h'r\dot{\phi}) &= Q_u \\ m(\dot{v} + ru + h'\ddot{\phi} - h'r^2\phi) &= Q_v \\ I_z\dot{r} + (I_z\theta_r - I_{xz})\ddot{\phi} - mh'(\dot{u} - rv)\phi &= Q_r \\ (I_x + mh'^2)\ddot{\phi} + mh'(\dot{v} + ru) + (I_z\theta_r - I_{xz})\dot{r} - (mh'^2 + I_y - I_z)r^2\phi & \\ +(C_{\phi_{fl}} + C_{\phi_{fr}} - mgh')\phi &= Q_\phi \end{aligned} \tag{2.28}$$

The wheel dynamics are adopted from the quarter car dynamics in equation 2.2, with the addition of and engine torque term ($T_e$) to account for the possible throttle input from the

driver:

$$J\dot{\omega}_i = (T_{e_i} - T_{b_i}) - F_{x_i} R_{w_i} \tag{2.29}$$

where $i$ denotes the wheel location ($e.g\ fl, fr, rl, rr$). Finally the tire forces ($F_{x_i}$ & $F_{y_i}$) are computed using a combined slip tire model which is further detailed in section 2.4

### 2.3.2 CarSim®

Developed in 1991 at the University of Michigan Transportation Research Institute [39], CarSim® software package provides realistic vehicle models with as many degrees-of-freedoms (DoF) for various simulation studies and for many test applications including the evaluation of control systems [40, 41, 42]. In this study, the models provided by CarSim® are downloaded into the MATLAB/Simulink environment, where the proposed control algorithms are implemented and the resulting vehicle characteristics are evaluated under given conditions. The vehicle models run with 15 mechanical DoF which account for 6 DoF for the sprung mass rigid body, 2 DoF for each suspension, single DoF on each wheel and a 1 DoF steering system; in addition to other dynamic DoF such as tire response (2 DoF lagged response), brake hydraulics and throttle lags [43]. Various chassis types are offered (Figure 2.6) based on standard European chassis styles such as B,C,D & E-classes as well as sports utility vehicles (SUVs). In this study specifically the D and E class sedan passenger cars and SUVs are utilized. Furthermore many test conditions can be modified including driver models, surface conditions (e.g. friction, bank angle, etc.), environmental conditions (e.g. gust wind, obstacle, etc.) or timing options for braking/throttling (Figure 2.6).

The vehicle model in CarSim is defined by fully nonlinear equations of motion as derived using first principles. The equations are in the form of a system of ordinary differential equations (ODEs). In CarSim vernacular, the program contains several built-in solvers. A solver in CarSim represents a complete set of equations of motion defining a particular combination of front and rear suspension types and a trailer (if included). Following paragraphs provide brief descriptions of modeling details on the individual elements of the vehicle and the environmental factors.

*Suspension:* Each wheel on the vehicle has vertical travel and rolling rotation as degrees of freedom. The front suspension is always modeled as fully independent, while rear suspensions may be independent, twist axle, or solid axle at the option of the user. Each

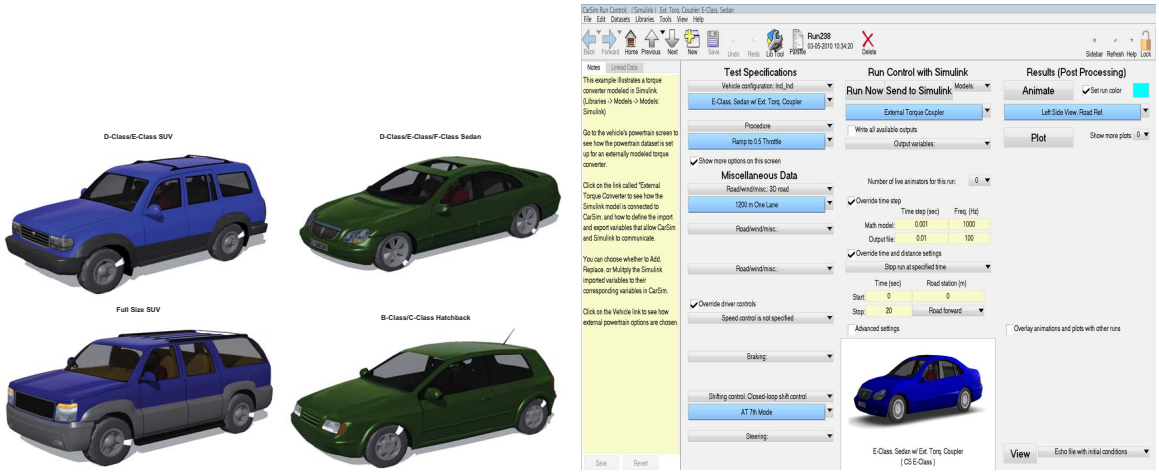


(a) Utilized vehicle models (b) User interface

Figure 2.6: CarSim® features

suspension contains full compliance effects in lateral / longitudinal motion and angular motion, and friction (hysteresis) effects in the suspension springs. All kinematics (camber, toe, etc.), spring stiffnesses, damping, and compliance can be defined by the user through lookup tables / curves, which can be fully nonlinear. For this reason, the suspension type need not be specified beyond "independent", as the solver uses kinematic curves (the consequence of whatever geometry may be present) rather than the geometry itself. The effects of roll and jacking forces are derived from the kinematic curves and the compliance effects, rather than as a consequence of conventional geometric analyses.

*Steering:* Complete vehicle steering mechanics are included in the CarSim model. The virtual driver can steer the steering wheel to any angle up to a user-definable maximum angle. The steer angle at the wheels is found by multiplying the steer angle through the steering rack ratio (user-defined tabular data). The actual angle at the wheel/tire is augmented by the angular effects of the compliance in the suspension. The compliance deflection is found as a result of the sum of moments in the suspension about the kingpin. Steering torque at the steering wheel is calculated by multiplying the total moment about the kingpin back through the steering system ratio. The driver steer angle can be defined as an open-loop function of time in the form of tabular data, or can be controlled by a virtual driver. The virtual driver will always try to follow a user defined driving path. A level of realism is added using a nominal response time lag, and a preview time. Preview time is the delay between

when the driver sees an upcoming event, such as a curve in the road, and when the vehicle must react to it.

*Brakes:* For the braking system in CarSim the input pressure (at the brake pedal) is controlled by either an open-loop control or the virtual driver. The pressure is proportioned to each brake by the master cylinder according to user-definable curves, which can be controlled independently for each wheel. Furthermore, the user can define braking torque as a function of pressure for each brake individually, allowing large amounts of flexibility in brake system control. Dynamics in the hydraulic brake fluid are modeled by a first order transient lag and a constant time delay. Both the "fluid dynamics time constant" and the "transport delay" can be defined for each brake individually. When the brakes are applied to a spinning wheel, the supplied torque causes the wheel to decelerate. This allows the braking torque to be calculated using Newtons second law. When the wheel locks up, however, the brake no longer does any work. Still, the braking torque does not go to zero, but rather supplies just enough torque to keep the wheel from spinning. These two braking situations represent two unique mathematical cases. Thus, when lockup is detected the solver will switch to a locked-up braking model. The brake system is replaced by a torsional spring and damper that winds up the wheel to resist the braking loads at the tire contact patch. The model switch occurs when the wheel reaches a rotation speed equivalent to a low user-defined forward speed, and will stay locked up until the torque in the torsional spring/damper is greater than the supplied braking torque.

*Powertrain:* CarSim uses a detailed powertrain model that includes engine torque output and fuel consumption, and detailed transmission effects. Torque and fuel consumption are both calculated as functions of engine RPM and throttle angle using user-defined tabular data. Torque is transmitted to either an automatic or a manual transmission that include the effects of the torque-converter or clutch, as well as efficiency and inertia that can be specified for each gear. Torque is transmitted to the driven wheels through the differential (final drive) ratio or alternatively, through an all-wheel drive system with user-defined front to rear torque-split. As with steering and braking, the throttle, shifting, and clutch can be controlled by the end user as open-loop functions of time. Alternatively the clutch (if applicable) and shift timing can be controlled by a shift schedule, and the throttle controlled by the virtual driver model.

*Tires:* CarSim allows the user to model tire forces using a default internal model (with or without nonlinear camber and overturning moment effects), the Pacejka 5.2 Magic Formula model, or any external model that can be programmed in C code or Simulink. The CarSim Internal Tire Model uses nonlinear tabular data of longitudinal force, lateral force, aligning moment, and overturning moment as functions of longitudinal slip, lateral slip angle, load, and camber angle. The required data represents typical quantities that are obtainable during experimental tire testing. The vertical load in the tire is found by treating the tire as a linear spring in the vertical direction, and so a stiffness coefficient must be supplied. Tire models such as the Magic Formula model represent methods of curve-fitting tire test data. Thus, it is presumed that by inputting tire test data directly into CarSim (which is designed to interpret and use it directly) the results should compare well with those found using equation based tire models.

*Aerodynamics:* Aerodynamic effects on the vehicle are included. Three forces and three moments are applied to the sprung mass at a point known as the aerodynamic reference point. Users may define the aerodynamic properties of the vehicle model by inputting six coefficients of drag (as functions of aerodynamic slip angle), vehicle reference length, location of the aerodynamic reference point, and vehicle frontal area. The user may also define the wind amplitude, wind heading, and air density for a given simulation using nonlinear tabular data, as a function of time.

**Solver Method**

The equations of motion of the CarSim vehicle system are in the form of a set of ODEs. The CarSim solver integrates the differential equations using a second-order implicit Runge-Kutta algorithm known as $RK2$. Second-order Runge-Kutta is best understood as a refinement of Euler's Method. Given the present value of the dependent variable y(t), Euler's method calculates the derivative $k_1 = dy/dt|_{t_0}$ and estimates the next value of y(t) to be $y_{t+h} = y_t + hk_1$. It is therefore considered a linear ones step method. It is simple to implement, but accuracy is low and the time step $h$ must be made very small in order to improve accuracy. Runge-Kutta integration methods sacrifice the linearity of Eulers method, but retain the one step format. Other integration methods exist which retain linearity but move into a multi-step format. With second order Runge-Kutta (RK2), a second estimate of the derivative is used to increase the accuracy. Knowing $y_t$ the derivative at the current time is found as

$k_1 = dy/dt|_t$. The derivative $k_1$ is sed to make an initial estimate for $y_{t+h}$ called $y^*_{t+h}$ and the derivative at $t+h$ is estimated using $y^*_{t+h}$ as $k_2 = dy/dt|_{t+h}$. The new value for $y$, called $y^{\bar{*}}$, is found to be $y^{\bar{*}} = y_t + h[(k_1+k_2)/2]$. Thus, the average of the two estimated derivative was used to estimate the new value of $y$. The $RK2$ method is summarized as Equation 2.30 and provides better results than the simplest form of Euler's method.

$$\begin{aligned} k_1 &= \left.\frac{dy}{dt}\right|_t^y h \\ k_2 &= \left.\frac{dy}{dt}\right|_{t+h}^{y+k_1 h} h \\ y_{t+h} &= y + \left(\frac{k_1+k_2}{2}\right) h \end{aligned} \tag{2.30}$$

Because Runge-Kutta methods are future-looking and do not rely on information from previous time-steps, it is easy to adapt the size of the time-step to increase or decrease accuracy as required. However, CarSim implements a fixed time-step in order to facilitate co-simulation abilities with external software packages, compatibility with experimentally measured tabular data, and ability to match constant step size test data. As a consequence, the solver in CarSim has no internal error-checking, and the end user must be cautious. It is recommended that simulations are carried out at several time-steps to verify the insensitivity of the model to further time-step refinement [ref].

## 2.4 Tire Models

Tires basically define the amount of forces and moments acting on a vehicle's chassis during its motion, which emphasizes the role of the utilized tire models in any study. There are numerous tire models developed so far to serve for different purposes and provides results at different accuracy levels. One can select a model depending on whether the problem in hand allows for the use of computational power required for a more theoretical model or requires faster processing that can be achieved with a more empirical model. Similarly, models have been developed to feature transient dynamics of the tire or its steady state characteristics (Table 2.1).

In this research, different models are used basically for two purposes; for estimation and control studies which provide analytical expressions to be substituted in the derivation of

Table 2.1: Classification of the common tire models used in research

| | **Steady State** | **Transient** |
|---|---|---|
| **Empirical Models** | Magic Formula, Nicholas-Comstock | SWIFT, SIMON, TM-Easy, SMAC |
| **Theoretical Models** | Dugoff, Brush, String, Burckhardt, Kiencke, Unitire | LuGre, Modified Nicholas-Comstock |

various observer dynamics, and for simulations studies where the developed control and estimation algorithms are tested.

### 2.4.1 A Modified Dugoff Tire Model for Estimation Studies

A control algorithm basically depends on the feedback of system states, which are rarely available for direct measurement. Most of the time, it requires an estimation scheme that takes in the system outputs (sensor measurements, etc.) and computes the system states for the control algorithm. This estimation scheme, similar to the control algorithm, requires a computationally lightweight but sufficiently accurate mathematical model of the system. Therefore tire models, which provide such analytical expressions, essentially provide the solution.

First model utilized in the estimation studies is the so-called Dugoff tire model. Dugoff et.al. published number of studies about the analytical modeling of tire-road interaction (circa 1970) [1, 44], which eventually yielded to this widely known model today. The model basically assumes a simplified contact patch geometry (Figure 2.7) where the line segment $0-1-2$ represents the centerline during a turning maneuver, hence the indicated slip angle ($\alpha$). Point 1 stands for the sliding boundary below which (line segment $0-1$) the tire tread is assumed to adhere to the ground perfectly. At point 1 the elastic stresses due to tread deformation ($\alpha$) starts to become saturated which yields the rubber to begin sliding relative to the ground until the stress values drop to zero at the tread liftoff point 2.

Assuming uniform pressure distribution over the contact patch (which is found to be a weak

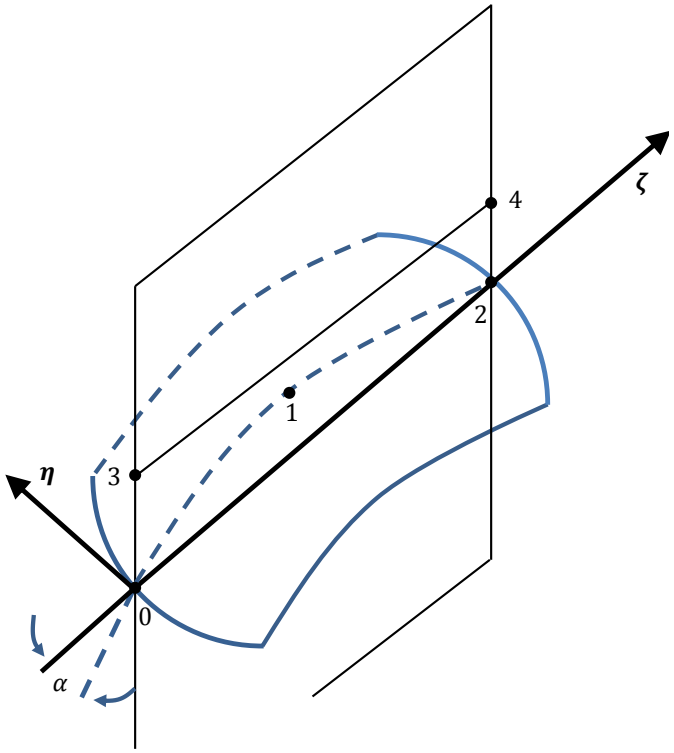


Figure 2.7: Simplified tire contact patch geometry (adopted from [1])

assumption, nevertheless yields to reasonable results), the resultant tire forces are given as a function of tire slip and surface friction as bellow:

$$F_x = C_\lambda \frac{\lambda}{1-\lambda} f(\zeta) \tag{2.31}$$

$$F_y = C_\alpha \frac{tan(\alpha)}{1-\lambda} f(\zeta) \tag{2.32}$$

where

$$\zeta = \frac{\mu F_z (1+\lambda)}{2\sqrt{(C_\lambda \lambda)^2 + (C_\alpha tan(\alpha))^2}}$$

and

$$f(\zeta) = \begin{cases} (2-\zeta)\zeta, & \text{if } \zeta < 1 \\ 1, & \text{if } \zeta \geq 1 \end{cases}$$

### 2.4.2 Tire Models Used in Simulation Studies:

As mentioned earlier the forces and moments acting on the vehicle body are generated at the tire-road contact patch. Therefore a successful simulation of the vehicle motion during a certain maneuver requires highly accurate modeling of the tire characteristics. Increasing the number of degrees-of-freedom and further parameterization might seem to be a solution at first; however such models (finite element models) require proportionally high computational power. The Brush model is an idealized representation of the tire in the tire-road contact region [38] which is assumed to be realized through a number of massless, elastic elements, the so-called bristles. Figure 2.8 depicts such a tire representation with the tire slip-angle ($\alpha$) and the forces acting on it. The base point of each bristle is attached to a circular belt, while the tip adheres to the road surface. The bristles are subjected to a level of stress due to the wheel load and surface friction which leads to their deformation. Brush model basically states that integrating these stresses on the bristles along the contact patch yields to the expressions for forces and moments generated on the tire. A major assumption is the parabolic stress distribution (as opposed to the Dugoff with uniform distribution) over the bristles. Furthermore, the tire carcass is assumed to be completely stiff neglecting the carcass deflections and the bristles are assumed to be linearly elastic disregarding the nature of the rubber characteristics.

Following the above assumptions the resulting tire forces can be given as follows. In the case of pure longitudinal slip ($\alpha = 0$), the longitudinal tire force becomes:

$$F_x = \begin{cases} C_\lambda \left(\dfrac{\lambda}{1+\lambda}\right) - \left(\dfrac{1}{3}\dfrac{{C_\lambda}^2 \left|\dfrac{\lambda}{1+\lambda}\right| \dfrac{\lambda}{1+\lambda}}{\mu F_z}\right) - \left(\dfrac{1}{27}\dfrac{{C_\lambda}^3 \left(\dfrac{\lambda}{1+\lambda}\right)^3}{(\mu F_z)^2}\right), & \text{for } |\lambda| \leq |\lambda_s| \\ \mu F_z sgn(\lambda), & \text{for } |\lambda| > |\lambda_s| \end{cases} \tag{2.33}$$

where $\lambda_s$ stands for the slip condition where the available frictional force becomes short to keep the tip of the tread element attached anymore and it phases into full slip condition. As for the case of pure side-slip ($\lambda = 0$), the lateral tire force and the aligning moment are

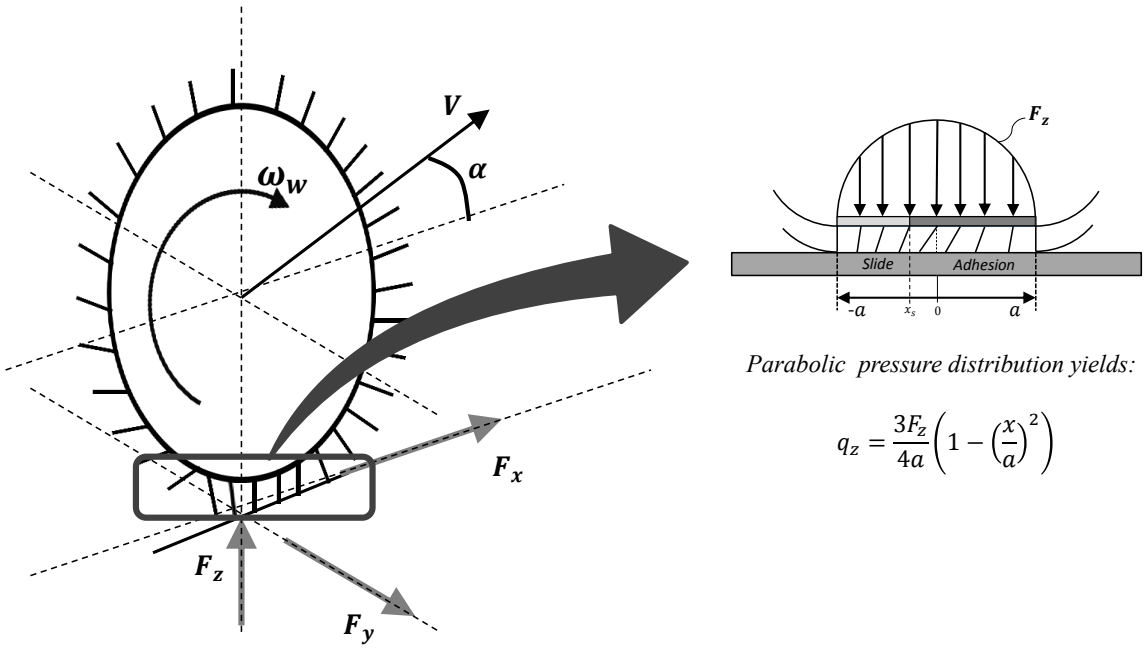


Figure 2.8: Simplified bristle geometry for the Brush tire model

defined as:

$$F_y = \begin{cases} -C_\alpha tan(\alpha) + \left(\frac{1}{3}\frac{{C_\alpha}^2|tan(\alpha)|tan(\alpha)}{\mu F_z}\right) - \left(\frac{1}{27}\frac{{C_\alpha}^3 tan^3(\alpha)}{(\mu F_z)^2}\right), & \text{for } |\alpha| \leq |\alpha_s| \\ -\mu F_z sgn(\alpha), & \text{for } |\alpha| > |\alpha_s| \end{cases} \quad (2.34)$$

$$M_z = \begin{cases} \frac{C_\alpha tan(\alpha)\alpha}{3}\left(1 - \left|\frac{C_\alpha tan(\alpha)}{3\mu F_z}\right|\right)^3, & \text{for } |\alpha| \leq |\alpha_s| \\ 0, & \text{for } |\alpha| > |\alpha_s| \end{cases} \quad (2.35)$$

where $\alpha_s$ stands for the slip-angle where, similar to the pure longitudinal case, the available frictional force becomes short to keep the tread element following a straight line anymore and a is the half of the contact patch length. Brush model is also modified for the case of a combined lateral and longitudinal slip. In that case the bristles will be deformed in a direction proportional to the magnitude of the stress levels in each direction. Nonetheless the method of computing the forces remains the same as integrating the stress expressions over the contact patch. Assuming isotropic tire properties (*e.g.* $C_\lambda = C_\alpha = C_s$) the resulting equations for longitudinal and lateral tire forces along with the aligning moment are defined

respectively as below:

$$F_x = F(\lambda, \alpha, \mu, \mu_{max}) \frac{\sigma_x}{\sqrt{\sigma_x^2 + \sigma_y^2}} \tag{2.36}$$

$$F_y = F(\lambda, \alpha, \mu, \mu_{max}) \frac{\sigma_y}{\sqrt{\sigma_x^2 + \sigma_y^2}} \tag{2.37}$$

$$M_z = \frac{2\alpha \left(1 - \left|\frac{C_s\sqrt{\sigma_x^2 + \sigma_y^2}}{3\mu F_z}\right|\right)^3}{\left|\frac{C_s\sqrt{\sigma_x^2 + \sigma_y^2}}{3\mu F_z}\right|^2 - 3\left|\frac{C_s\sqrt{\sigma_x^2 + \sigma_y^2}}{3\mu F_z}\right| + 3} \tag{2.38}$$

where

$$F(\lambda, \alpha, \mu, \mu_{max}) = \begin{cases} \mu F_z \left(1 - \left(\frac{C_s\sqrt{\sigma_x^2 + \sigma_y^2}}{3\mu F_z}\right)^3\right), & \text{for } \left|\sqrt{\sigma_x^2 + \sigma_y^2}\right| \leq \left|\frac{3\mu F_z}{C_s}\right| \\ \mu F_z sgn(\alpha), & \text{for } \left|\sqrt{\sigma_x^2 + \sigma_y^2}\right| > \left|\frac{3\mu F_z}{C_s}\right| \end{cases}$$

and

$$\sigma_x = \frac{\lambda}{\lambda + 1}, \qquad \sigma_y = \frac{tan(\alpha)}{\lambda + 1}$$

Another practical solution has come out to be as developing relatively lightweight analytical expressions with constants that are to be found empirically. A very well-known such model is the so-called Magic Formula (MF) developed by Hans Pacejka [45], which is also implemented in the simulation studies carried out for this research. The MF basically defines the lateral and longitudinal tire forces in addition to the tire aligning moment as follows:

$$F_x = D_x sin\left(C_\lambda arctan\left(B_x\lambda - E_x(B_x\lambda - arctan(B_x\lambda))\right)\right) S_{vx} \tag{2.39}$$

$$F_y = D_y sin\left(C_\alpha arctan\left(B_y\alpha - E_y(B_y\alpha - arctan(B_y\alpha))\right)\right) S_{vy} \tag{2.40}$$

$$M_z = D_t sin\left(C_t arctan\left(B_t\alpha - E_t(B_t\alpha - arctan(B_t\alpha))\right)\right) S_{vt} \tag{2.41}$$

where $B$ represents the effect of the tire stiffness, $C$ defines the shape of the trigonotmetric sine function, $D$ stands for the peak values as the sine function can take maximum value of unity, $E$ is known as the curvature factor which helps with better defining any possible local deformations, and the final terms $S_{vy}$, $S_{vx}$ and $S_{vt}$ represent the amount of the resulting force and moment curve's shift from the origin as the tire might behave differently during

braking and acceleration even under the same conditions. On a side note, $C_t$ represents the torsional stiffness of the tire. These parameters can be obtained by testing the tire under the conditions to be simulated.

The tire models described above characterize the tire at its steady-state, in other words they ignore any variations with respect to time, which largely holds true under constant surface friction conditions. However, if the surface friction is varying considerably during the maneuver, the transient dynamics might become effective enough to invalidate the steady-state assumptions. A collaboration between the Lund and Grenoble universities yielded to the development of a new tire model, named as LuGre model after the names of the collaborating institutes, to account for the tire's transient dynamics. Based on a similar simplified tire representation using bristles as in the Brush model, the LuGre model accounts for the variations of the bristle deflections with respect to both time and position, hence allowing to simulate transient behavior. A lumped and distributed model is developed first as a proof of concept and for computational convenience. Next a more complex distributed model is developed which, as opposed to the point contact assumption in the lumped model, assumes a contact area on which different pressure distribution schemes can be applied depending on the type of application. In this study an average lumped model is utilized which offers similar results to a detailed distributed model by keeping the number of states that describes the friction minimum. This is accomplished by defining a mean friction state as shown below:

$$\dot{\bar{z}} = v_r - \left( \frac{\sigma_0 |v_r|}{g(v_r)} + \kappa \omega_w \right) \bar{z} \tag{2.42}$$

where

$$g(v_r) = \left( \mu_c + (\mu_s - \mu_c) e^{-\left| \frac{v_r}{v_s} \right|^{\alpha}} \right) \mu_{max}$$

and $\mu_c$ represents the normalized Coulomb friction, $\mu_s$ is the normalized static friction, $\mu_{max}$ is the maximum road surface friction, $v_s$ is the Stribeck relative velocity details about which is provided in [**?**] and is omitted here as it is out of the scope of this research and $v_r$ is the relative velocity of wheels to the vehicle chassis ($v_r = R\omega_w - v$). The term $\kappa$ stands for the pressure distribution effect which in this study is taken as a constant by assuming a uniform distribution scheme. Using these equations the resulting tire force is expressed as:

$$F(t) = (\sigma_0 \bar{z}(t) + \sigma_1 \dot{\bar{z}} + \sigma_2 v_r) F_z \tag{2.43}$$

where $\sigma_0$, $\sigma_1$ and $\sigma_2$ are constants that represent rubber longitudinal stiffness, rubber longitudinal damping and viscous relative damping respectively.

# Chapter 3

# Adaptive Vehicle Stability Control

## 3.1 Introduction

Stability control systems have drawn great interest since their introduction in the late 1980s [46, 47]. They have evolved dramatically especially over the past decade thanks to the rapid advancements in the computational power of the on-board electronics. The principle idea of a stability control system is to assist the driver during a severe steering maneuver and prevent any possible spin or drift out, sometimes even by intervening the driver commands (Figure 3.1a). Three major methods have been proposed so far for these systems to interact with the vehicle dynamics: differential braking, active steering and active torque distribution (Figure 3.1b). In addition to these, active suspensions are becoming available with the emerging technology which is used in a number of integrated control schemes.

Systems which use differential braking utilize the on board anti-lock braking system (ABS) and apply the individual wheel brakes according to a known strategy to generate a correcting yaw moment on the vehicle body. Their performance heavily relies on the performance of the onboard ABS. Active steering systems allow the stability controller to intervene with the driver's steer command and implement any correction when necessary. A well-studied active steering system is steer-by-wire. It is adapted from the aeronautic term fly-by-wire which basically refers to the idea of replacing the manual control mechanisms with electronic (wired) based equivalents. However steer-by-wire systems are not considered for commercial applications yet, mostly due to concerns about reliability and capital costs. As a result,

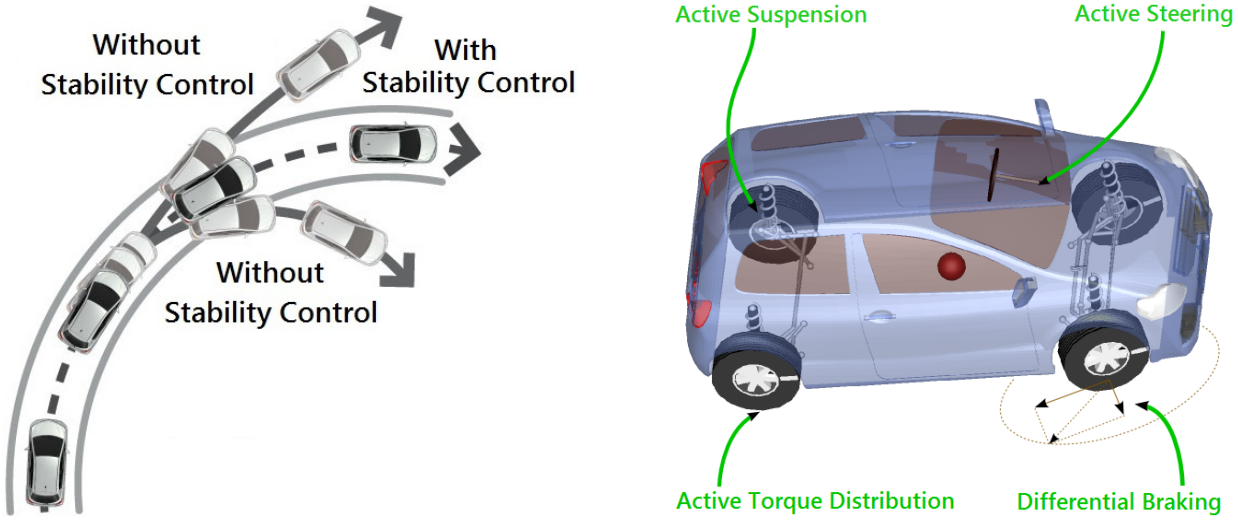


(a) Role of stability control (b) Conventional stability control systems

Figure 3.1: The functioning of stability control systems

mechanical based active front steering systems have recently been introduced into the market. Active torque distribution is another popular method for stability control. It makes use of an advanced differential mechanism in the driveline to distribute the engine torque onto the wheels in a way that it can control the resulting yaw moment on the vehicle body. As summarized in Chapter 1, the effectiveness of such stability control systems has allowed them to become almost ubiquitous in modern vehicles. They have already become a requirement and almost standardized by many countries. This naturally triggers further research on the subject to further push their performance and to find new avenues for improved safety.

## 3.2 Literature Review

The earliest introduction of a commercial stability control system was done by Mercedes-Benz and Robert Bosch GmbH where they introduced the Electronic Stability Program (ESP®). Since then a considerable number of studies have been done on various control schemes based on the three aforementioned systems as well as on their combinations. These studies can be grouped into a fewer number of titles which would form the mainstreams in the subject. One of these mainstreams is about utilizing individual control systems to their utmost possible performance and mostly refers to the initial studies. Among these

individual systems, differential braking based ones (e.g. ESP) attracted more attention due to the widely used ABSs on board. A number of commercial systems followed ESP, such as BMW's Dynamic Stability Control (DSC) [48], GMs Stabilitrak [49] or Active Handling System [50] and Toyotas Vehicle Stability Control (VSC) system [51], all based on active braking of individual wheels. On the other hand, valuable academic studies lead the way to the improvement of these commercialized systems. In [52], Pilutti et.al. investigated three different control designs based on a linearized two degree-of-freedom vehicle model integrated with brake dynamics and the authors concluded that saturation of the brake actuators play a cardinal role in the effectiveness of the active braking based stability controllers. Another important study was done by Ghoneim et.al. [53] where they studied the performance of two controllers, a yaw-rate feedback system and a full-state (yaw-rate and sideslip) feedback system. The authors developed a Luenberger observer to be able to obtain sideslip information and concluded that the additional information from the observer improved the controller performance; however it is also critical to accurately estimate the variable which might easily introduce abrupt errors into the system. A similar work is done by Fukada [54] where he investigates combining an observer based method with numerical integration to find chassis sideslip while dealing with tire nonlinearities and disturbances such as road slant. Nishio et.al. [55] follow the same path and reports the results of an application of the estimator on a differential braking based control system. A more recent study by Baffet et.al. [56] employs an extended Kalman filter and estimates lateral tire forces and friction in addition to chassis sideslip.

Active steering based controllers have drawn great interest from academia until recently commercial systems were released into the market which still do not use complete steer-by-wire technology. The essential contribution in this area is done by Ackerman [57, 58, 59, 60]. In these studies Ackerman principally analyzed decoupling of yaw rate which defines the rotational dynamics of the vehicle body from lateral acceleration which is directly related to the slip of the vehicle body in lateral direction. As a result, the control designs were not affected by the lateral disturbances such as side-winds or road slants. In [61] Isermann introduced a development methodology for a fault-tolerant steer-by-wire system and used a brake-by-wire application as a proof of concept. Mammar et.al. [62] and You et.al. [63] took this one step further and analyzed H control schemes for active steering based stability control systems. Another noteworthy study was done by Hsu and Gerdes in [64] where, different from the other studies, they investigated a steer-by-wire vehicle at the limits of

handling and proposed a control algorithm using feedback linearization.

The third general method in stability control is active drive torque distribution which is based on distributing the engine torque on the right and left side wheels (rather than front and rear as in the traction control systems) to generate a yaw moment on the chassis which would eventually stabilize the vehicle when needed. A major advantage of these systems is that they do not reduce vehicle's acceleration as opposed to the active braking based systems. An introductory investigation was done by Ikushima and Sawase [65] which reported the results of a torque distribution based yaw-feedback control application on an actual vehicle. Huchtkoetter and Gassmann [66] studied an advanced differential mechanism that would aid in various commercialized control algorithms. Similarly Osborn and Shim [67] study the application of an advanced differential mechanism which would allow individual wheel torque control together with a PI stability control scheme and report significant improvement. Finally, recent studies focus more on advanced control schemes such as [68] where the authors employ internal mode control for robustness.

Another mainstream in the subject deals with the coordination of the individual control systems from an upper level controller point of view. These decentralized systems have been developed under different names such as Integrated Chassis Control (ICC), Global Chassis Control (GCC) or Unified Chassis Control (UCC). Trachtler [69] details such a system, so called Vehicle Dynamics Management (VDM), which suggests an upper-level control strategy based on the yaw-rate feedback to handle the active braking, steering and suspension systems. Another analysis is done by Hac and Bodie [70] where the authors investigate the stability problem on a simplified vehicle model, the stability effects of small perturbations in the tire-forces characteristics and of chassis control subsystems (lower lever controllers), and eventually the performance of an upper level controller (UCC) that integrates an active brake and an active suspension system. Similar studies investigating the integration of active braking and suspension systems are also done by Smakman [71, 72], and by Duda and Berkner [73] where the authors focused more on reducing the activation of the braking system to increase the ride comfort together with stability. In [74] and [75] Hwang et.al. investigate the performance of an integrated active steering and active braking system. The authors study two methods for integration, a supervisory algorithm which controls individual systems and a so-called unified algorithm which requires combining the physical control units onboard and they report very close performance results for both algorithms. Also in [76]

and [77] Nagai et.al. analyze integrating an active braking system based on model matching control method with active rear and front steering systems respectively. Selby et.al. in [78] report the improvements that can be achieved by coordinating active steering with differential braking. A common conclusion of these studies states that despite the improvements in the system performance one needs to be careful about the saturation regions of the individual controllers as the braking system might run the tires into saturation while the active steering system still tries to stabilize the vehicle. A good analysis of these saturation regions is done by He et.al. in [79] at the end of which the authors propose a metric to determine the vehicle operating ranges and thereby the desired individual control system to employ. Active steering and active suspension combination has drawn less interest than the other two among research groups. An investigation of such an integration is done by March and Shim in [80] where the authors focus on the handling ability of the system. Chen et.al. in [81] study the system from a broader point of view and report improvements for ride comfort as well as handling.

The integrated control schemes have an indisputable improvement over the individual controllers. Nevertheless adopting a decentralized integration methodology introduces additional complications such as saturation of one system disregarding the other(s) or integrating a system that has indirect effect on stability (eg. suspension system). A solution to these issues is found by deriving a centralized control algorithm that can command on multiple controllers in a unified fashion. Due to its top-down design strategy, a centralized control structure can be developed more comprehensively by taking all systems into account and thus it is expected to provide better performance. The last mainstream to be discussed in this study considers such stand-alone systems. An early investigation is done by Matsumato and Tomizuka in [82] where the authors develop an optimal control law using linear quadratic regulator (LQR) theory and report performance variations by switching between front and rear wheel steering and traction control. Similar studies followed again using optimal control techniques [83, 84] or robust control techniques such as $H_{\text{inf}}$ analysis [85] or $\mu$-synthesis [86]. An interesting subtitle under this mainstream is the multilayer structures. The systems developed using such structure implements the control law which is still derived using unified approach through a lower level loop-control design. Although such a strategy reminds the decentralized controllers, a major difference between them is that the lower level loop-control in this method that implements the upper-level control law is developed considering the coupled dynamics of the actuators unlike the decentralized systems which commands the

individual lower level controllers separately. Optimal control is the most popular technique for lower level loop-control design. Good examples of such systems are given by Mokhiamar and Abe in [87] where a sliding mode control (SMC) is proposed for upper level control, by Hattori et.al. in [88] or by Shen et.al. in [89, 90, 91, 92] where again SMC strategy is adopted for upper level control.

## 3.3 Motivation

A common need in the vehicle stability algorithms summarized above is to obtain information about system states (e.g. lateral velocity, chassis side-slip) or axle forces, which are not directly available from sensors on board a vehicle due to cost associated with them. Therefore observer schemes are required to estimate these values which are in general based on chassis kinematics and linear approximations to tire force and moment properties. Nevertheless, due to the nonlinearities in tire characteristics and intrinsic deviations in estimation schemes (such as integral errors, or deviations due to simplifications in system dynamics), the resulting estimates might become overwhelmed with cumulating inaccuracies which yields the control signals to deteriorate. Figure 3.3 shows results of an example simulation study designed for lateral velocity estimation scheme. Given the double lane change maneuver in Fig. 3.3a, a D-class sedan vehicle model is simulated using CarSim® software to obtain vehicle dynamics parameters. Based on the bicycle vehicle mode summarized in Chapter 2, multiple observers (Direct, Luenberger, Kalman) are designed and implemented to have a better judgment on possible performance variations.

The results indicate that other than the direct estimation method which is taken as a reference model and is actually not real-time implementable [93], the common observers yield to significant overshoots especially around the turn points during the given maneuver where the vehicle approaches neutral steer characteristics. Similar issues develop in the estimation of other vehicle states as well, such as vehicle side-slip or lateral axle forces. Various solutions have been proposed to address this problem, mostly by integrating additional sensor inputs into the estimation scheme such as inputs from inertial navigation system (INS) and/or global positioning system (GPS) [94, 95], or inputs from optical sensors [96]. Nevertheless these solutions come with costly sensor units and high computational power requirements; and moreover they still employ indirect methods to estimate the parameters of interest.

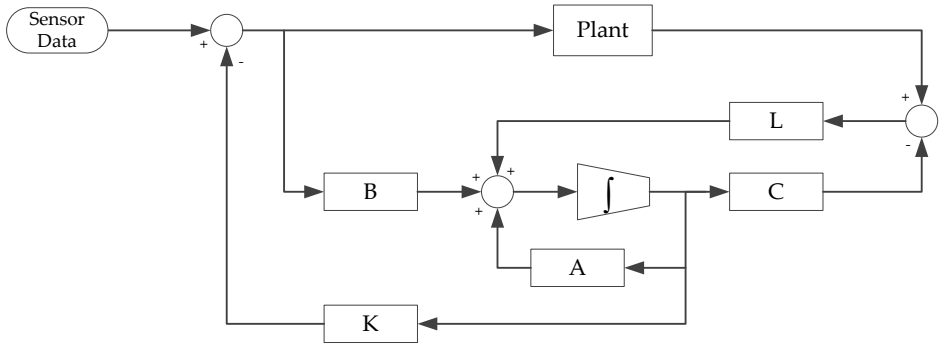


(a) Block diagram expression for Luenberger observer

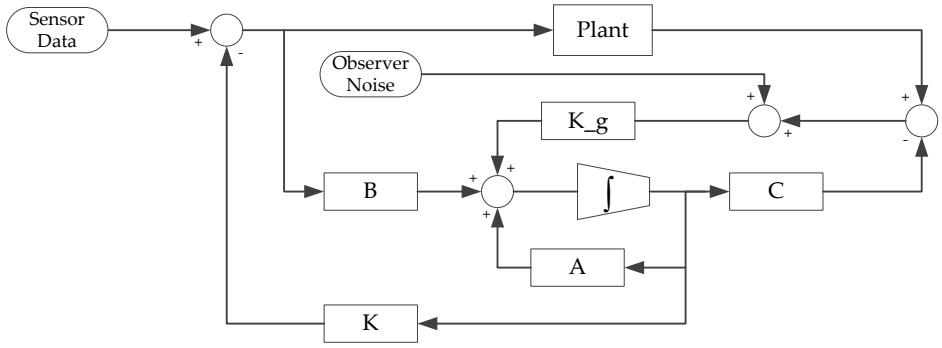


(b) Block diagram expression for Kalman filter

Figure 3.2: Observer designs for lateral velocity estimation

This study proposes the use of a sensor fusion approach which integrates a smart tire system with a model based observer to obtain information about tire slip-angle variations. The smart tire system provides information about tire slip-angle by directly monitoring tire-road contact which alleviates possible intrinsic estimation errors of the model based observer. In what follows an adaptive stability control algorithm is developed based on the tire slip-angles. Using the tire slip-angle as the parameter of interest provides two major advantages. One is that the strong correlation between tire slip angle and vehicle drive characteristics as summarized in Chapter 2 is utilized. The typical stability controllers are generally based on a yaw-rate feedback which might retard the controller performance due to the intrinsic time lag in the generation of yaw motion on the vehicle chassis. This could be better explained by analyzing the transients of the system states during a lateral maneuver. Figure 3.4 shows the results of the tire slip-angle response and chassis yaw-rate for a sinusoidal steering input. The results depict a noticeable lag between the two responses. This phenomenon can be explained by looking into the dynamics of lateral force at the tire-road contact patch. As

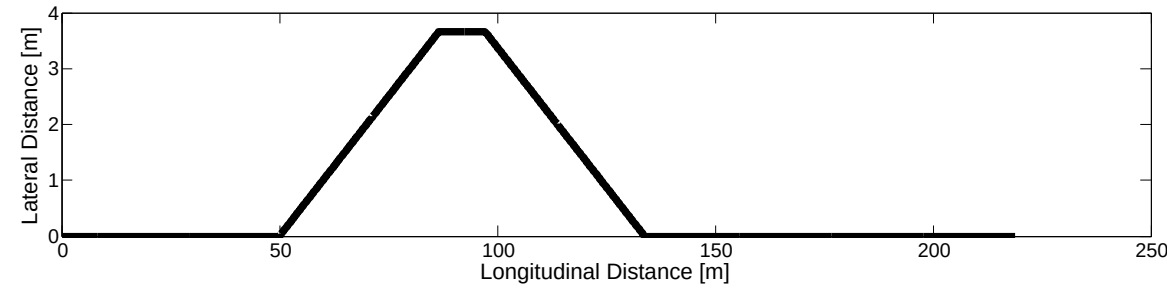


(a) DLC Maneuver

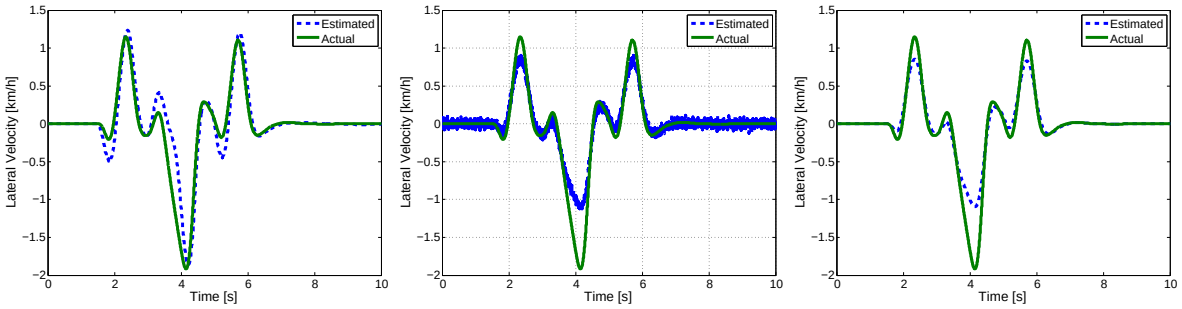


(b) Direct estimation results (c) Kalman estimation results (d) Luenberger estimation results

Figure 3.3: Observer designs for lateral velocity estimation

summarized in [97] the tire slip-angle is initiated by the generation of the lateral tire force after a given steering input, which is then followed by the generation of chassis side-slip and yaw motions on the vehicle chassis. The other advantage is the presence of tire slip-angles in the linearized vehicle lateral dynamics model that gives way to manipulate this model to present the tire slip-angles as its states in the development of the control laws which is directly based on the stability characteristics of a vehicle.

The proposed control algorithm follows the steps of the latter mainstream by integrating Active Front Steering (AFS) and Direct Yaw Control (DYC) schemes. The smart tire system provides successful dynamic tire slip-angle information in the linear region of tire force curve and the model based observer meets the default by estimating the tire slip-angle in the nonlinear region when necessary. With the addition of vehicle yaw rate and steering wheel angle signals from chassis based sensors, the control algorithm computes corrective steering and yaw moment values which are to be implemented through AFS and DYC units. To compute these inputs, Lyapunov's direct stability method is followed which carries out an adaptation law along the way. As a result the control system becomes more robust against variations in driving conditions such as surface friction. The steering input is implemented

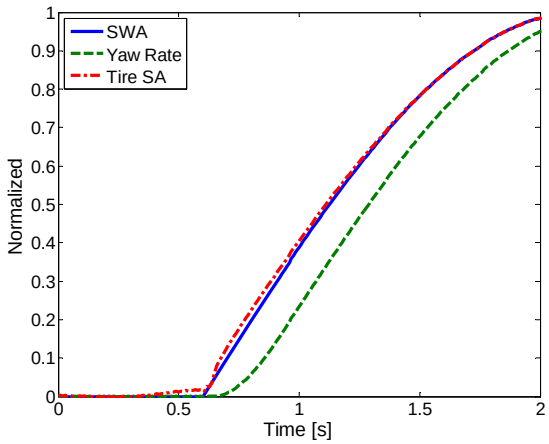


Figure 3.4: Comparison of vehicle state response time

as an auxiliary input to the drivers whereas for the DYC command a lower level optimal force distribution algorithm is developed. Based on the corrective yaw moment, this lower level control algorithm optimizes the wheel brakes forces to be implemented by utilizing current tire force information from the developed model based observer. The rest of this chapter goes into the details of the proposed algorithms for these tasks. Section 3.4 explains the sensor fusion approach with smart tire based tire slip-angle estimation method and the model based observer scheme. Sections 3.5 and 3.6 summarize the derivation of the control laws as well as the results from the simulations carried out. The chapter is concluded by discussing the results and benefits of the proposed systems.

## 3.4 Tire Slip-Angle Estimation

The sensor fusion approach followed for tire slip-angle estimation integrates the smart tire system with a model based observer scheme that uses a Sliding Mode Observer (SMO) to estimate tire forces and a Luenberger Observer to obtain tire slip-angles.

### 3.4.1 Smart Tire based Estimation

This section presents an implementation strategy for the dynamic estimation of the tire-slip angle using the developed smart tire system prototype. The algorithm development for the

smart tire system starts by logging and analyzing data from the system under different test conditions. The analyses aim to find the synthetic parameters that are the most sensitive to the variations in tire slip-angle values. Through extensive parametric studies, a strong interdependence appeared between the magnitude of the lateral acceleration signal in time domain and the tire slip-angle variations. The magnitude of the lateral acceleration signal was characterized by estimating the signal power (absolute amplitude of the signal) on a per revolution basis as depicted in Figure 3.5a. Another key parameter is identified as the tire loading condition which basically defines the proportion between the signal power and the rate of change of variation in the slip-angle values. The tire load information can also be obtained from the smart tire system using the radial acceleration signals. Similar to the tire slip-angle, the radial signals are correlated to the instantaneous vertical load by computing the signal power which strongly correlates to the applied vertical load. Figure 3.5b indicates the variation in radial signal power under different load conditions and the distinct boundaries demarcating the change in the instantaneous load.

Considering these two synthetic parameters, a line fitting algorithm is employed to estimate the tire slip angles. The proposed method provides successful estimate of tire-slip angles in the linear range of operation. Figure 3.6 shows the results of a sample application using smart tire signals during a steer sweep motion. Despite this limitation the smart tire method provides sufficient information for the proposed control algorithm because the algorithm, as in most other controllers based on linearized mathematical models, aims to maintain the system trajectory in the linear region. Nevertheless, to ensure robust performance and guarantee system convergence even during the vehicle maneuvers which show highly nonlinear tire characteristics, a sensor fusion approach, combining the smart tire system with a model based observer is used. The model based estimation methodology uses a tire force estimator in conjunction with a Luenberger observer to make dynamics estimates of the tire slip-angle. Details regarding the methodology adopted to estimate the tire slip angle using an observer based approach are presented in the following section.

### 3.4.2 Model based Observer Derivation

The proposed observer scheme makes use of lateral and longitudinal force information obtained from SMO using a random walk model and utilizes a Luenberger observer to output the tire slip-angle. As their dynamics differ, the derivations for longitudinal and lateral force

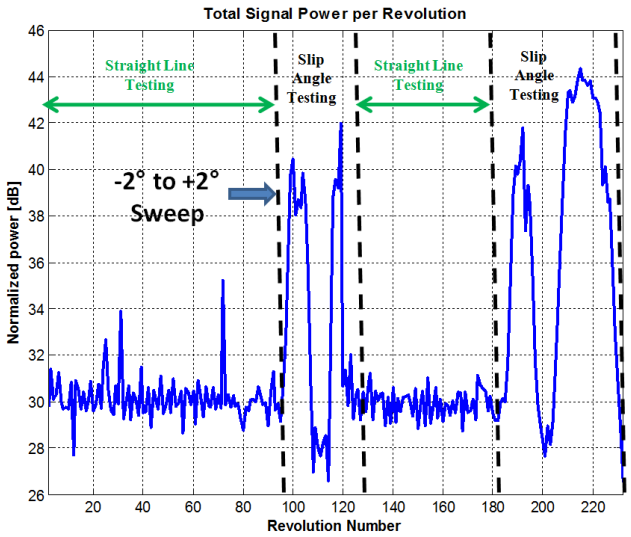


(a) Lateral acceleration signal vs. slip-angle variations

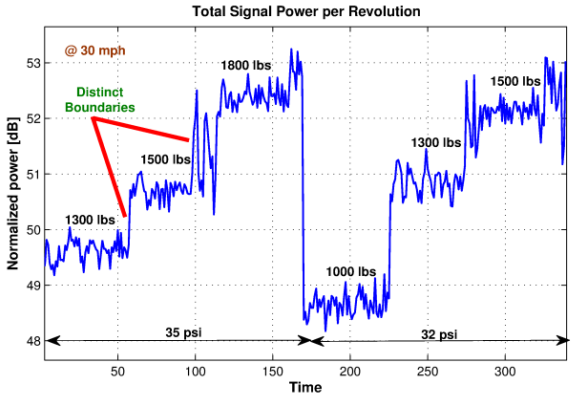


(b) Radial acceleration signal vs. wheel load variations

Figure 3.5: Variation in the instantaneous amplitude of the lateral and radial acceleration signal power regarding slip angle and wheel load

estimation are considered in separate subsections.

### Longitudinal Force Estimation

The first approach to estimate the tire longitudinal force is based on a simplified wheel dynamics model. The dynamic equation for the angular motion of the wheel is given as:

$$J_w \dot{\omega}_i = T_{w_i} - T_{b_i} - F_{x_i} R_{w_i} - F_{rr_i} R_{w_i} \tag{3.1}$$

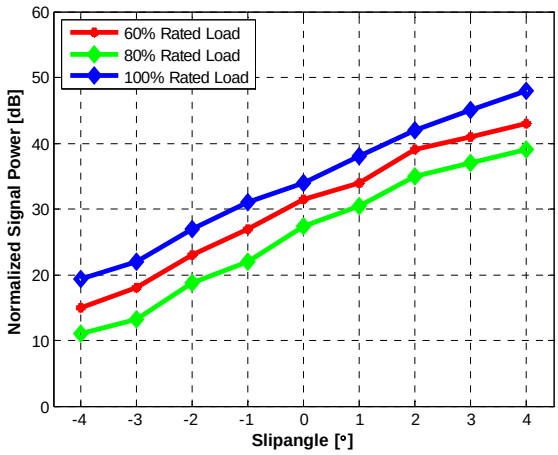


Figure 3.6: Variation in instantaneous amplitude of the lateral acceleration signal as function of the tire-slip angle under different loading conditions

where the subscript $i = fl, fr, rl, rr$ is used to separately represent the four wheels of the vehicle. $T_{w_i}$, $T_{b_i}$, $R_{w_i}$, $F_{rr_i}$ and $F_{x_i}$ represent the drive and brake torque delivered to each specific wheel, the effective radius of the tire, the rolling resistance force and the longitudinal tire force of that specific wheel respectively. Rearranging equation 3.1 yields an expression for the longitudinal force as:

$$F_{x_i} = \frac{T_{w_i} - T_{b_i} - J_w \dot{\omega}_i}{R_{w_i}} - F_{rr_i} \tag{3.2}$$

where the wheel drive torque $T_{w_i}$ can be estimated using the engine torque, the engine angular velocity, and the wheel angular velocity [98]. It is assumed that the brake pressure of each wheel is an available signal. Therefore, the brake torque $T_{b_i}$ can be computed by the brake gain ($K_{b_f}$, $K_{b_r}$). The wheel rolling resistance force, $F_{rr_i}$, is given by the expression:

$$F_{rr_i} = 0.005 + 3.24 \cdot 10^{-2} (R_{w_i} \omega_i)^2 \tag{3.3}$$

Even though equation 3.2 presents a relatively simple (open-loop) method to estimate the longitudinal tire force, it is not advisable to use this approach, since in realworld conditions, finding the time derivative of angular wheel speed signals ($\dot{\omega}_i$) can pose some challenges. To avoid the need of taking derivatives, a sliding mode observer (SMO) based estimation scheme is proposed. Using the sliding mode structure, the state estimates ($\hat{\omega}_i$) evolve according to the wheel dynamics model in eq. 3.1, the force model, $\dot{F}_{x_i} = 0$ (i.e. tire forces modeled as a

random walk model) and the sign of the measurement estimation error (difference between actual $\omega_i$ and estimated $\hat{\omega}_i$ angular wheel speed) as:

$$J_w\dot{\hat{\omega}}_i = (T_{w_i} - T_{b_i}) - \hat{F}_{x_i}R_{w_i} - F_{rr_i}R_{w_i} + k_1 sgn(\omega_i - \hat{\omega}_i) \tag{3.4}$$

$$\dot{\hat{F}}_{x_i} = k_2 sgn(\omega_i - \hat{\omega}_i) \tag{3.5}$$

where $k_1$ and $k_2$ are the observer gains and sgn(.) denotes signum function. The results (Figure 3.7) show that the estimated longitudinal force using the proposed observer formulated using equations 3.4 and 3.5 ensures stable estimation of the tire longitudinal force.

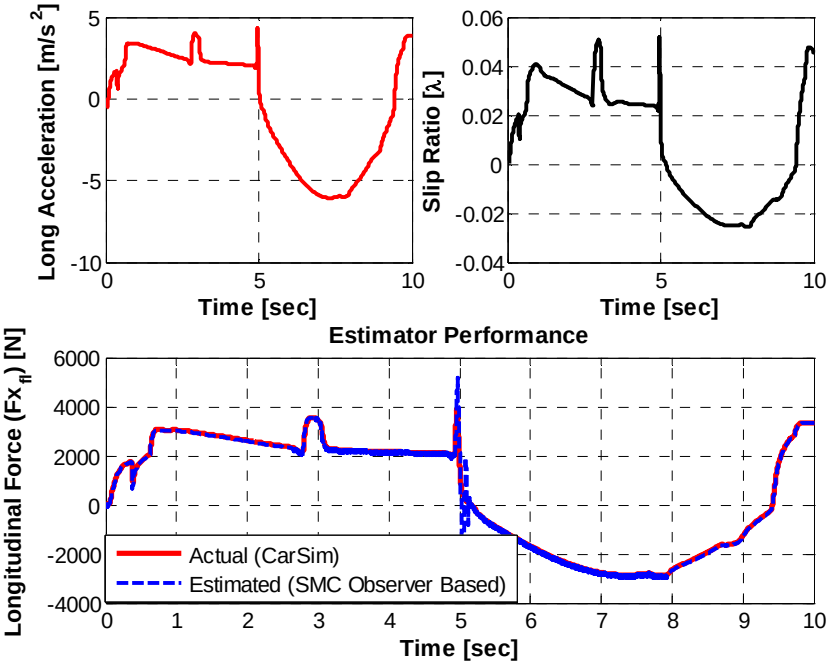


Figure 3.7: Results for the proposed SMO scheme for longitudinal tire force estimation

**Lateral Force Estimator:**

The same SMO structure is utilized for lateral forces as well. A four wheel vehicle model is considered to derive the vehicle rigid body dynamics:

$$\dot{u} = \frac{F_{x_{fl}} + F_{x_{fr}} + F_{x_{rl}} + F_{x_{rr}}}{m} + rv \tag{3.6}$$

$$\dot{v} = \frac{F_{y_{front}} + F_{y_{rear}}}{m} - ru \tag{3.7}$$

$$\dot{r} = \frac{\left(F_{x_{fr}} + F_{x_{rr}}\right)(t_r/2) - \left(F_{x_{fl}} + F_{x_{rl}}\right)(t_r/2)}{I_z} + \frac{l_f F_{y_{front}} - l_r F_{y_{rear}}}{I_z} \tag{3.8}$$

The tire lateral forces are modeled as the sum of on the sides of the chassis for front and rear axles ($F_{y_{front}}$, $F_{y_{rear}}$) and again with a random walk model:

$$\begin{aligned} \dot{F}_{y_{front}} &= 0 \\ \dot{F}_{y_{rear}} &= 0 \end{aligned} \tag{3.9}$$

The vehicle dynamics are described by the following state and measurement equations:

$$\begin{aligned} X &= [x_1, x_2, x_3] = [F_{y_{front}}, F_{y_{rear}}, r] \\ Y &= [y_1, y_2] = [a_y, r] \end{aligned} \tag{3.10}$$

Vectors $\hat{X}$ and $\hat{Y}$ represent the state estimations and the measurement estimations where the measurements are modeled as:

$$\hat{y}_1 = \frac{\hat{x}_1 + \hat{x}_2}{m}, \qquad \hat{y}_2 = \hat{x}_2 \tag{3.11}$$

where m is the vehicle mass. The estimation errors for states and measurements are denoted respectively as:

$$\begin{aligned} e_x &= [x_1 - \hat{x}_1, x_2 - \hat{x}_2, x_3 - \hat{x}_3] \\ e_y &= [y_1 - \hat{y}_1, y_2 - \hat{y}_2] \end{aligned} \tag{3.12}$$

Finally the resulting state estimates evolve according to the four-wheel vehicle model given in eq.3.6-3.8, to the random walk force model given in eq. 3.9 and the sign of the measurement

estimation errors, which can be written in open form as:

$$\begin{aligned}
\dot{\hat{x}}_1 &= k_{11} sgn(e_{y_1}) + k_{12} sgn(e_{y_2}) \\
\dot{\hat{x}}_2 &= k_{21} sgn(e_{y_1}) + k_{22} sgn(e_{y_2}) \\
\dot{\hat{x}}_3 &= \frac{1}{I_z}\left(\frac{t_r}{2}\left(\left(F_{x_{fr}} + F_{x_{rr}}\right) - \left(F_{x_{fl}} + F_{x_{rl}}\right)\right)\right) + l_f \hat{x}_2 - l_r \hat{x}_1 + k_{31} sgn(e_{y_2})
\end{aligned} \tag{3.13}$$

where $k_{11}$, $k_{12}$, $k_{21}$, $k_{22}$, $k_{31}$ are the observer gains. $F_{x_{ij}}$ is the longitudinal force estimate for the individual wheels obtained using the estimation scheme proposed above. A complete study for the convergence of the SMO is presented in [99]. The performance of the observer was evaluated for a sweep steering input which can run the tire forces into the saturation region. Figure 3.8 indicates that the observer can cope with the given extreme maneuver and provide robust estimates of the lateral force values.

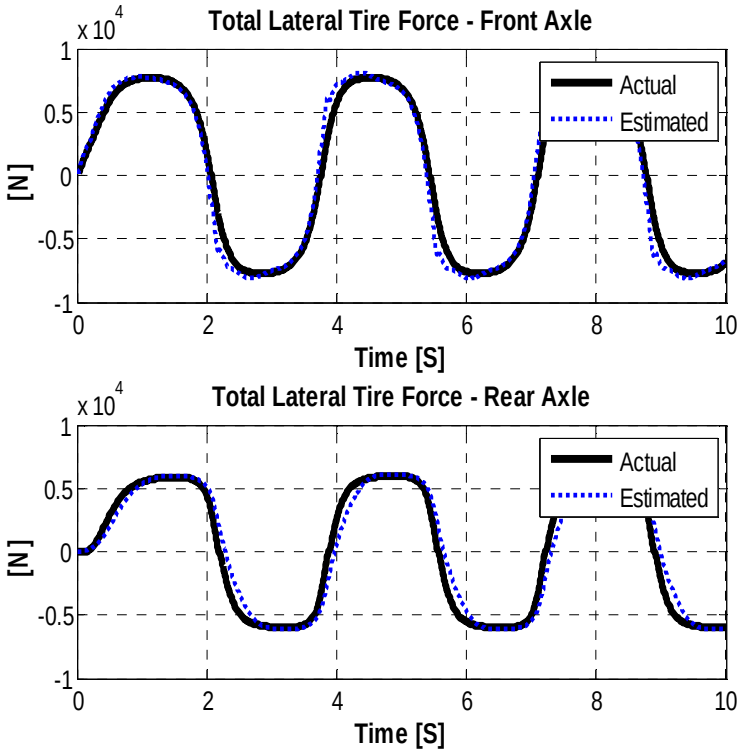


Figure 3.8: Results for the proposed SMO scheme for lateral tire force estimation

**Luenberger Observer**

To finally estimate the tire slip angle, an update equation for the front slip angle is derived as a function of the tire forces. Using the kinematic relation for front and rear slip angles (eq. 2.11 and 2.12) the update equation for the front slip angle can be derived by taking their time derivatives.

$$\dot{\alpha}_f = \dot{\delta} - \frac{\dot{v} + l_f \dot{r}}{u} \tag{3.14}$$

$$\dot{\alpha}_r = \frac{l_r \dot{r} - \dot{v}}{u} \tag{3.15}$$

Substituting expression for $v_y$ and $r$ from equations (3.7) and (3.8) respectively into equation (3.14) yields:

$$\begin{aligned} \dot{\alpha}_f = {} & \dot{\delta} + r - \left(\frac{1}{mu} + \frac{l_f^2}{I_z u}\right)(F_{y_{fl}} + F_{y_{fr}}) - \left(\frac{1}{mu} - \frac{l_f l_r}{I_z u}\right)(F_{y_{rl}} + F_{y_{rr}}) \\ & - \frac{t_r l_f}{2 I_z u}\left\{(F_{x_{fr}} + F_{x_{rr}}) - (F_{x_{fl}} + F_{x_{rl}})\right\} \end{aligned} \tag{3.16}$$

Thus the following equation is integrated to update $\alpha_f$:

$$\begin{aligned} \dot{\hat{\alpha}}_f = {} & \dot{\delta} + r - \left(\frac{1}{mu} + \frac{l_f^2}{I_z u}\right)(F_{y_{fl}} + F_{y_{fr}}) - \left(\frac{1}{mu} - \frac{l_f l_r}{I_z u}\right)(F_{y_{rl}} + F_{y_{rr}}) \\ & - \frac{t_r l_f}{2 I_z u}\left\{(F_{x_{fr}} + F_{x_{rr}}) - (F_{x_{fl}} + F_{x_{rl}})\right\} \\ & + k(m a_y - F_{y_{fl}} - F_{y_{fr}} - F_{y_{rl}} - F_{y_{rr}}) \end{aligned} \tag{3.17}$$

where $k$ is the observer feedback gain and $a_y$ is the measured lateral acceleration. The update law for the rear tire slip-angle $\alpha_r$ is obtained using the same approach:

$$\begin{aligned} \dot{\hat{\alpha}}_r = {} & \left(\frac{l_f l_r}{I_z u} - \frac{1}{mu}\right)(F_{y_{fl}} + F_{y_{fr}}) - \left(\frac{l_r^2}{I_z u} - \frac{1}{mu}\right)(F_{y_{rl}} + F_{y_{rr}}) \\ & - \frac{t_r l_f}{2 I_z u}\left\{(F_{x_{fr}} + F_{x_{rr}}) - (F_{x_{fl}} + F_{x_{rl}})\right\} - r \end{aligned} \tag{3.18}$$

Using equations (3.18) and (3.18) tire slip-angle values are successfully estimated provided that the tire forces are made available. Figure (3.9) shows the performance of the algorithm under double lane change and fishhook maneuvers.

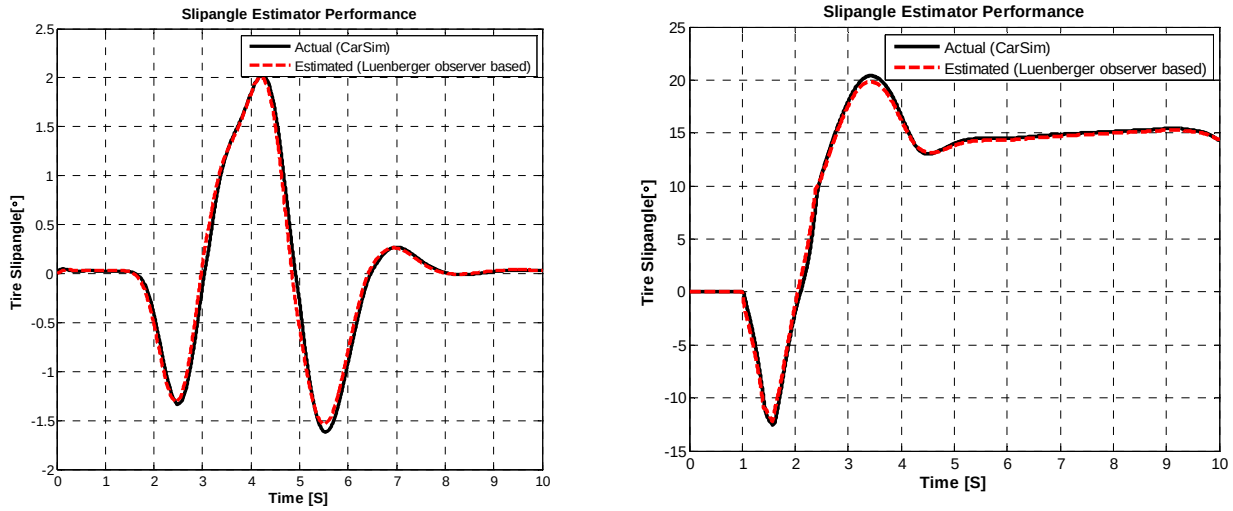


(a) Double lane change maneuver

(b) Fishook maneuver

Figure 3.9: Tire slip-angle estimation performance

## 3.5 Tire Slip-angle based Stability Control

The direct relationship between the tire-slip and vehicle lateral dynamics provides a good measure of the possible improvements in stability control. This section details the derivation of an adaptive chassis stability control algorithm based on direct Lyapunov method. As mentioned before, the developed control system benefits from AFS and DYC schemes. The control laws make use of the tire-slip angle information provided by smart tire system. The derivation of the control algorithm is based on the bicycle model as summarized in Chapter 2. An auxiliary yaw moment is augmented into the equations of motion as a control input:

$$m(\dot{v} + ur) = 2C_f\alpha_f + 2C_r\alpha_r \tag{3.19}$$

$$I_z\dot{r} = l_f(2C_f\alpha_f) - l_r(2C_r\alpha_r) + M_b \tag{3.20}$$

The auxiliary input ($M_b$) represents the moment applied on the vehicle chassis for maintaining stability. Based on the tire slip-angle dynamics as defined in equations 3.14-3.15) the governing equations of the conventional bicycle model can be redefined with the front and

rear tire-slip angles as the states of the system:

$$I_z\dot{\alpha_f} = -(a_{11})\alpha_f - (a_{12})\alpha_r + I_z(\dot{\delta} + r) - (l_f/u)M_b \tag{3.21}$$

$$I_z\dot{\alpha_r} = -(a_{21})\alpha_f - (a_{22})\alpha_r + I_z r + (l_r/u)M_b \tag{3.22}$$

where

$$a_{11} = \left(\frac{2C_f(I_z + l_f^2 m)}{mu}\right) \quad a_{12} = \left(\frac{2C_r(I_z - l_f l_r m)}{mu}\right)$$
$$a_{21} = \left(\frac{2C_f(I_z - l_f l_r m)}{mu}\right) \quad a_{22} = \left(\frac{2C_r(I_z + l_r^2 m)}{mu}\right)$$

The steering term $\delta$ in equations (3.21) and (3.22) accounts for the sum of the driver steering input and the additional input from the AFS controller:

$$\delta = \delta_d + \delta_c$$

Next manipulating these governing equations and rewriting them in the state-space form yields:

$$\begin{bmatrix} I_z & 0 \\ 0 & I_z \end{bmatrix} \begin{bmatrix} \dot{\alpha_f} \\ \dot{\alpha_r} \end{bmatrix} + \begin{bmatrix} a_{11} & a_{12} \\ a_{21} & a_{22} \end{bmatrix} \begin{bmatrix} \alpha_f \\ \alpha_r \end{bmatrix} - \begin{bmatrix} I_z(\dot{\delta}_d + r) \\ I_z r \end{bmatrix} = \begin{Bmatrix} U_1 \\ U_2 \end{Bmatrix} \tag{3.23}$$

where $U_1$ and $U_2$ represent the control law:

$$\begin{Bmatrix} U_1 \\ U_2 \end{Bmatrix} = \begin{bmatrix} I_z & -(l_f/u) \\ 0 & (l_r/u) \end{bmatrix} \begin{Bmatrix} \dot{\delta}_c \\ M_b \end{Bmatrix}$$

Choosing the state vector $x = [\alpha_f \quad \alpha_r]^T$, the system can be rewritten in short form as $A\dot{x} + Bx + C = U$. Following that a candidate Lyapunov function (eq 3.24) is defined based on the system dynamics (A and B) and by including a set of adaptation parameters. A major advantage in using the Lyapunov method is that it allows computing control law for guaranteed asymptotic stability without the need for the analytical solutions of system

equations.

$$V(x,t) = \frac{1}{2}\left[\tilde{x}^T A\tilde{x} + \tilde{p}^T \Gamma \tilde{p}\right] + \int \tilde{x}^T B\tilde{x} dt \tag{3.24}$$

where $\Gamma$ and $p$ define the adaptation law which ensures system stability in case of parameter variations. In this study the adaptation parameters are selected as the front and rear cornering stiffness values ($C_f$ and $C_r$) to be able to adapt the controller to the variations in the road surface conditions. As the Lyapunov's criteria state [100], being able to define a positive definite candidate function and demonstrating that its rate of change in time always decreases (negative definite) would allow one to comment about system's stability. The positive definiteness of equation 3.24 can be guaranteed by selecting a positive diagonal $\Gamma$ matrix. In what follows differentiating the candidate function gives:

$$\dot{V}(x,t) = \tilde{x}^T A\dot{\tilde{x}} + \tilde{p}^T \Gamma \dot{\tilde{p}} + \tilde{x}^T B\tilde{x} \tag{3.25}$$

where $\tilde{x} = x - x_d$ defines the error. Expanding the terms in equation (3.25) and using the symmetry of matrices $A$ and $\Gamma$ it can be rewritten as:

$$\dot{V}(x,t) = \tilde{x}^T \left(-Bx - C - U - A\dot{x}_d + Bx - Bx_d\right) + \tilde{p}^T \Gamma \dot{\tilde{p}} \tag{3.26}$$

where the control law can be defined as $U = \hat{A}\dot{x}_d + \hat{B}x_d + \hat{C} - D\tilde{x}$ with $D$ as the control gain and $\hat{}$ denoting the estimated values using the adaptation law which is defined by further simplification of equation (3.26). Letting the general form of the adaptation law defined by:

$$H\tilde{p} = \tilde{A}\dot{x}_d + \tilde{B}x_d + \tilde{C} \tag{3.27}$$

where $p = [\tilde{C}_f \quad \tilde{C}_r]^T$ and substituting into equation 3.26 yieds:

$$\dot{V}(x,t) = -\tilde{x}^T D\tilde{x} + \tilde{p}^T \left(\Gamma\dot{\tilde{p}} + H^T\tilde{x}\right) \tag{3.28}$$

Asymptotic stability of the system is ensured by satisfying $\dot{V}(x,t) < 0$ which can be realized by selecting a positive definite controller gain matrix $D$ and zeroing the terms inside the parentheses which also define the adaptation parameters as:

$$\begin{aligned} \dot{\tilde{p}} &= -\Gamma^{-1} H^T \tilde{x} \\ p &= p_0 + \int (-\Gamma^{-1} H^T \tilde{x}) dt \end{aligned} \tag{3.29}$$

Finding out the form of the adaptation parameters, the control laws can finally be written:

$$M_b = \left(I_z\dot{\alpha}_{r_d} + \hat{a}_{21}\alpha_{f_d} + \hat{a}_{22}\alpha_{r_d} - I_z\dot{\psi} - D_{22}(\alpha_r - \alpha_{r_d})\right)(u/l_r) \tag{3.30}$$

$$\dot{\delta}_c = \left(I_z\dot{\alpha}_{f_d} + \hat{a}_{11}\alpha_{f_d} + \hat{a}_{12}\alpha_{r_d} - I_z(\dot{\delta}_d + \dot{\psi}) - D_{11}(\alpha_f - \alpha_{f_d})\right)(1/I_z) + (l_f/I_z u)M_b \tag{3.31}$$

The desired slip-angle values ($\alpha_{f_d}$ and $\alpha_{r_d}$) are derived by using the definitions for steady state steering to be able to negotiate a turn with radius R and for the lateral force acting on the front and rear axles during the turn:

$$\delta_{ss} = \frac{L}{R} + \left(\frac{m_f}{2C_f} - \frac{m_r}{2C_r}\right)\frac{u^2}{R} \tag{3.32}$$

$$F_{y_f} = m_f u^2/R = 2C_f\alpha_f$$

$$F_{y_r} = m_r u^2/R = 2C_r\alpha_r \tag{3.33}$$

where $m_f = l_r m/L$ and $m_r = l_f m/L$. Using equations 3.32 and 3.33 the desired slip-angle values can be written as:

$$\alpha_{f_d} = \frac{m_f\delta u^2}{2C_f\left(L + \left(\frac{m_f}{2C_f} - \frac{m_r}{2C_r}\right)u^2\right)} \qquad \alpha_{r_d} = \frac{m_r\delta u^2}{2C_r\left(L + \left(\frac{m_f}{2C_f} - \frac{m_r}{2C_r}\right)u^2\right)} \tag{3.34}$$

The control laws in the above equations can be implemented in various ways. The steering input is relatively easier as an Active Front Steering (AFS) mechanism can be assumed available so that the steering can be simply added to the driver's input. Whereas for the yaw moment signal a full lower level control algorithm is needed since there is no direct method to implement the resulting value above. This problem of implementing a *correcting* yaw moment on the vehicle chassis is generally known as Direct Yaw Control (DYC). The DYC can be implemented through different methods on the vehicle chassis (*e.g.* torque distribution, differential braking). In this study a differential braking method is utilized which administers individual brakes to generate the required yaw moment on the chassis. Initially, a rule based algorithm is developed to select appropriate wheel(s) to brake with respect to the vehicle's momentary understeer/oversteer characteristics and the direction of turn. The decisions about these conditions are made by monitoring the desired (eq. 3.34) and actual slip angle values and the direction of the turn. Table 3.1 summarizes the rules

used for such a differential braking method. Finding which wheel to brake, the required brake torque is simply calculated by using:

$$T_b = \frac{M_b R_w}{t_r/2} \tag{3.35}$$

Table 3.1: Brake rules for the DYC implementation

| $\alpha_{actual}$ | $\alpha_{actual} - \alpha_{desired}$ | $M_b$ | Wheel to brake |
|---|---|---|---|
| - | actual > desired | + | FR |
| - | actual > desired | - | RL |
| - | actual < desired | + | |
| - | actual < desired | - | |
| + | actual < desired | + | RR |
| + | actual < desired | - | FL |
| + | actual > desired | + | |
| + | actual > desired | - | |

## 3.6 System Validation using Simulation

The developed control algorithm is implemented and evaluated using numerical analysis. The algorithm is implemented in the MATLAB/Simulink environment and the vehicle dynamics are simulated using the CarSim commercial software. A D-class sedan vehicle model is downloaded into Simulink environment and integrated with the control algorithm. The system is then evaluated under an evasive double lane change (DLC) maneuver at a given initial speed which is kept constant by the driver model.

The desired path for the evasive DLC is selected as given in Figure 3.3a, the system is first tested on a high-friction ($\mu = 0.8$) surface with an initial speed of $30m/s$. The given speed easily runs an uncontrolled vehicle unstable, whereas the controlled vehicle seems to cope with it and successfully negotiates the turn. Figure 3.10a and 3.10b represent the AFS and

DYC commands computed using the Lyapunov's direct stability method. Compared with the driver's steering on Figure 3.10a, the AFS command seems in reverse which suggests that it applies a corrective counter-steer which cannot easily be done by the inexperienced daily-driver but is achieved through AFS without disturbing the driver. Figure 3.11a shows the trajectory of vehicle's CG and Figure 3.11b shows the yaw rate of the vehicle, which also comply with the above inference that the control algorithm can successfully stabilize the vehicle under these challenging conditions. Shown in Figure 3.12 are the traction performances for the front and rear tire-slip angle values compared to the desired values as in equation 3.34. Slight variations in the rear slip-angles can be accounted by the time lag in the slip-angle generation at the rear tires as summarized in section 3.3. Another point to note is that the controller maintains the slip-angle values in the linear range of the tire force-moment curve where the smart tire is capable of providing successful slip-angle estimations. The results also indicate that the controller helps to maintain an understeer behavior during the turn as desired.

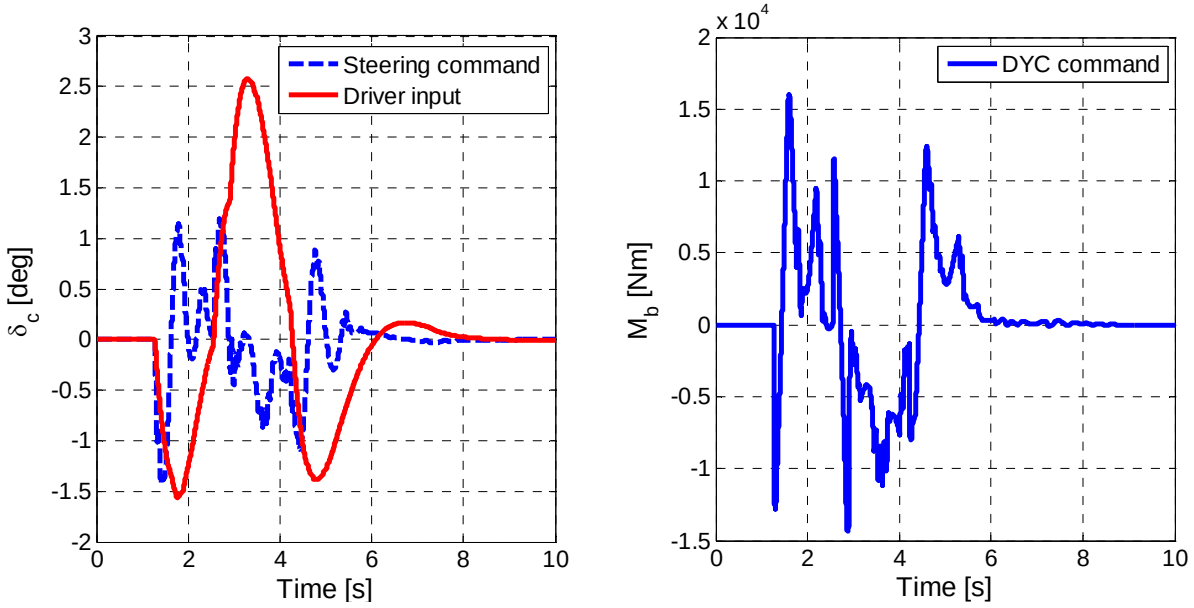


(a) Steering input

(b) Corrective yaw moment input

Figure 3.10: Control signals for high-$\mu$ condition

Figure 3.13 presents the wheel and vehicle speed variations and the applied brake torque values during the turn to help evaluating the lower level (optimal force allocation) controller performance.

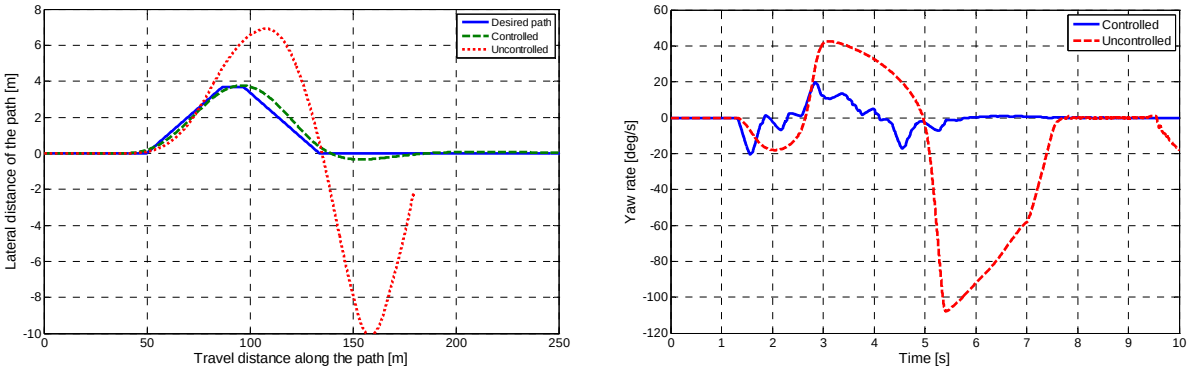


(a) Vehicle CG path

(b) Chassis yaw-rate response

Figure 3.11: Vehicle response comparison on high-$\mu$ condition

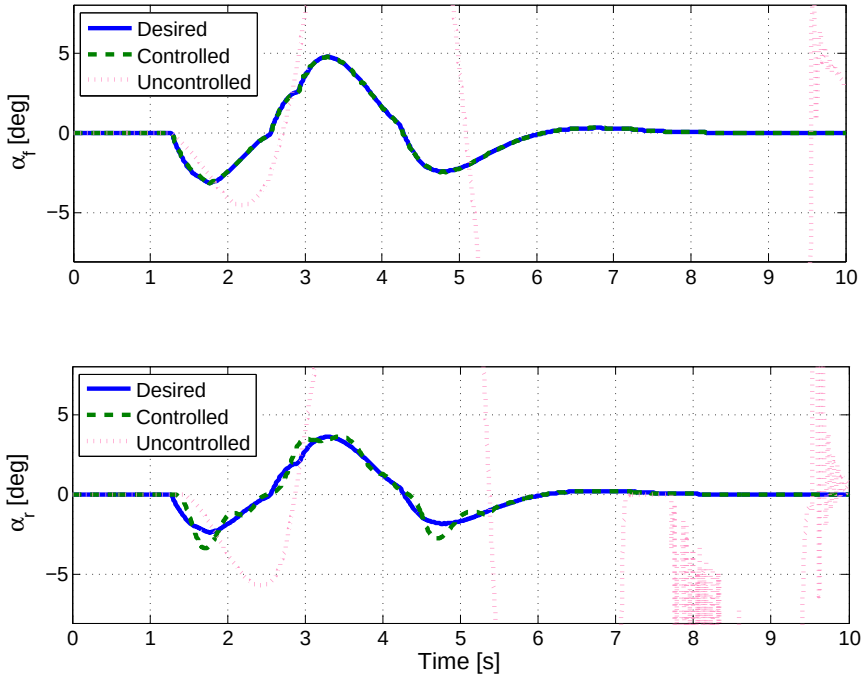


Figure 3.12: Front and rear tire-slip angle values for the controlled and uncontrolled vehicles compared to the desired values

Finally Figure 3.13 shows the variations of the adaptation laws for the front and rear axle cornering stiffness values. Also shown are the design and nominal values. The design value corresponds to the cornering stiffness of the tire under static load and on a unity friction

surface whereas the nominal value varies with the surface friction. The front and rear axle design values are taken as $120,000 N/rad$ and for the high-friction surface ($\mu = 0.8$) the nominal value is expected to become 80% of the design value. As can be deduced from equation 3.29 the adaptation law is directly related to the integration of the error between the desired and actual slip angles. As a result, the front axle value in Figure 3.14 converges to the design value due to the minimal error in the front slip angle whereas the rear axle value converges to the nominal value.

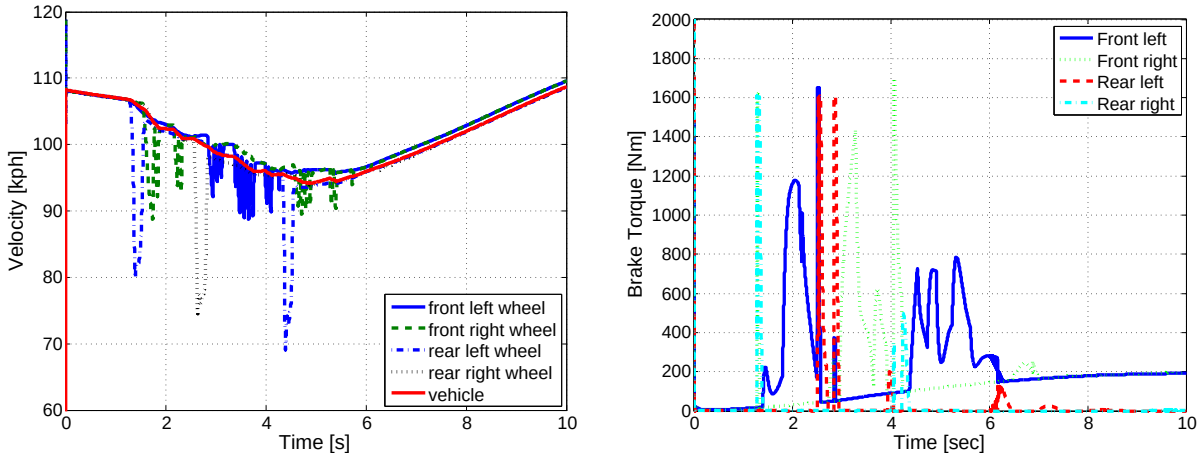


(a) (b)

Figure 3.13: Vehicle and wheel speeds

In what follows the system is tested on a low friction surface ($\mu = 0.25$). Figure 3.15a shows the CG trajectory at a reduced initial speed ($11 m/s$) and indicates that the controlled vehicle again can initiate the turn whereas the uncontrolled vehicle goes unstable very early on.

Figure 3.16 represents the controller commands for AFS and DYC systems during the low friction maneuver. The AFS control implements higher reverse steering which is again very significant in stabilizing the vehicle. Due to the lower force capacity from the tires on a low friction surface, the brake system would not be as effective, hence the lower magnitudes in the DYC command.

Figure 3.17 is also good indicator for the performance of the controller on the low friction surface. The desired front and rear tire-slip values are tracked satisfactorily and the variations of the wheel and vehicle speeds are still in a quite reasonable range. Finally, shown in Figure 3.19 are the adaptation values of the front and rear axle cornering stiffness'. Both converge very close to the nominal value of $26,000 Nm$, which is about 20% of the design value,

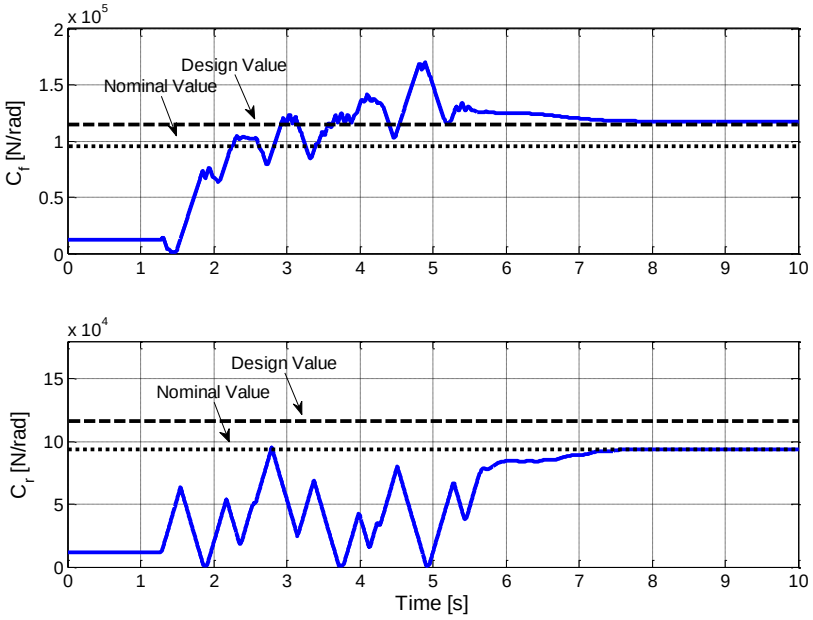


Figure 3.14: Adaptation of the front and rear axle cornering stiffness values

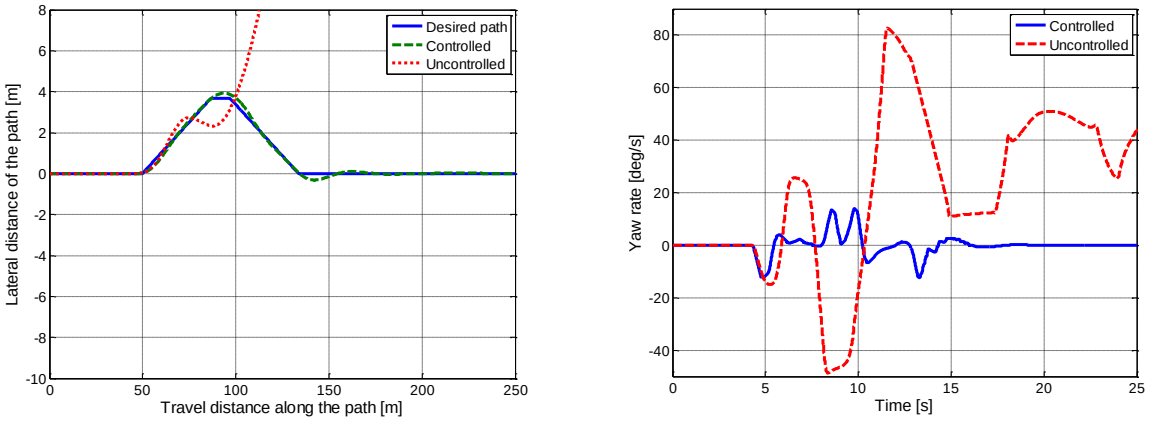


(a) Trajectory followed by vehicle's CG

(b) Yaw rate compared for controlled and uncontrolled systems

Figure 3.15: Low-$\mu$ surface test results

$120,000Nm$.

To conclude the simulation efforts, a comparison study is conducted to have a better judgment on the performance of the proposed algorithm. Another stability control algorithm based on vehicle yaw-rate feedback is implemented in the same environment and executed

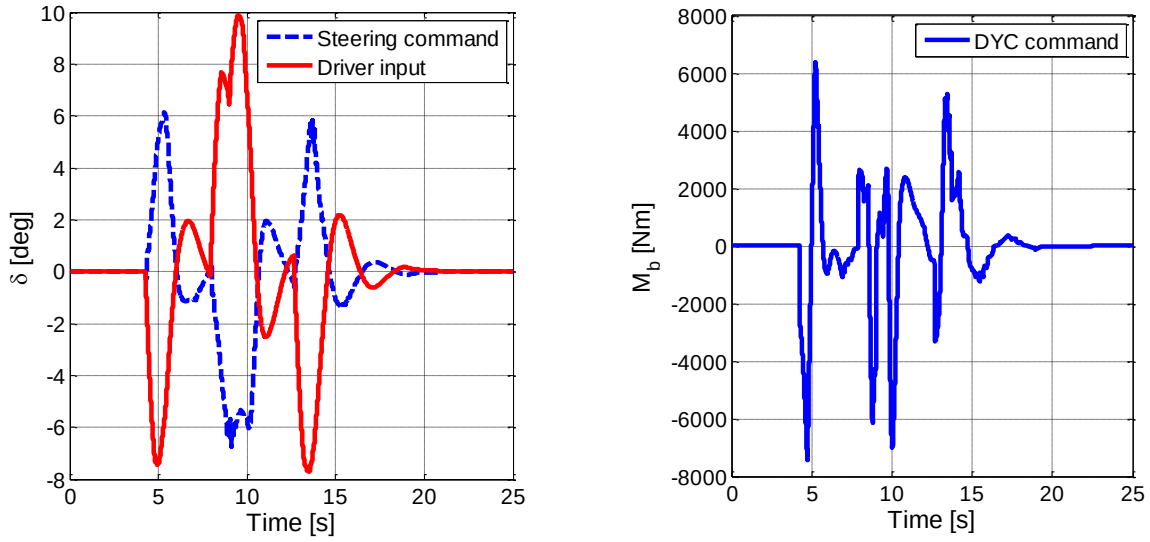


(a) Steering input ($\delta_c$) (b) Corrective yaw moment ($M_b$)

Figure 3.16: Control signals for low-$\mu$ surface testing

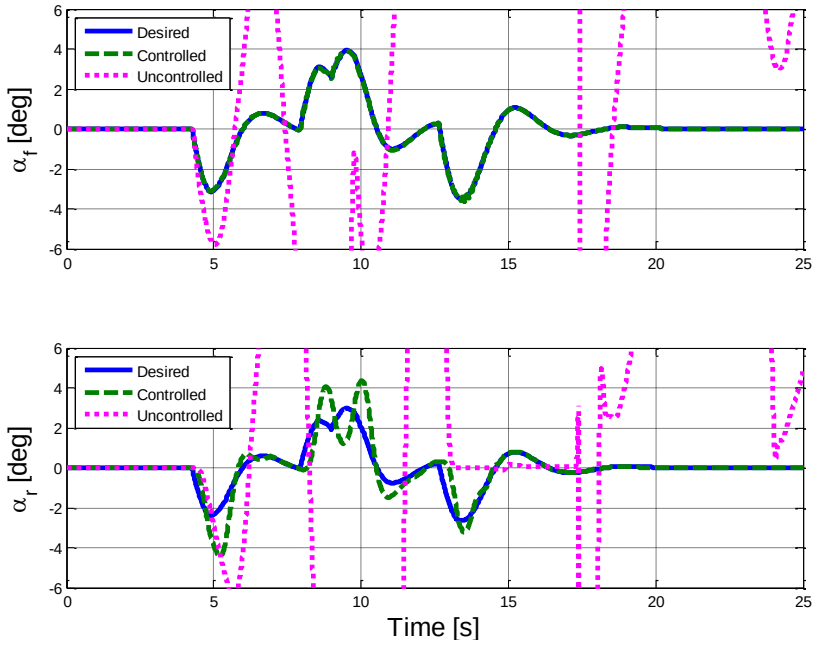


Figure 3.17: Front and rear tire-slip angle values for the controlled and uncontrolled vehicles compared to the ideal values

the same DLC maneuver. Figure 3.20 shows the comparison of the resulting control laws

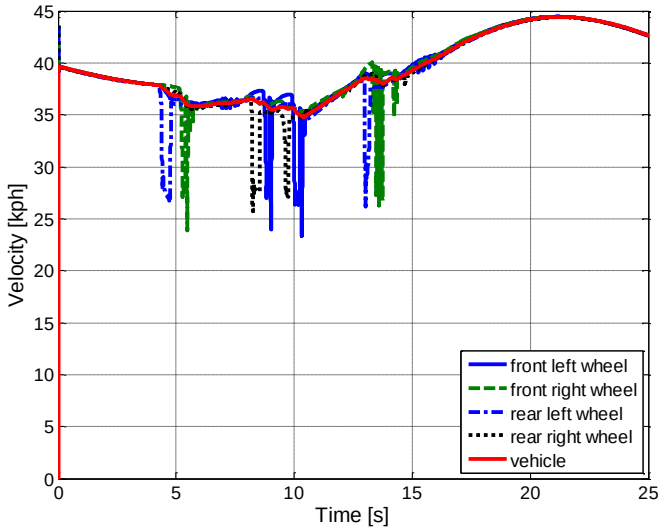


Figure 3.18: Wheel and vehicle velocity variation during low friction surface test

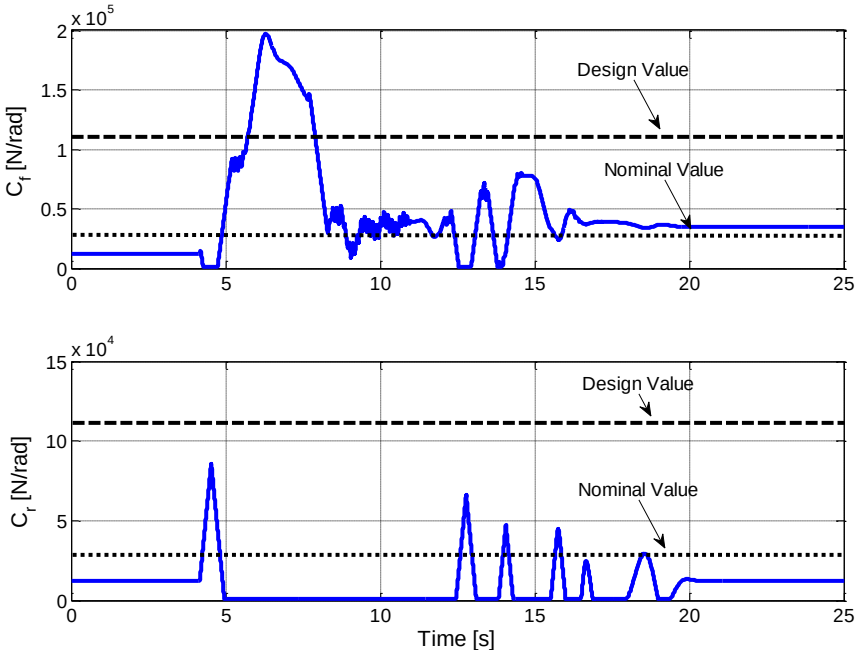


Figure 3.19: Adaptation of the front and rear axle cornering stiffness values during low friction surface test

for each algorithm. As the results indicate, the slip-angle based control algorithm yields to a considerable reduction in the control signals, which eventually impose less loads on the actuators and lower levels of interference with the driver's inputs. In addition, Figure 3.20b

indicates that the proposed algorithm results in lower levels of desired yaw moment values, as a result lower braking action is required.

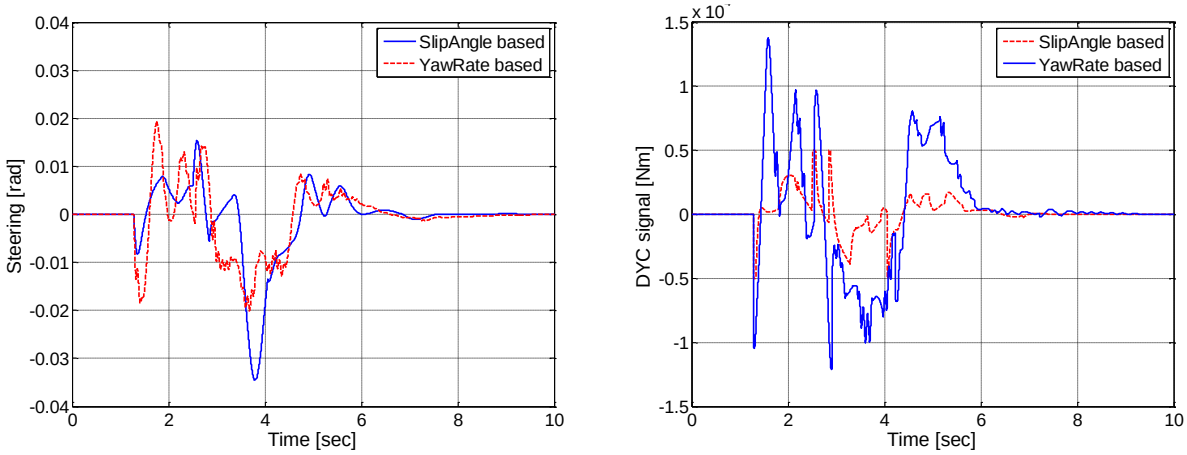


(a) Steering input ($\delta_c$) comparison

(b) Corrective yaw moment ($M_b$) comparison

Figure 3.20: Comparison of control efforts for slip-angle and yaw rate based control algorithms

## 3.7 Conclusion

This chapter details the derivation of an adaptive vehicle stability control algorithm based on tire slip-angle. The first part summarizes the implemented tire slip-angle estimation methodology that utilizes the so-called sensor fusion approach. Integrating the smart tire technology with a model based observer scheme, the method provides robust tire slip-angle information in both linear and saturation regions of the tire force-slip curve. In what follows, the derivation of the control algorithm is presented. The resulting control laws are implemented by integrating active front steering (AFS) and direct yaw control (DYC) methods to intervene with the driver's inputs. The DYC part is implemented by designing another lower level control algorithm that optimally distributes the wheel brake forces.

The algorithms are evaluated using numerical analysis in MATLAB/Simulink environment and using vehicle model from CarSim software. The results of simulation studies indicate that the algorithm successfully intervenes with the steering and braking mechanisms and stabilize the system during the given evasive lane change maneuver. Choosing the adaptation

parameters as the tire cornering stiffness, the algorithm is also capable of running on a lower friction surface condition. A comparative study provides a better measure of improvements and advantages using the proposed algorithm. Same simulations executed for the yaw-rate based control algorithm indicate that proposed algorithm impose less oscillations on the AFS system, which also yields to lower levels of interference with the driver inputs. Similarly the proposed algorithm requires lower levels of desired yaw moment values, which leads to fewer loads on the brake/traction dynamics. Another merit of this algorithm is that it eliminates the need for the lateral velocity variable which would require a state estimator and would introduce more uncertainty into the system.

# Chapter 4

# Advanced Anti-lock Braking

## 4.1 Introduction

Conventional anti-lock braking systems (ABS) provide vehicles the ability to achieve shorter stopping distance and also mediate to maintain directional control and stability. The main objective of the ABS algorithm is to maximize the tire longitudinal traction by preventing the wheels from being locked during braking. This also helps to maintain control on the steering as the tires do not pass the limit for saturation and allows steering input to remain effective. The generic ABS control approach is based on wheel slip and wheel angular acceleration control [101, 102]. The principle of the operation in a typical ABS is simply formed on limited cycling of longitudinal wheel slip in a desired range [103]. The algorithm sets certain bounds for wheel angular acceleration and wheel angular speed and uses a complex rule set to decide for the pressure mode of the actuator. Nevertheless, these conventional ABSs do not take the varying tire force-moment characteristics on different types of road surfaces into consideration, which naturally have their own appropriate operating conditions. The forces and moments generated at the tire-road contact patch are altered by driver input based on various handling maneuvers. Vehicle dynamic behavior is primarily controlled through three driver inputs, and these driver inputs indirectly control the vehicle motion by affecting the tire forces. The forces experienced through the tires are actually the primary forces affecting vehicle handling dynamics, and the magnitude of these forces that can be transferred from the tire to the driving surface are limited by the contact patch area, the vertical load on the tire and the coefficient of friction between the tire and road surface. Moreover, as stated by

the friction ellipse theory [104], the total friction force acting between the tire and the road cannot exceed the maximum value determined by the friction coefficient ($\mu$) and the vertical load $F_z$. A decrease in the lateral force is expected as the longitudinal force increases, and vice versa. This ultimately leads to the conclusion of inefficient braking performance as well as unexpected consequences when the vehicle encounters a road surface that is not defined in the ABSs default settings.

Therefore, knowledge about the road surface friction condition is essential for propelling new designs in vehicle control systems. On the other hand, lack of knowledge about friction leads to developing over-conservative design rules which might result in reduced driving performance. In normal driving conditions the frictional force is not fully utilized and the developed tire force will be somewhere in the interior of the friction circle. With the force generated at the tire-road contact, a relative motion arises between the tire structure and the road surface, referred as the tire slip The relation between the resulting tire force and this slip motion depends on many factors, namely, tire inflation pressure, vertical load, tire wear, temperature, etc., and also contains information about the maximum surface friction condition. When the tire is exposed to excitation with high utilization, beyond the point corresponding to the maximum available friction force, the tire is sliding and the resulting tire force directly corresponds to the friction coefficient. This interdependence allows for estimation of the surface friction condition using the smart tire technology, which is then to be utilized in improvement of the ABS logic to adapt itself to the most appropriate operating points for the corresponding surface condition.

The goal of this chapter is to present an implementation strategy for a new adaptive ABS control algorithm that makes use of a surface friction estimation algorithm to adapt itself to possible variations in friction condition. The estimation algorithm integrates two methods for satisfactory results: a smart tire based method with a model based observer. The smart tire based estimation uses a method that characterizes the terrain using the measured frequency response of the tire vibrations whereas the model based observer makes use of a Brush model together with tire force estimations to obtain the maximum surface friction. In what follows, a new ABS algorithm is developed that can adapt an initially defined rule-set to the variations on the surface friction conditions. As mentioned earlier the conventional ABS algorithms define multiple rule-sets to cope with such variations. The proposed algorithm allows simplifying the rule-set by only defining rules for the applied brake torque and

wheel slip in advance and adapting them dynamically to the varying surface conditions.

## 4.2 Background

The ABS is one of the earliest developed active safety systems together with the traction controllers. As mentioned earlier, ABS is originally developed to prevent wheels from locking up for better braking and stability performance. Modern ABSs, on the other hand, also strive to maximize the wheel brake forces by controlling the tire slip ratio to operate around an optimum value, which varies w.r.t. the road surface characteristics as depicted in Figure 4.1.

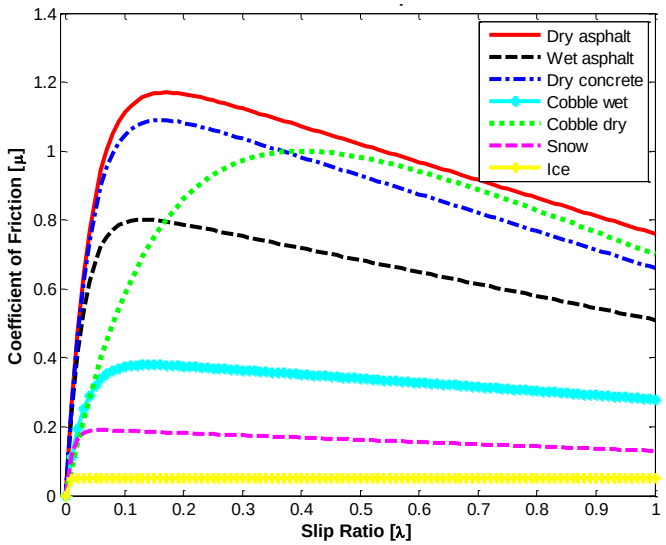


Figure 4.1: Tire force-moment characteristics as a function of road surface conditions

The basic function of an ABS is to either hold or release the braking pressure on the wheels if there is a danger of the wheels locking. At the same time, the ABS needs to re-permit application of the brakes again once the danger of locking has been averted. It could also hold or release the braking pressure; all in order to keep the slip ratio at the wheel from exceeding the given optimum value. Depending on the number of wheels the ABS is expected to control, it can be implemented with four channels four sensors, three channels three sensors or one channel one sensor. Each of these channels is to be controlled by a solenoid valve, and depending on the state of these valves, brake pressure on the wheel can be held even, released or increased. Open valve allows the brake to be controlled by the driver by allowing the amount of brake pressure desired by the driver to be applied to the brake. Closing the

valve isolates that brake from the master cylinder which yields to holding the brake pressure and preventing it from increasing even if the driver pushes the brake pedal harder. Finally when the valve is in the release position, the pressure from the brake is released. In this position, not only is the brake isolated from any further braking actions of the driver, but the amount of braking pressure on the wheel is actively reduced. These three states allow adjusting the amount of brake pressure desired by the driver to be applied to the brake by avoiding any wheel lock-up situation.

ABS algorithms typically utilize wheel speed measurements to predict if the wheels will lock and if the danger of locking has been averted. The process of determining whether or not the wheel is going to lock is called prediction. Prediction point slip is defined as the wheel slip at the instant the control unit predicts for the first time in a brake cycle that the wheel is going to lock. The process of determining whether or not the danger of locking has been averted is called reselection. Reselection point slip is defined as the wheel slip at the instant it is predicted for the first time in a brake cycle that the danger of locking is averted.

A number of other factors influence the working of an ABS in addition to surface friction. One major factor is the rate of the brake torque application which depends on the brake pedal action during the first cycle, and depends on the pressure build characteristics of the modulator in the subsequent cycles. Another factor is the initial longitudinal velocity of the vehicle as it determines how quickly the vehicle can come to a stop. The brake effort distribution from front to rear also makes a significant difference. Reul et.al. in [105] present results of an analysis that summarizes two major methods for the improvement of vehicle brake systems in general. One method relates to maximization of the available surface friction which requires adjusting the tire and surface physical properties and is not discussed in this research. After quoting the strong dependence between slip oscillations and brake performance [106], the second method proposes controlling the oscillations of the operating slip point for improved braking. Two synthetic parameters surface to accomplish this task; the tire load which helps to maximize the tire's road holding capacity and the wheel brake force which aims to maximize the tire grip level and which is the focus of this study. Numerous logic based ABS control systems have been developed and reported in literature to address the use of these methods and to improve brake performance in the presence of the above variations.

A pioneering and widely cited study for the application of anti-lock brakes in automobiles is by Guntur and Ouwerkerk [107, 108], which contain a good discussion of various implementation strategies with different prediction and reselection rule sets. Other more recent studies work on different control methodologies and other benefits from ABS. In [109], Taheri studies performance of a new sliding mode based nonlinear control algorithm integrated with four wheel steering. Yeh et.al. in [110, 111] introduce a four-phase ABS control algorithm with the addition of a high and low pressure hold states. They also investigate an analytical derivation method for a stability guaranteed rule-set in [112]. Sliding mode control (SMC) constitutes a large portion in ABS algorithm studies especially due to its robust nature against uncertainties in the brake hydraulics. Another widely cited study that uses SMC is by Drakunov et.al. [113] where the authors take a simplified brake hydraulics model as well as the uncertainties in the optimal slip value corresponding to the current road surface into account. A similar study that uses a SMC scheme is by Unsal and Kachroo [114] where the authors study a sliding mode observer (SMO) scheme and develop a real-time implementable control law based on slip ratio estimations from the SMO. Another mainstream in the development of brake controllers is the development and use of the LuGre tire model which allows accounting for the tire transient characteristics. A number of studies have been conducted specifically under the California PATH program [115, 116, 117], where the authors investigated the integration of LuGre model in brake dynamics and proposed control algorithms again using a SMC scheme. Due to its coherent nature with rule-based control, Fuzzy logic algorithms constitute another large part in this research. In [118] Keshmiri et.al. study the performance of fuzzy based controllers on varying road surface conditions and conclude that fuzzy logic by itself does not always provide best braking action. Habibi and Shahri propose the integration of SMC and Fuzzy logic in [119] to overcome this problem. More recent studies in the subject take advantage of the advancements in the onboard electronics and propose using control algorithms of higher complexity. Petersen et.al. study a gain scheduling scheme based on slip optimization in [120, 121]. A robust control algorithm that uses linear matrix inequalities (LMI) scheme to gain schedule the brake torque is proposed by Baslamisli et.al. in [122]. Finally Dae Keun et.al study an implementation strategy for model predictive control scheme based on nonlinear brake dynamics in [123]. A common assumption in these recent studies is the availability of an electronic brake system (brake-by-wire) replacing the hydraulic brakes that might yield to crucial time lags.

A common practical problem in the above summarized ABS systems is the availability of

wheel slip information which cannot be measured with any feasible sensor system available on current vehicles in the market. Often the only measurements available to the ABS system are measurements of the individual wheel speeds at the four wheels.

## 4.3 Estimation of Surface Friction Condition

This section provides a brief overview of the friction estimation method utilized for in the development of the proposed ABS algorithm. A so called sensor fusion approach is followed which basically integrates a model based observer scheme with the smart tire based estimations of the surface friction condition. An integral approach is followed due to the argument that each method provides robust results at different levels of excitation on the tire. The level of excitation here basically refers to the range of slip ratio the tire experiences. The smart tire is capable of providing successful estimations in the linear slip range whereas the model based observer can cope with the nonlinear dynamics if the tire is driven into the saturation region. The summary of each method is given below in substantial details.

### 4.3.1 Smart Tire Based Surface Classification

The smart tire based approach characterizes the road surface using the frequency response of the tire vibrations logged using the prototype system. The effect of various test conditions (tire load, translational speed, tire pressure) on the tire vibration spectra are studied by varying each of these parameters during testing of the instrumented tire. More details of the procedure are provided in [35]. The power spectrum of each accelerometer signal from these tests is computed using Welchs averaged modified periodogram method [124]. The results as shown in Figure 4.2 indicate a marked difference especially in the concentration of the higher frequencies on the spectrum of the circumferential acceleration signals. These variations present an opportunity to characterize the road condition using the tire vibration pattern information.

Another significant demarcation is seen in the level variations in signal power between the pre-trailing and post-trailing domains of the signal. Due to the presence of more prominent variations, the analysis is pursued by only using the pre-trailing portion of the vibration signals. In what follows, the PSD content of the signal is executed through band-pass filters

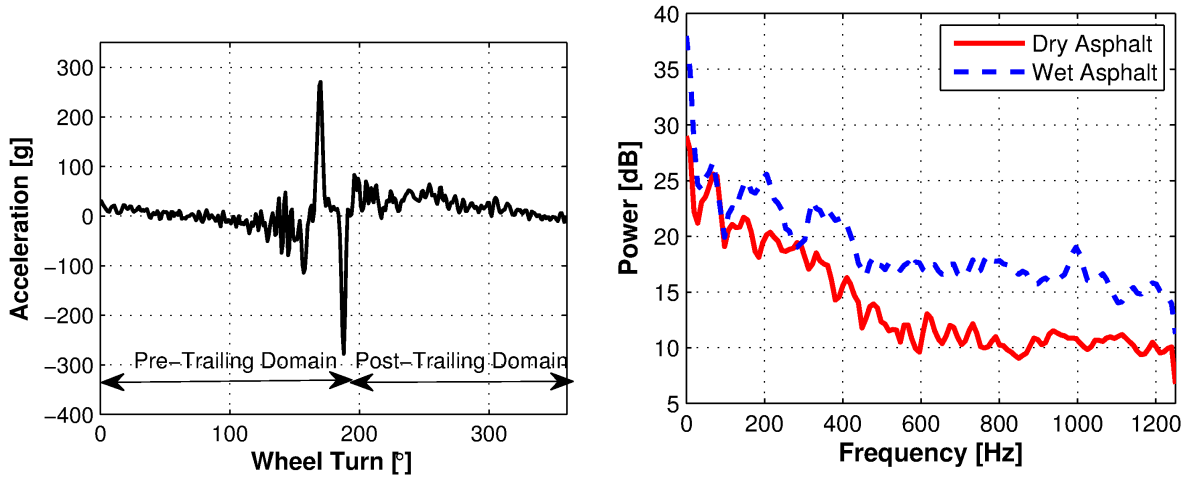


(a) Circumferential Acceleration Signal (b) Power spectrum density (PSD)

Figure 4.2: Frequency response analysis of the smart tire signals

to distinguish between the low frequency (e.g. $10 - 500Hz$ band) and high frequency (e.g. $600Hz$ to $2500Hz$) contents.

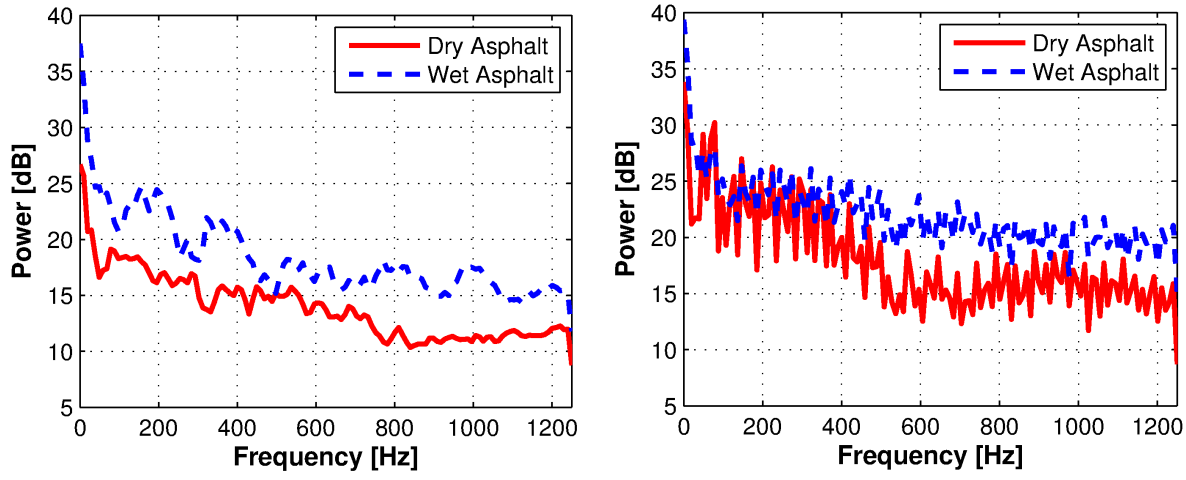


(a) Pre-trailing domain PSD (b) Post-trailing domain PSD

Figure 4.3: PSD analysis of pre-trailing and post-trailing signal domains

After filtering the frequency response of the smart tire signal, the change in the vibration level ratio (R) between the two frequency contents is measured. It is evident from results that the vibration level ratio (R) increases when the tire was tested on the wet road surface relative to when the tire was tested on the dry road surface. This change in the vibration level

ratio can be attributed to the increased slippage of the tire, and thus it has been confirmed that the slipperiness of a road surface can be decided by setting a proper threshold value. For this purpose, a fuzzy logic classification approach [35, 125] is utilized to classify among different surface conditions w.r.t. the given vibration ratios. Based on the interdependence of the given test conditions (tire load, translational speed, and tire pressure) and the way they affect the vibration spectra of a tire, a set of linguistic rules are developed. The classifier performance was validated on smooth asphalt, regular asphalt, rough asphalt and wet asphalt (Figure 4.5).

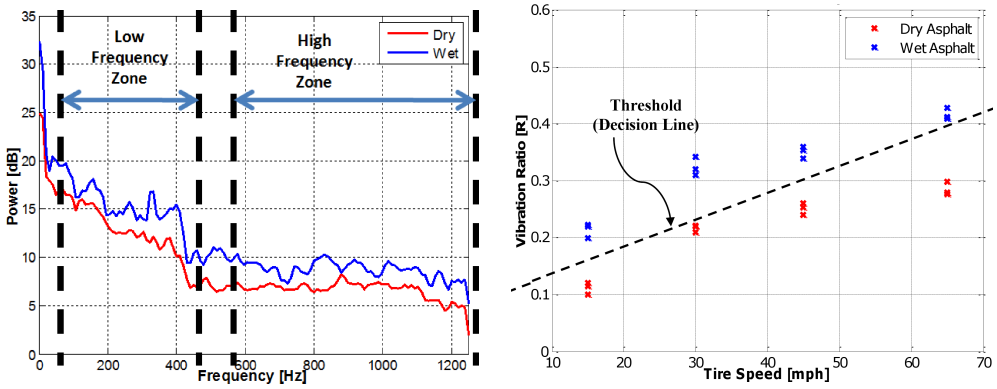


(a) Distinction of high and low frequency domains

(b) Vibration ratio on dry and wet surface conditions

Figure 4.4: Computation of the vibration ratio (R) on different surface conditions

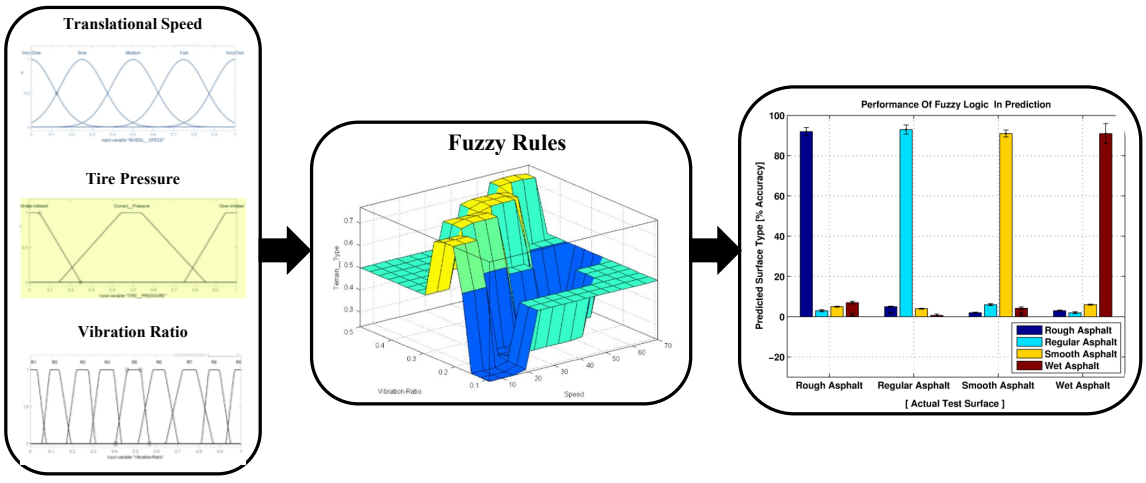


Figure 4.5: Fuzzy logic algorithm to classify the current surface condition

As mentioned earlier, the smart tire based classification algorithm results in robust estimation

of surface condition in the range of wheel slips that correspond to the linear tire force curve. Nevertheless, higher levels of excitation on the tire triggers additional modes of vibration which disrupts the correlation summarized above. The increasing misclassification rate under high slip conditions are attributed to the increased vibration levels in the circumferential acceleration signal due to the stick/slip phenomenon linked to the tread block vibration modes (Figure 4.6). Therefore a model based approach is followed to estimate road surface friction under high-slip conditions.

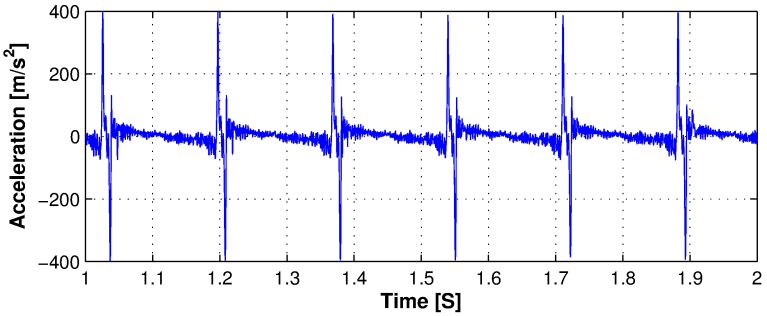


(a) Circumferential acceleration under low slip conditions

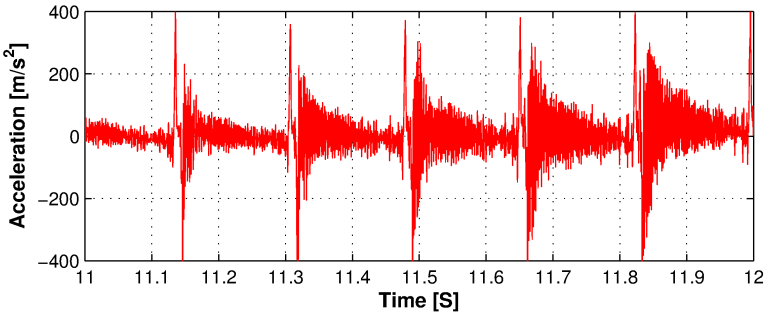


(b) Circumferential acceleration under high slip conditions

Figure 4.6: Variation in the vibration levels under low and high slip conditions

### 4.3.2 Model Based Surface Friction Observer

To develop a robust road surface friction coefficient ($\mu_max$) estimation technique, a tire model based observer scheme is used. The observer scheme basically requires the tire force ($F_x$), wheel load ($F_z$) and slip ($\lambda$) information and in turn estimates the surface friction condition. The details of providing each of the listed parameters are given as follows. The sliding mode observer scheme detailed in Chapter 3 is utilized for tire longitudinal force estimation.

Numerous methods have been proposed to estimate the dynamic wheel load information, such as recursive least squares (RLS) [126, 127] or Kalman filters [128]. In this study, a smart tire based estimation method is taken as the basis. The method utilizes a novel signal processing algorithm using the intelligent tire radial acceleration signal. The algorithm is based on two synthetic parameters, the contact patch length (CPL) and the radial acceleration signal amplitude. In addition, a strong dependence of both these parameters is observed on the tire rolling speed and inflation pressure. Having identified parameters that are sensitive to the tire normal load, a relationship between these system inputs/parameters (rolling speed, inflation pressure, contact patch length and signal amplitude) and the system output (tire normal load) is established using an explicit artificial neural network (ANN) [129] based formulation. In what follows, the selected ANN is trained for various learning rate and termination criteria [130] and modeled to make highly complex, nonlinear and multidimensional associations between selected input parameters and output. Further details on the selected ANN are provided in [35]. The results indicate acceptable degree of accuracy in the predictions of the tire load across the full range of the tire operating conditions (Figure 4.7).

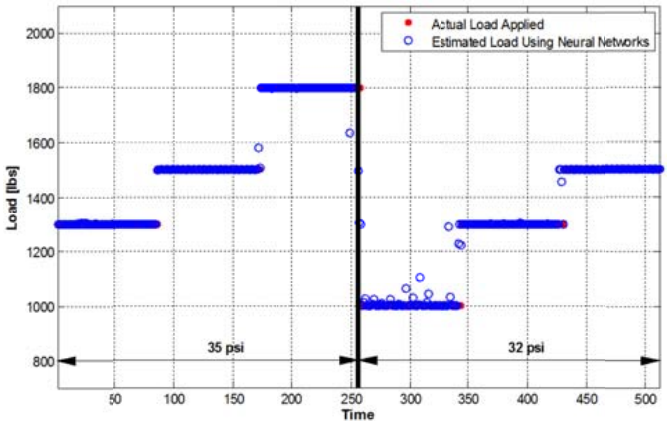


Figure 4.7: Smart tire based wheel load estimation performance.

Next parameter of interest for the model based observer is the tire longitudinal stiffness ($C_\lambda$). Satisfactory performance of the wheel dynamics-based observer in the small slip ($|\lambda| < 3\%$) region provides us with an opportunity to adaptively estimate $C_\lambda$ of the tire using an on-line parameter estimation algorithm. Equation (18) can be rewritten into a standard parameter

identification form as follows:

$$y(t) = \phi^T(t)\theta(t) \tag{4.1}$$

where $y(t) = F_x$ is the system output (from the wheel dynamics-based observer), $(t) = C_\lambda$ is the unknown parameter and $\phi^T(t) = \lambda$ is the measured slip ratio. The unknown parameter $(t)$ can be identified in real-time using the parameter identification approach. The RLS algorithm as summarized in [131] provides a method to iteratively update the unknown parameter at each sampling time to minimize the sum of the squares of the modeling error using the past data contained within the regression vector, $\phi(t)$. The performance of the RLS algorithm is evaluated with simulations where the road surface is designed to have sudden friction coefficient changes and the vehicle maneuver is straight driving with intermittent gas pedal presses. Figure 4.8 indicates the resulting estimates can track the variations in the friction condition of the terrain.

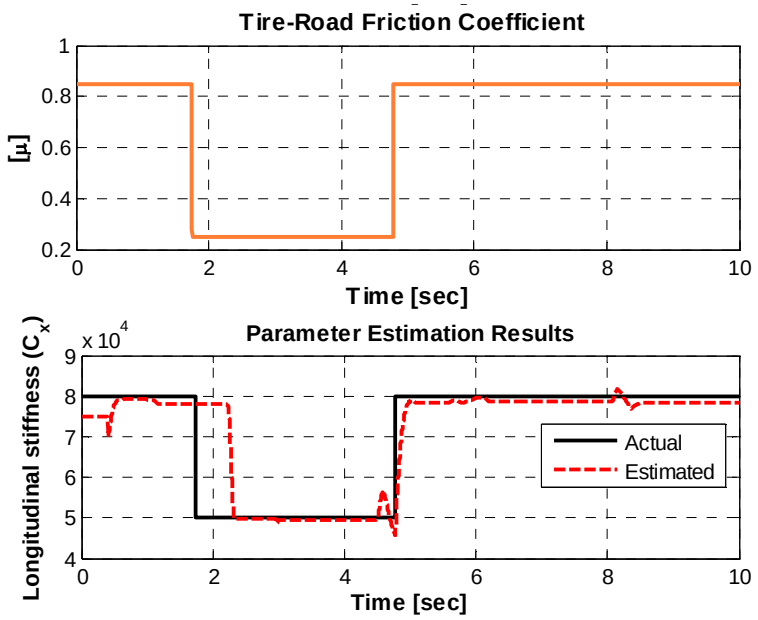


Figure 4.8: Fuzzy logic algorithm to classify the current surface condition

The last parameter required for friction estimation is the wheel slip ratio which can be obtained from the wheel and vehicle speed information. A field tested algorithm, which is also followed in this study, is provided by Savaresi and Tanelli in [132]. The main idea of the proposed algorithm is to estimate the vehicle speed differently according to the current vehicle status, so as to account for the different motion conditions. Specifically, the status of the vehicle is used to model the condition in which the vehicle speed is very low, constant,

accelerating or braking condition. Once the vehicle status is set, the estimated vehicle speed is computed based on the following observations. When the vehicle has very low or constant speed, the estimated vehicle speed can be obtained as the average of the four wheel speeds, as basically the slip is equal to zero for all wheels. When the vehicle is accelerating, instead, as the driving wheels have a non-zero longitudinal slip due to traction force, the estimated vehicle speed must be obtained as the average of the non-driving wheels. Finally, the braking condition is considered as the most critical, and it requires an appropriate integration procedure of the accelerometer signal.

Having identified the required parameters, a tire model-based closed-loop feedback observer is utilized. The estimator concept used here relies on the Dugoff tire model which has been summarized in Chapter 2. In its simplest formulation, the model describes the relationship between the tire force ($F_x$) and the slip ($\lambda$) as a function of tire stiffness ($C_\lambda$) and the surface friction coefficient ($\mu_{max}$). The above estimations yield the friction coefficient as the only unknown in the model, hence executing the inverse model provides expressions for $\mu_{max}$ as the following. The intermittent function $f(\xi)$ is given in terms of the tire force $F_x$:

$$f(\xi) = \frac{F_x(1-\lambda)}{C_\lambda \lambda} \tag{4.2}$$

Next. the piecewise function to define $\zeta$ can be defined:

$$\xi = \begin{cases} 1 - \sqrt{1 - f(\xi)}, & f(\xi) < 1 \\ 1, & f(\xi) \geq 1 \end{cases} \tag{4.3}$$

Finally the surface friction can be computed from the inverse expression as below:

$$\mu_{max} = \frac{2(C_\lambda \lambda)\zeta}{F_z(1-\lambda)(1-A_s V_s)} \tag{4.4}$$

where$A_s$ is a constant for the friction reduction factor and $V_x$ represents the slip linearized speed parameter ($V_s = u(\lambda)$). Figure 4.9 shows the estimator performance evaluated on a jump-$\mu$ condition during braking. The results indicate that the observer successfully converges to the actual values, nevertheless with an initial time lag. This time lag is mainly caused by the lack of excitation as mentioned earlier. Hence the sensor fusion approach by integrating the model based observer with the smart tire estimations yield to the suc-

cessful estimation of the surface friction in a substantially wide range of tire excitation levels.

Next section introduces an adaptive rule-based wheel slip control algorithm proposed to improve the ABS performance. The algorithm aims to gain-schedule a simplified rule-set to the variations in surface conditions estimations provided by the methods summarized above.

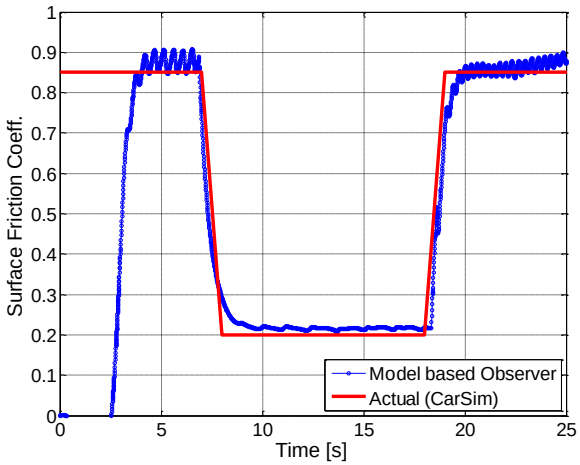


Figure 4.9: Model based surface friction estimation performance.

## 4.4 A Self-Tuning Anti-lock Brake System Algorithm

In a vehicle brake system, the applied brake torque can be basically considered as a function of longitudinal tire slip and tire force. Current ABS algorithms define rule-sets that are based on vehicle and/or wheel speed and acceleration to regulate the brake pressure. These limits are meant to keep the system trajectory bounded around a peak point that corresponds to the maximum applicable brake force as long as possible for the shortest stopping distance. The principle of the proposed algorithm is to define such rules that will define adaptive limits w.r.t. possible variations on the surface friction conditions, which will confine the system trajectory to a stable limit cycle.

The control algorithm is based on the quarter car model summarized in Chapter 2. If the motion of the wheel is extended to two dimensions, then the effect of tire slip-angle on the force-moment curve also must be considered. As mentioned earlier, there exists a strong dependency between the lateral and longitudinal tire force-moment characteristics

defined by the friction circle phenomena. Nevertheless, the range of the slip-angle variation in a daily driving situation, which generally remains in the stable region, yields only to a reasonable trade-off as indicated in Figure 4.10. Furthermore stability control algorithms, as summarized in Chapter 3, works to confine the slip-angle in the stable region to maintain driver's control abilities and vehicle stability. Therefore, the following derivations in this study omit the effect tire slip-angle on the tire force-slip curve.

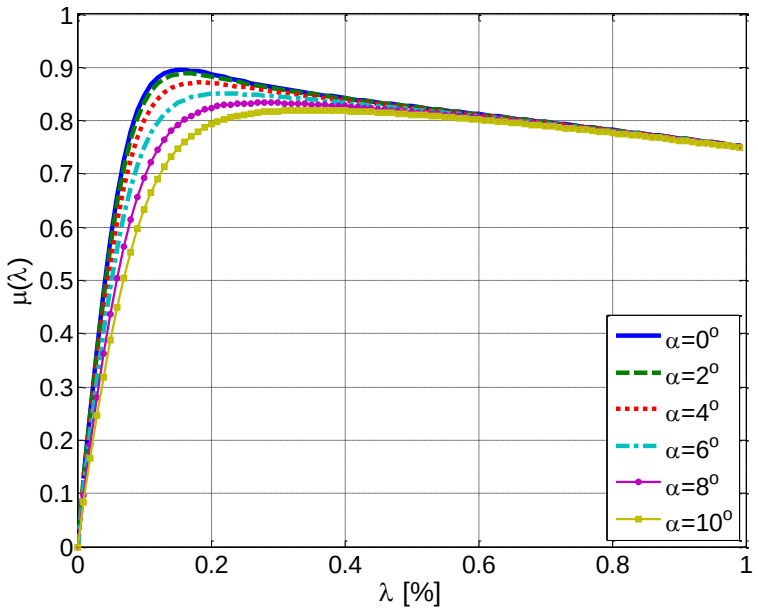


Figure 4.10: Tire force-slip curve and slip-angle relation.

In what follows, the wheel slip dynamics can be defined as below using the quarter car model dynamics and the expression for wheel slip which is reduced from eq. 2.3 by only considering the braking case ($\max(v, R_w\omega) \rightarrow v$):

$$\begin{aligned} \dot{\lambda} &= \frac{d}{dt}\left(\frac{v - R_w\omega}{v}\right) \\ &= -\frac{R_w\dot{\omega}}{v} + \frac{R_w\omega}{v}\frac{\dot{v}}{v} \end{aligned} \tag{4.5}$$

The wheel dynamics can be defined by substituting for the wheel and vehicle acceleration

terms above from the quarter car model detailed in Chapter 2

$$\begin{aligned} \dot{v} &= -\frac{1}{v}\left(\frac{1}{m}(1-\lambda)+\frac{R_w^2}{J}\right)F_z\mu+\frac{1}{v}\frac{R_w}{J}T_b \\ &= \frac{R_w}{Jv}\left(T_b-\underbrace{R_wF_z\mu\left(1+\frac{J(1-\lambda)}{mR_w^2}\right)}_{T_e}\right) \end{aligned} \tag{4.6}$$

where $T_e$ is referred as the equilibrium torque. It is worth to note that $T_e$ defines the isoclines in the phase plane $T_b$ vs. $\lambda$ as it zeros the rate of change of the slip when equal to the applied brake torque $T_b$. The wheel slip control problem is essentially to regulate the value of the longitudinal slip $\lambda$ to a given setpoint $\lambda_s$ and apply optimal braking force that corresponds to the maximum value along the tire force-slip curve as long as possible until the vehicle reaches a safe speed. The slip set-point can be obtained from a set of constants as in the conventional rule-based ABS algorithms or it can also be commanded from a higher-level control system such as ESP. In either case, the controller must be robust with respect to uncertainties in the tire characteristics, the brake pads/discs, the variations in the road surface conditions, the load on the vehicle, etc. In this study an adaptation scheme is developed with a four-phase rule based algorithm to remove steady-state error due to model inaccuracies and in particular due to the surface friction coefficient $\mu_{max}$. The proposed control algorithm can be seen as a minimum-seek algorithm to optimize the threshold values in a four-phase rule set (prediction, hold-high, reselection and hold-low) w.r.t. the variations in the surface friction condition.

The optimized rule set is to be devised as an appropriate switching logic to confine the trajectory of the wheel slip dynamics (4.5) inside the adapted thresholds as well as to induce a limit cycle on the system. The evolution of limit cycles in piecewise linear functions such as the brake dynamics has been studied extensively. Two good examples are by Wellstead and Pettit in [133] and [134] using graphical methods (Bond graphs) and by Goncalves in [135] where the author analyzes stability of piecewise linear systems using linear matrix inequalities (LMI). Similarly, Tanelli et.al. in [136, 137] study limit cycles specifically in ABS and compose conditions for the existence of a limit cycle in an ABS integrated wheel dynamics. The given conditions basically define the interrelations between the defined thresholds among themselves and between the system isocline ($T_e$), and can be summarized as follows.

Condition 1 states that the upper threshold for the maximum allowable brake torque (prediction line) should not be allowed to intersect with the isocline. Condition 2 states the threshold for the lower threshold for minimum allowable brake torque (reselection line) has to intersect with the isocline. Finally Condition 3 indicates that the slip condition of the system trajectory that corresponds to when the trajectory intersects with the reselection line has to be lower than the slip condition at the intersection of the reselection line and the isocline in the saturation region of the tire force-slip curve. These conditions are utilized in this study to develop the constraints expressions so that they will be expected to guarantee to induce a limit cycle when set. The rule-set are defined by the following notations

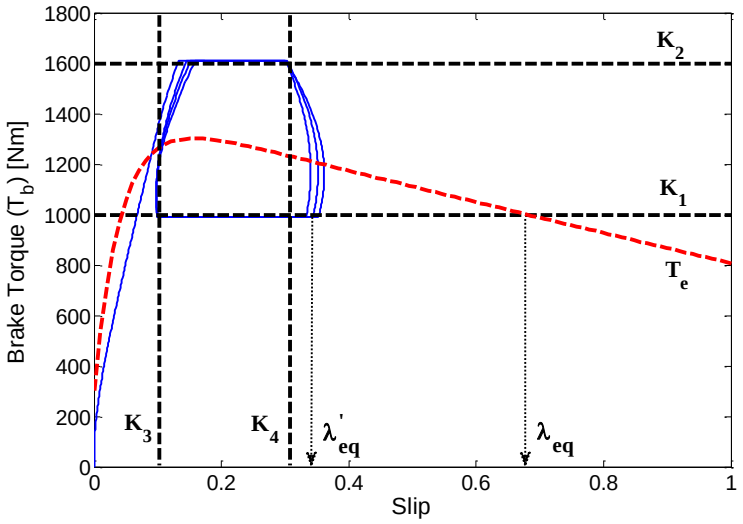


Figure 4.11: System constraints depicted on phase plane.

$$K_1 < T_a < K_2$$
$$K_3 < \lambda_a < K_4$$

Based on these conditions and the above notation, the inequality constraints to guarantee the existence of a limit cycle are defined.

$$\begin{aligned} C_1 \rightarrow K_2 &> T_e(\mu_{max}, \lambda_s) \\ C_2 \rightarrow K_1 &> T_e(\mu_{max}, 1) \\ C_3 \rightarrow K_1 &< T_e(\mu_{max}, \lambda_s) \\ C_4 \rightarrow \lambda'_{eq} &< \lambda_{eq} \\ C_5 \rightarrow K_3 &< \lambda_s \end{aligned} \tag{4.7}$$

where $\lambda_{eq}$ defines the slip condition when the isocline crosses $K_1$ threshold, and $\lambda'_{eq}$ states the slip conditions when the system trajectory crosses the same threshold. To carry out the optimization of this rule-set, a cost function is structured by the system state ($\lambda$), control inputs ($\mathbf{U}$) and the system constraints. Let the wheel slip dynamics (4.6) have the equilibrium point ($T_{b_s}$, $\lambda_s$) The proposed cost function can be written as:

$$J = \int \frac{1}{2}\left((\lambda - \lambda_s)Q(\lambda - \lambda_s) + (U - U_s)^T R(U - U_s)\right) + \xi(\dot{\lambda} - \dot{\lambda}_{sensor}) + \eta^T C \tag{4.8}$$

where $Q \in \mathbb{R}$ and $R \in \mathbb{R}^{6x6}$ refer to control gain values, $\dot{\lambda}_{sensor}$ is the rate of change of wheel slip as measured or computed by sensor readings, $C \in \mathbb{R}^5$ states the constraints, $\xi$ stands for the costate and $\eta^T \in \mathbb{R}^5$ refers to the Lagrange multipliers. The inequality constraints for the rule-set and control input are reformulated as equalities to be able to implement them into the cost function, so that the solution can be executed in a single run. To be able to accomplish this transformation proxy inputs are augmented into the constraint equations. The proxy inputs do not actually affect the system dynamics however indicate the level of offset of the system trajectory from the designated thresholds.

$$\begin{aligned}
K_2^2 - \left[R_w F_z \mu_{max}\left(1 + \frac{J(1-\lambda_s)}{mR_w^2}\right)\right]^2 &= U_1^2 \geq 0 \\
K_1^2 - (R_w F_z \mu_{max})^2 &= U_2^2 \geq 0 \\
\left[R_w F_z \mu_{max}\left(1 + \frac{J(1-\lambda_s)}{mR_w^2}\right)\right]^2 - K_1^2 &= U_3^2 \geq 0 \\
\lambda_{eq}^2 - (\lambda'_{eq})^2 &= U_4^2 \geq 0 \\
\lambda_s^2 - K_3^2 &= U_5^2 \geq 0
\end{aligned} \tag{4.9}$$

The equality constraints are then given as:

$$\begin{aligned}
C_1 &= U_1^2 - K_2^2 + \left[R_w F_z \mu_{max}\left(1 + \frac{J(1-\lambda_s)}{mR_w^2}\right)\right]^2 \\
C_2 &= U_2^2 - K_1^2 + (R_w F_z \mu_{max})^2 \\
C_3 &= U_3^2 + K_1^2 - \left[R_w F_z \mu_{max}\left(1 + \frac{J(1-\lambda_s)}{mR_w^2}\right)\right]^2 \\
C_4 &= U_4^2 - \lambda_{eq}^2 + (\lambda'_{eq})^2 \\
C_5 &= U_5^2 - \lambda_s^2 + K_3^2
\end{aligned} \tag{4.10}$$

Substituting eq. 4.10 into eq. 4.7 completes the definition of the cost function. Analytically solving the optimization problem for this cost function is neither likely nor feasible; therefore numerical methods are utilized to compute the solutions. The minimization of the proposed cost function is accomplished by solving for its differential when it converges to zero ($dJ = 0$). In what follows, the differential of the cost function is given as:

$$dJ = \frac{\partial J}{\partial \lambda} d\lambda + \frac{\partial J}{\partial \mathbf{U}^T} d\mathbf{U} + \frac{\partial J}{\partial \eta^T} d\eta \tag{4.11}$$

The solution can be obtained by equating each partial derivative to zero which provides a system of equations to be solved for the adaptive threshold values. The partial derivative of the cost function w.r.t. the system state $\lambda$ provides a single equation which can be solved to find the system costate $\xi/$

$$\begin{aligned} \frac{\partial J}{\partial \lambda} d\lambda &= \left( Q(\lambda - \lambda_s) + \xi \frac{\partial \dot{\lambda}}{\partial \lambda} \right) d\lambda = 0 \\ &\rightarrow \quad Q(\lambda - \lambda_s) + \xi \frac{\partial \dot{\lambda}}{\partial \lambda} = 0 \end{aligned} \tag{4.12}$$

To be able to compute $\partial\dot{\lambda}/\partial\lambda$, the tire forces $F_x$ can be approximated by the widely accepted Burckhardt model (eq. 2.4) as in the stability analysis completed in Chapter 2. Having the surface friction information, the tire force-slip curve can be reconstructed to find corresponding model coefficients by using a linear regression algorithm. After calculating the costate $\xi$ that zeros the first partial derivative, the partials of the cost function w.r.t. the inputs and the Lagrange multipliers are computed. The partial of the cost function w.r.t. the input vector augmented with the proxy inputs $\mathbf{U} = [U_1 - U_6 \quad T_b]^T$ provides a set of 6 equations.

$$\begin{aligned} \frac{\partial J}{\partial \mathbf{U}^T} d\mathbf{U} &= \left[ \frac{\partial J}{\partial U_1} \frac{\partial J}{\partial U_2} \frac{\partial J}{\partial U_3} \frac{\partial J}{\partial U_4} \frac{\partial J}{\partial U_5} \frac{\partial J}{\partial U_6} \frac{\partial J}{\partial T_b} \right] d\mathbf{U}_{(6x1)} \\ &\rightarrow \quad \left[ \frac{\partial J}{\partial U_1} \frac{\partial J}{\partial U_2} \frac{\partial J}{\partial U_3} \frac{\partial J}{\partial U_4} \frac{\partial J}{\partial U_5} \frac{\partial J}{\partial U_6} \frac{\partial J}{\partial T_b} \right] = 0 \end{aligned} \tag{4.13}$$

In the computation of the above set of equations, the input control gain $\mathbf{R}$ is taken as a positive semi-definite diagonal weight matrix that individually penalizes the input offsets.

The set of equations can be reformulated as:

$$\begin{aligned} \frac{\partial J}{\partial \eta^T} d\eta &= (\mathbf{C}^T)_{(1x5)} d\eta_{(5x1)} \\ &\rightarrow \mathbf{C} = \mathbf{0}_{(5x1)} \end{aligned} \tag{4.14}$$

The resulting 11 equations can be solved simultaneously by numerical analysis for the unknown thresholds and the Lagrange multipliers. To be able to find the threshold values, the proxy inputs $U_{1-5}$ are assumed to be zero as it is the goal of the constructed optimization scheme. The equations are then implemented in MATLAB/Simulink environment and solved numerically utilizing the Levenberg-Marquardt [138] algorithm (LM). The LM algorithm is a very widely used optimization algorithm based on nonlinear least squares minimization. To briefly summarize, the algorithm initially approximates the equations by their linearization. A new estimate for the subsequent iteration is assumed by adding an infinitesimal value $\check{\partial}$ on the predefined initial guess. In what follows, the differentiation of the system is solved for this infinitesimal value. If either the parameter vector at the calculated step or the reduction of sum of squares from the latest parameter vector fall below predefined limits, the algorithm stops and the last parameter vector is considered to be the solution. Further details of the algorithm is omitted here not to distract off of the course of this research but can be found in [139]. A disadvantage of the LM algorithm is its sensitivity to the initial guess for the parameters to be solved. Depending on the level of nonlinearity and the number of minima of the given set of equations, the algorithm might deviate from a feasible result. Therefore extra attention must be paid to the initial estimates of the sought parameters. On the other hand an advantage of this algorithm is that it does not require the system of equations to be square which fits to the problem in hand. The following section provides the results of the evaluation of the proposed algorithm using numerical analysis.

## 4.5 System Validation using Simulation

The proposed algorithm above is evaluated using a nonlinear 8 degree-of-freedom (DOF) vehicle model detailed in Chapter 2, which captures the rotational dynamics of the four wheels in addition to the vehicles longitudinal, lateral, roll and yaw motions. A finite state machine (FSM) is implemented in Simulink to select the control actions according to the threshold values computed in the proposed algorithm. The FSM is composed of four discrete

states, e.g. rise, hold-high, release, hold-low, each of which has an associated control action as their names imply. The transition between these states takes place when the system trajectory hits the adaptive threshold value.

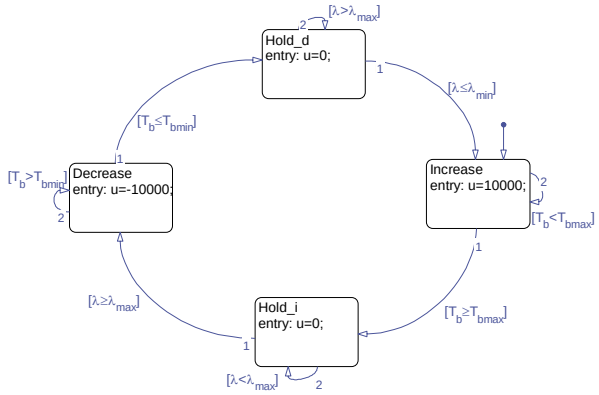


Figure 4.12: FSM description of the ABS state switching logic

The brake torque input is assumed to be implemented by a constant actuator rate at a nominal value of $10kNm/s$ which is proven to be a feasible value by Petruccelli et.al. in [140]. The wheel & vehicle longitudinal speed and the control of the longitudinal slip ratio over time are known as the two key parameters in quantifying ABS performance. Each of these key parameters will be presented to show the system performance for both a high-$\mu$ ($\mu_{max} = 0.85$) surface, representative of dry asphalt and a low-$\mu$ ($\mu_{max} = 0.3$) surface, representative of an icy surface. A series of straight line braking maneuvers are executed on different surface conditions. The dynamics of the adaptive threshold values are shown in the following figures. The results indicate that the solution algorithm allows the threshold values to converge to effective values before the ABS starts to operate; therefore yields to stable brake behavior.

Figure 4.13 shows the results for the adaptation of the threshold values $K_1$ to $K_4$ and the respective system parameters, $T_b$ and $\lambda$. The front tires seem to experience less slip oscillations and as a result can handle higher brake torque values. This can be grounded on the load transfer towards the front wheels which increases the tires road holding capacity and accordingly the increases the applicable brake force capacity. Whereas the rear tires experience a drop in the wheel loads which yields to the opposite effect and yields to higher levels of slip oscillations. Another point worth to note is that the brake torque for the front tires maintain almost constant around the maximum applicable value, which will not be possible due to the leaks and lags in a hydraulic brake system. In this numerical analysis,

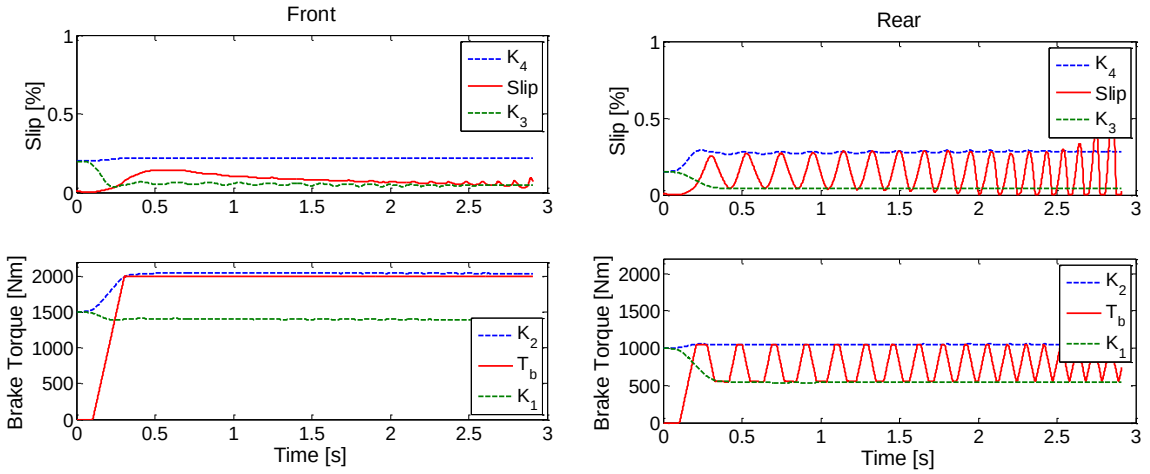


(a) Threshold evolution and system dynamics at front wheel

(b) Threshold evolution and system dynamics at rear wheel

Figure 4.13: Results for the threshold adaptation and system dynamics on high-$\mu$ surface condition

only the mechanical lag is introduced into the model. Given an initial velocity of $25m/s$, the algorithm yields to a satisfactory braking performance on the high-$\mu$ condition. The vehicle comes to a complete stop after $2.91s$ at around $40.12m$. Figure 4.14 also shows the wheel and vehicle speeds variations.

Figure 4.15 shows the adaptation characteristics of the threshold values on the low-$\mu$ surface. As the surface friction level decreases, the tires road grip capability minimizes which also yields to higher levels of slip oscillations. Nevertheless the prediction and reselection rules successfully maintain stability of the brake system.

Figure 4.15 depicts the braking performance of the adaprive control algorithm in the low-$\mu$ surface. Given the same initial speed ($u_0 = 25m/s$), the vehicle comes to a complete stop after $6.44s$ at about $87.05m$.

Both tests show satisfactory braking performance under challenging conditions. The algorithm can confine the system specifically inside the prediction and reselection lines while maintaining the slip ratio within a close proximity to the desired slip (Figure 4.16). The increasing levels of slip oscillations towards the end of the braking occurs due to the decreasing velocity which yields to infinitely fast open loop wheel slip dynamics which the solution

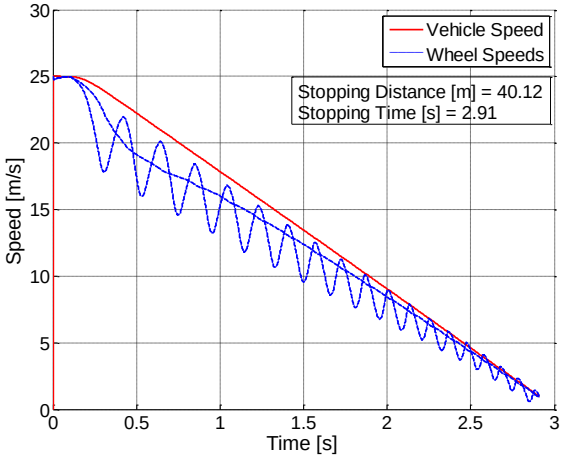


Figure 4.14: Braking performance of the proposed algorithm on high-$\mu$ surface

algorithm cannot cope with. Furthermore uncertainties such as load transfer or road bank might also cause increasing levels of slip oscillations.

To get a better measure of the improvements in the performance of the proposed intelligent tire based ABS algorithm, it is compared to a conventional ABS algorithm used in modern day vehicles. The details of the algorithm are provided by Day and Roberts in [103]. It utilizes a rule-based method to maintain longitudinal wheel slip in a certain range on the information provided by angular wheel speed and acceleration sensors. The following methodology explains the adopted selection criteria for the acceleration/deceleration thresholds.

- Wheel deceleration threshold ($-a$): The relationship between the wheel-deceleration and slip curves for different initial braking velocities ($10-40m/s$) was studied. Clearly, for high velocities, the deceleration threshold should be set at higher values. In contrast for low initial velocities the threshold should be decreased. A reasonable selection for this threshold could be the 10% slip value. Such a selection will be able to provide 10% slip for high initial braking velocities and slip exceeding 10%, but still lower than 20% for lower velocities.

- Wheel acceleration threshold ($+a$): This threshold is used to mark a positive tendency in the wheel acceleration. Appropriate threshold values are $3-6m/s^2$.

- Wheel acceleration threshold ($+A$): This threshold denotes a recovery from the pre-

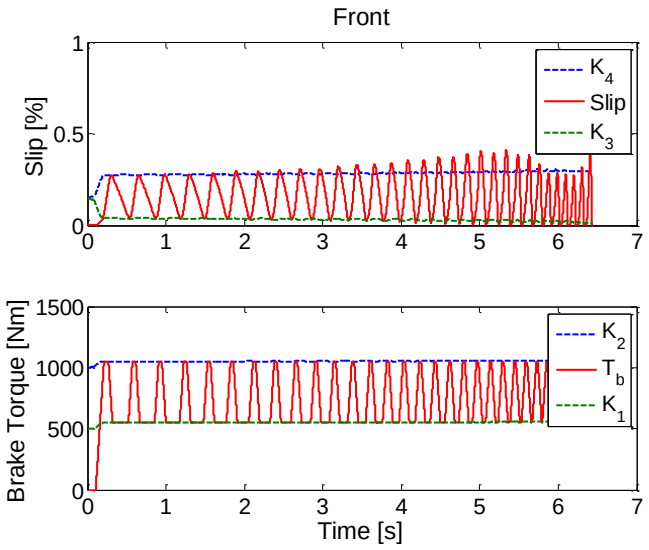


(a) Threshold evolution and system dynamics at front wheel

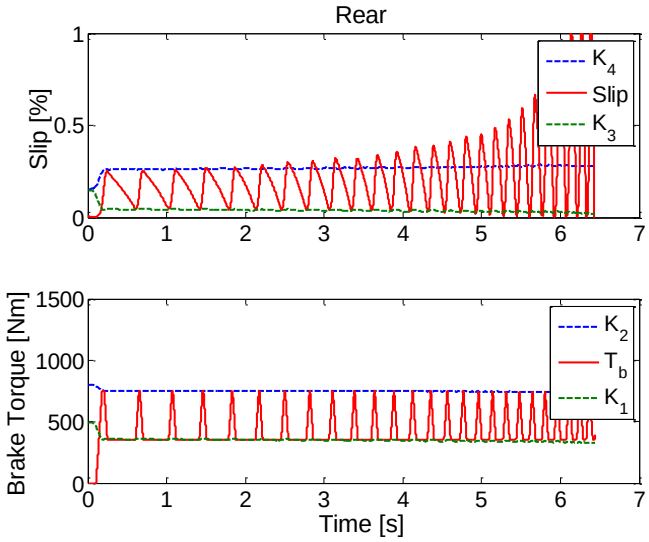


(b) Threshold evolution and system dynamics at rear wheel

Figure 4.15: Results for the threshold adaptation and system dynamics on low-$\mu$ surface condition

dicted lock and is higher than $(+a)$. Selection of too high values of $(+A)$ threshold results in higher recovered wheel speed and lower slip values. Suitable threshold values are $9 - 12m/s^2$.

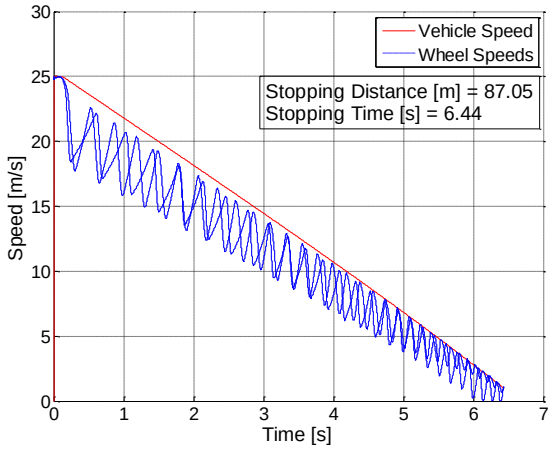


Figure 4.16: Braking performance of the proposed algorithm on low-$\mu$ surface

The summary of the triggering signals and threshold values are given in Table 4-1.

Table 4.1: Triggering signals and threshold values for the baseline ABS

| **Command** | **Triggering Signal** | **Threshold Value** |
|---|---|---|
| **Hold** | $-a$ | $-50m/s^2$ |
| **Decrease** | $> slip$ | $20\%$ |
| **Stop Decrease** | $+a$ | $4m/s^2$ |
| **Increase** | $+A$ | $10m/s^2$ |

Figure 4.17 a and b show the performance of the baseline ABS model on high-$\mu$ and low-$\mu$ surfaces, respectively. Given an initial velocity of $25m/s$, the results show that the vehicle requires $44.86m$ to come to a complete stop on the high-$\mu$ surface, whereas on the low-$\mu$ surface this distance is $108.25m$. Clearly, executing the described adaptive threshold based ABS control algorithm shows an improved braking performance respective to the conventional algorithm. The longitudinal slip quickly averages around the calculated desired slip ratio after brake application and oscillates about this point for the remainder of the braking maneuver with the help of the adaptive threshold values, until the ABS cut- off speed is reached. The result of staying within these close boundaries is an increase in the average longitudinal braking force available to the tire.

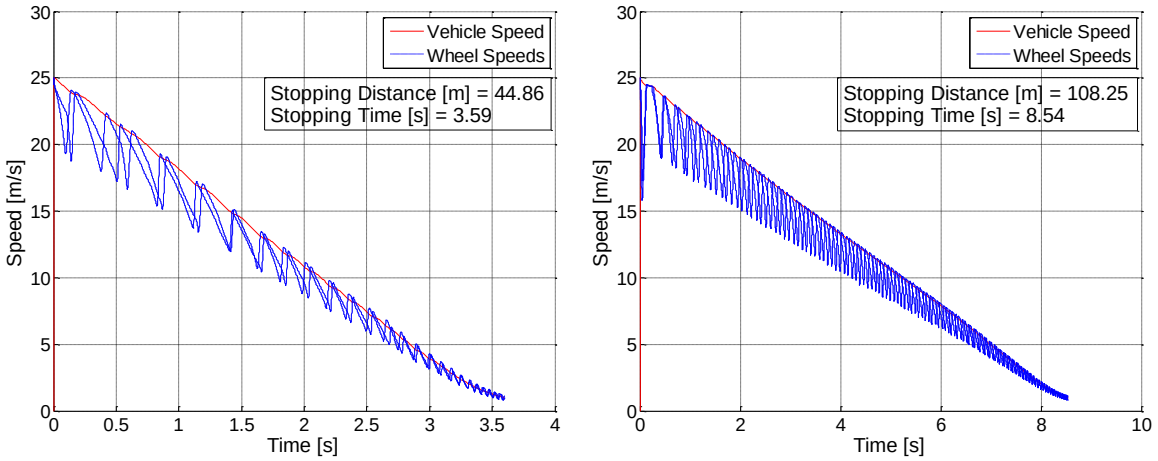


(a) High-$\mu$ surface testing

(b) Low-$\mu$ surface testing

Figure 4.17: Braking performance of the conventional ABS algorithm on straight line braking

The comparative phase plane analysis shown in Figure 4.18 depicts the system trajectory behavior using the adaptive threshold and conventional ABS algorithms. As the figures indicate, the adaptive threshold algorithm significantly reduces the variations in the applied brake torque without excessive disturbance in the slip oscillations that might cause instability as it is guaranteed intrinsically by the predefined constraints. Consequently, this reduction in the brake torque variations yields to a shorter stopping distance which might distinguish between a crash or safe brake scenario.

Finally the proposed algorithm is evaluated on surface conditions with varying friction levels. First a jump-$\mu$ condition is implemented where the surface friction coefficient is assumed to jump from high to low at $15m$ and then back to high after $30m$ (Figure 4.19). This maneuver can be very harsh for many conventional rule-based ABS logics as these sudden changes cannot be easily apprehended due to the lack of surface friction information and might lead to instabilities. On the other hand the proposed algorithm adapts the ruleset definitions with respect to these variations and thereby maximizes the brake force utilization. Figure 4.20 depicts the adaptation of the threshold values and the resulting brake torque and slip variations. Obtaining the surface friction from the estimation scheme, the algorithm computes the optimal threshold values for improved braking performance and guaranteed stability as well. Next the system is put on test under slip-$\mu$ condition where the left wheel are kept on the same jump-$\mu$ surface while the right wheels are driven on high friction. Figure

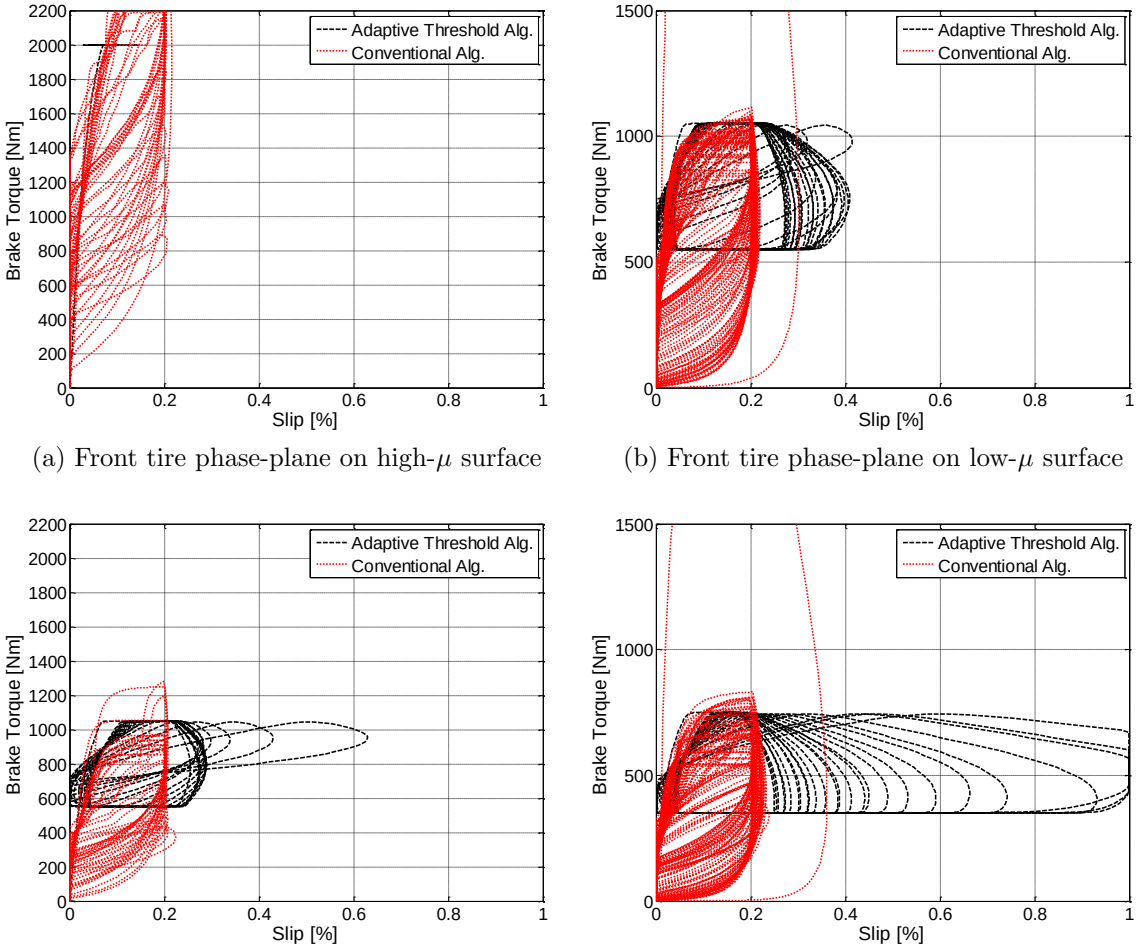


(a) Front tire phase-plane on high-$\mu$ surface

(b) Front tire phase-plane on low-$\mu$ surface

(c) Rear tire phase-plane on high-$\mu$ surface

(d) Rear tire phase-plane on low-$\mu$ surface

Figure 4.18: Phase plane comparison of adaptive threshold and conventional ABS algorithms in high-$\mu$ and low-$\mu$ tests

4.22 summarizes the results in the same manner to underline the adaptation of thresholds on the left wheel brakes while maintaining an optimal level for avoiding any lock-up scenario on the right hand side. The phase-plane of the system similarly proves guaranteed stability while providing admirable braking performance.

It is clear from the executed simulations that the effect of the varying friction coefficient is significant, but the proposed algorithm handles these unexpected changes in the road surface conditions quite well. With the momentary surface condition information from the smart tire integrated estimation scheme the proposed algorithm copes with the variations by adapting the threshold values. The comparison between the time histories of tire slip (Figure 4.20 and

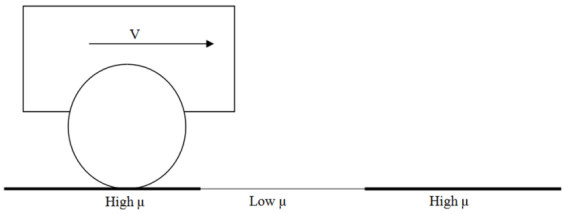


Figure 4.19: Jump-$\mu$ test condition

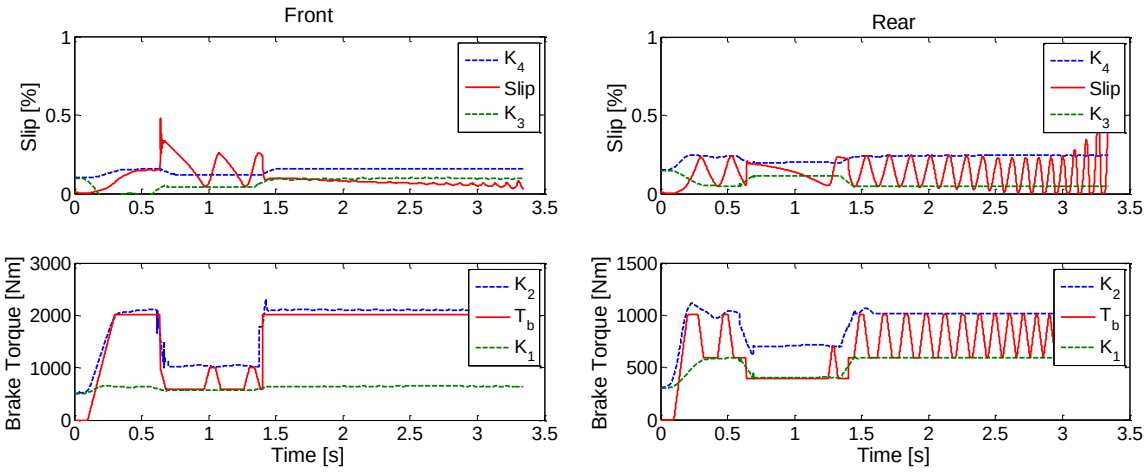


(a) Threshold evolution and system dynamics at front wheel

(b) Threshold evolution and system dynamics at rear wheel

Figure 4.20: Results for the threshold adaptation and system dynamics on jump-$\mu$ surface condition

4.22) clearly shows how the instantaneous information about the change of friction coefficient allows the ABS controller to prevent wheel lock-up during the jump from high friction to low friction. This can be attributed to the fact that the adaptive threshold algorithm yields to a significant reduction in both frequency and amplitude of the oscillations in the applied brake torque as well as in slip. Figure 4.23 is a good indicator for this reduction, which compares the resulting phase plane ($T_b$ vs. $\lambda$) of each algorithm at front and rear tires. As summarized in the introduction, the reduced oscillation levels helps to maximize the tire grip level in which manner it also allows higher brake forces to be applied. As a result, the adaptive algorithm yields to considerable improvement in the braking performance by decreasing the stopping distance significantly. Figure 4.25 shows the vehicle and wheel speed variations in comparison between the two algorithms.

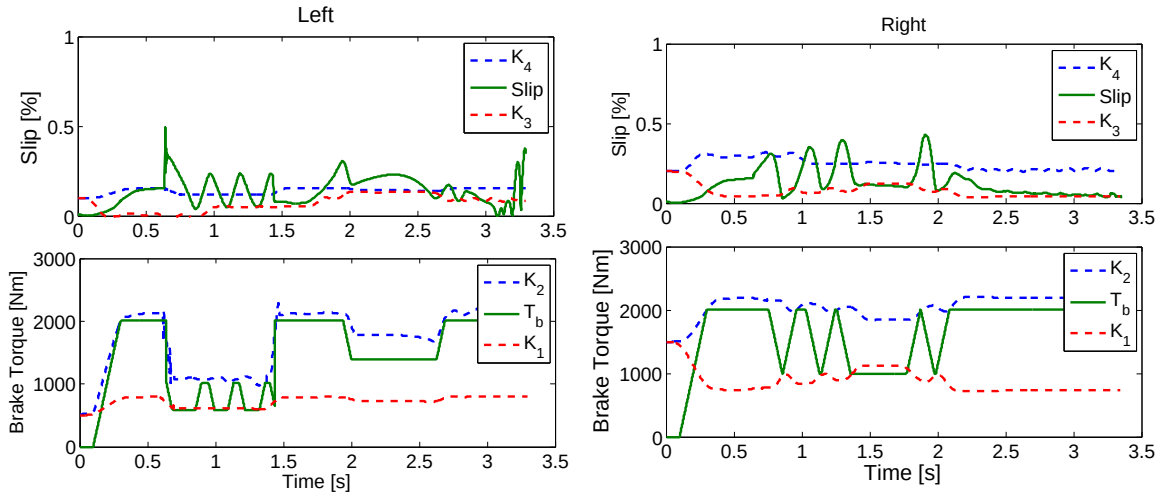


(a) Threshold evolution and system dynamics at left wheel

(b) Threshold evolution and system dynamics at right wheel

Figure 4.21: Results for the threshold adaptation and system dynamics on split-$\mu$ surface condition

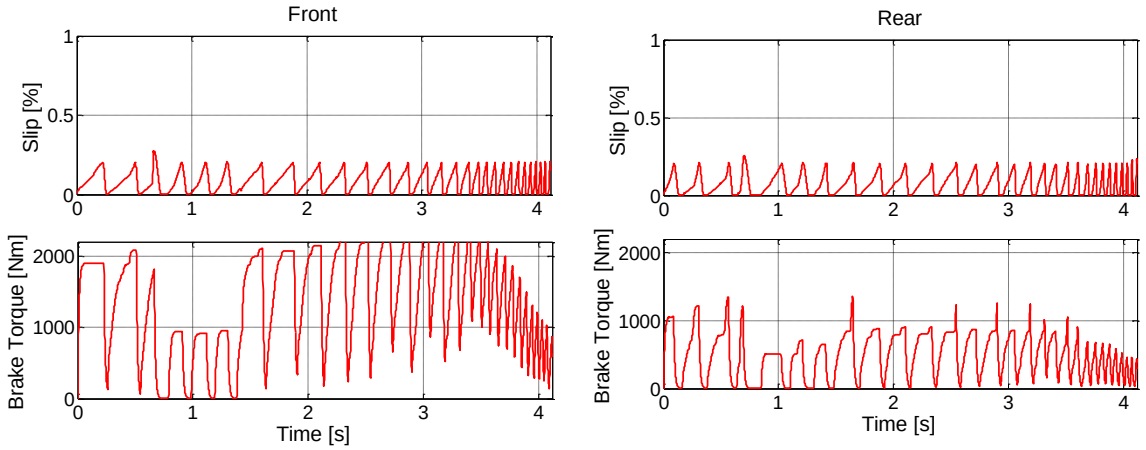


(a) Brake torque and slip performance for front tire

(b) Brake torque and slip performance for rear tire

Figure 4.22: Results for the conventional ABS algorithm on jump-$\mu$ surface condition

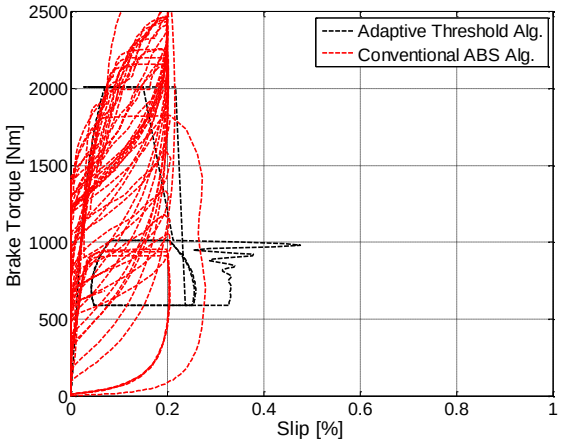


(a) Front tire phase plane on jump-$\mu$

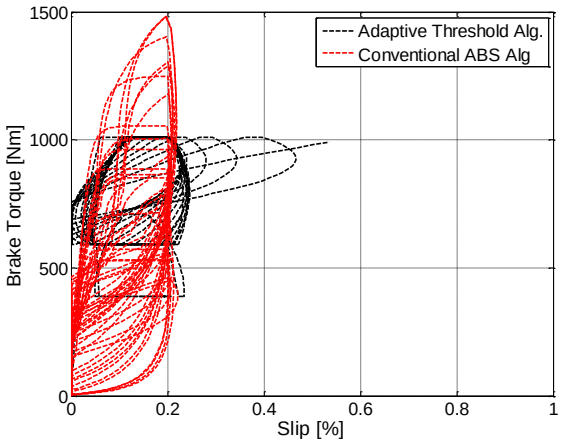


(b) Rear tire phase plane on jump-$\mu$

Figure 4.23: Phase plane comparison of adaptive threshold and conventional ABS algorithms in jump-$\mu$ test

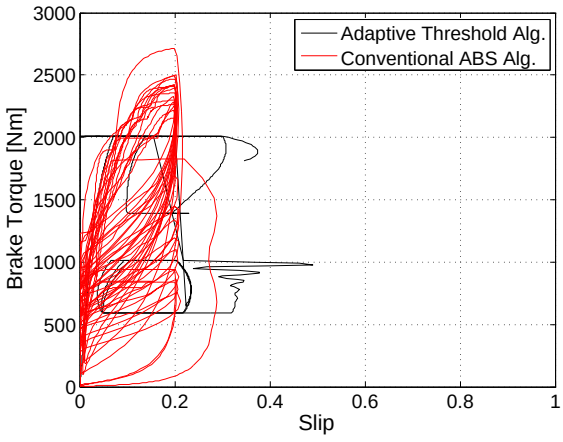


(a) Front tire phase plane on split-$\mu$

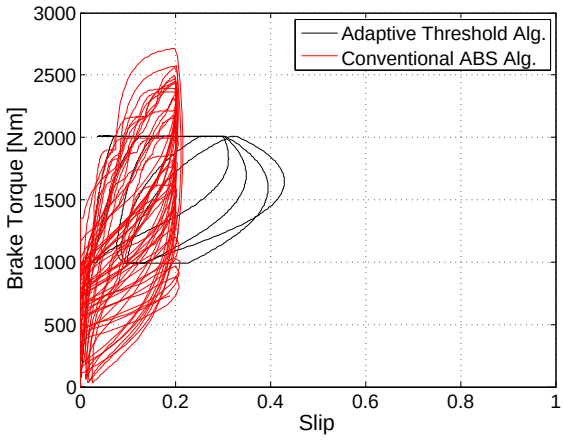


(b) Rear tire phase plane on split-$\mu$

Figure 4.24: Phase plane comparison of adaptive threshold and conventional ABS algorithms in split-$\mu$ test

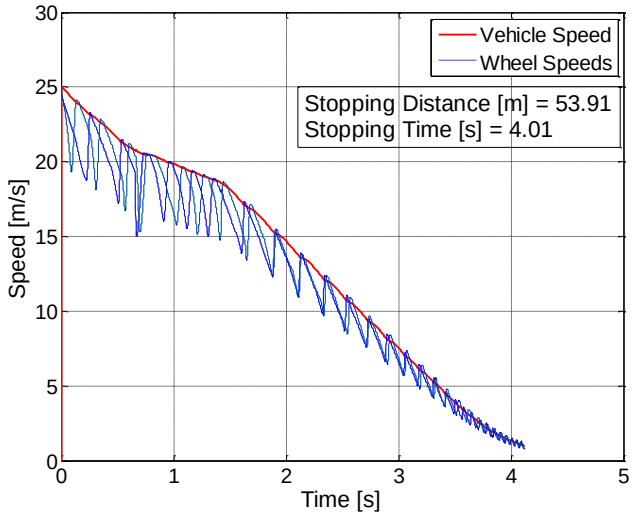


(a) Conventional ABS algorithm performance

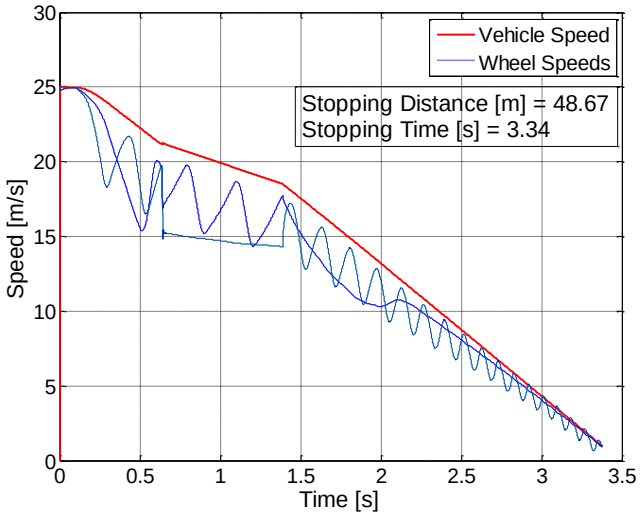


(b) Adaptive threshold algorithm performance

Figure 4.25: Comparison of algorithm performances in jump-$\mu$ surface test

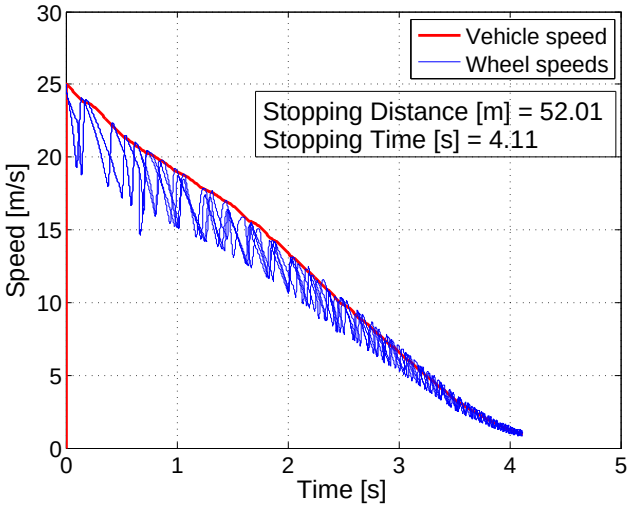


(a) Conventional ABS algorithm performance

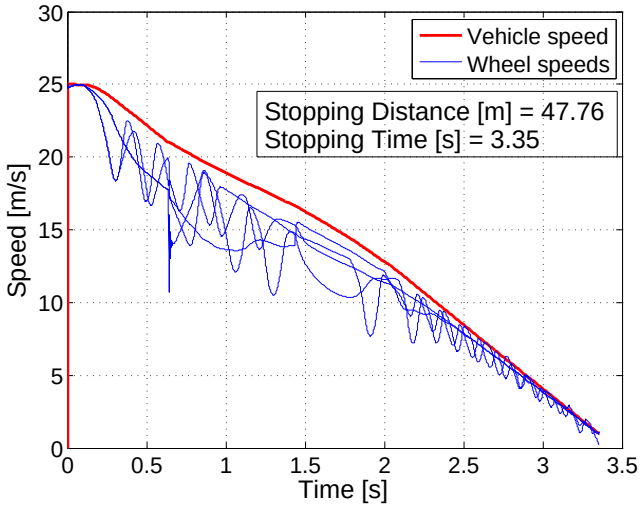


(b) Adaptive threshold algorithm performance

Figure 4.26: Comparison of algorithm performances in split-$\mu$ surface test

## 4.6 Conclusion

This chapter presents a road surface condition classification system through the integration of a smart tire system with a model based observer, which is later employed in an adaptive rule-based ABS algorithm developed based on the optimization of brake thresholds. Simulations are carried out on a series of braking maneuvers to examine the possible improvements with the proposed ABS algorithm in braking performance, assuming that the additional information concerning road surface condition could be provided by the sensor fusion method. The results reveal that the proposed algorithm significantly reduces the oscillations in the applied brake and slip values which yields to an increase in the tire road grip levels and thereby in the applied brake force. Impressive improvements are obtained for the executed straight line braking tests the results from the numerical analyses. Table 4.2 compares and summarizes the results for both algorithms.

Table 4.2: Summary of the system evaluation using numerical analysis

| | High-$\mu$ surface | | Low-$\mu$ surface | |
|---|---|---|---|---|
| | Stopping Distance [m] | Improvement over baseline [%] | Stopping Distance [m] | Improvement over baseline [%] |
| Conventional ABS | 44.86 | - | 108.25 | - |
| Adaptive Threshold | 40.12 | 10.56 | 87.05 | 19.58 |
| | Jump-$\mu$ surface | | Split-$\mu$ surface | |
| | Stopping Distance [m] | Improvement over baseline [%] | Stopping Distance [m] | Improvement over baseline [%] |
| Conventional ABS | 53.91 | - | 52.01 | - |
| Adaptive Threshold | 48.67 | 9.72 | 47.76 | 8.17 |

In the light of these results, the following conclusions can be drawn. The actual road surface

condition information provided by an integrated estimation approach using smart tire technology can be used to develop an adaptive rulebased ABS algorithm. The adaptive nature of the proposed algorithm provides significant performance improvements with less slip and brake torque oscillations which underline that knowing the actual road surface condition can be quite favorable for enhancing the current ABS models and reducing the vehicle stopping distance significantly. In addition, following the same approach (rule-based) as in the conventional ABS algorithms allows the proposed algorithm to be implemented on the currently available braking systems without the requirement of major modifications.

# Chapter 5

# Integrated Vehicle Control Systems

## 5.1 Introduction

The studies detailed in Chapters 3 and 4 provide strong arguments on the utilization and advantages of the smart tire technology in vehicle control applications. The proposed control algorithms yield to considerable performance improvements in the addressed vehicle states, namely the stability and braking dynamics. Nevertheless the daily driving conditions might easily pose more complicated operation conditions which require multiple of such controllers to activate simultaneously. On the other hand, the co-existence of several control subsystems without coordination can cause various drawbacks. For example, a major practical issue is that the design of software and hardware becomes more complicated due to the dramatically increased number of sensors and signal transmission requirements. Another critical issue is that, because of the possible function overlapping among these systems, there will be inevitable conflicts in their control objectives and control actions. If not coordinated, the performance of these systems might get worse than that of individual systems or even worse than a passive system without any active control. For example, anti-lock braking systems (ABS) and electronic stability programs (ESP) are both based on the tire slip ratio control, however the primary objective of an ABS is to maintain the slip ratio around the optimal value (normally corresponding to peak longitudinal friction coefficient), while the objective of ESP is to control wheel slip ratios properly for vehicle stability improvement via braking the selected wheels, requiring optimum use of the available lateral force.

As a result, the ensuing challenge becomes successful integration of these control systems to cope with such conditions while maintaining a comfortable ride, and based on the above summary, the two key problems of integrated vehicle dynamics control to be solved are:

- to avoid the conflicts and interventions among different subsystems;
- to exploit the potentials of each subsystems by communication and coordination among the sub-systems since different systems have different action domains.

The synthesis of such integrated control schemes has been studied extensively; Chapter 3 provided an exhaustive literature review focusing on the stability control applications. Common aliases for these methods are *Integrated Vehicle Dynamics Control* or *Integrated Chassis Control* (ICC). Despite the abundant number of publications, the definition for ICC systems is not standardized. Nevertheless, the expected attributes from such a system are definitive, i.e. they need to coordinate multiple subsystems systematically according to control objectives and actions in terms of both software and hardware, rather than simply putting the subsystems altogether.

Inspired by this challenge, this chapter describes the derivation of an ICC algorithm for vehicle stability control. The first application takes the algorithms derived in Chapters 3 and 4 as the basis and employs a dynamic control allocation algorithm to successfully integrate the two. The control allocation task intends to deploy the wheel brake forces to generate the desired yaw-moment on the vehicle chassis and it is accomplished through an optimization procedure utilizing a weighted least squares method. The resulting control signals are then implemented via the ABS to avoid any possible wheel lock-up scenarios while providing sufficient braking performance. As a result, combined with the additional steering input, the system maintains vehicle yaw stability even during a challenging evasive double lane change maneuver as given in Chapter 3. The next focal point of the chapter is the introduction of a new adaptive control methodology, namely the $\mathcal{L}_1$ adaptive control method, to replace the upper-level stability control algorithm. The considerable advantages this new method introduces are: it proposes an architecture that yields to robust performance while allowing fast adaptation so long as the actuator dynamics concede; and it extends the adaptation of system dynamics from selected parameters to non-linear functions of time and states. The subsequent sections detail these applications and present results of simulation studies for evaluating the proposed systems' performances.

## 5.2 Integrated Stability Control based on Lyapunov Direct Method

As summarized above, a decentralized implementation of active safety systems might easily impair the vehicle performance and even destabilize the system due to objective conflicts. A major challenge in the integration of control systems is the inherently coupled vehicle dynamics states. To tackle with such issues, the control algorithm needs to be derived considering a so-called *centralized* or *multi-layered* structure where the control inputs should be implementable considering lower level control and actuator dynamics; and any possible objective conflict is taken care at an upper-level algorithm. Based on these terms, this section combines the studies in Chapters 3 and 4 and forms an integrated vehicle control system by dynamically allocating the required brake forces with respect to the applied yaw-moment and actuator dynamics.

### 5.2.1 Control Allocation Problem

Control allocation deals with the problem of distributing a given control demand among an available set of actuators. Most existing methods are static in the sense that the resulting control distribution depends only on the current control demand. In this study a method for dynamic control allocation is proposed, in which the resulting control distribution utilizes time varying system dynamics as well as the distribution in the previous sampling instant. As a result, the method extends regular quadratic programming control allocation by also penalizing the actuator rates. This also leads to a frequency dependent control distribution which can be designed to account for different actuator bandwidths. The control allocation problem is posed as a constrained quadratic program which provides automatic redistribution of the control effort when one actuator saturates in position or in rate. When no saturation occurs, the resulting control distribution coincides with the control demand fed through a linear filter.

The existence of a redundancy in the set of existing actuators set (e.g. four wheel brakes) allows for more than one combination of actuator activities to yield to the same generalized control action, and hence give the same overall system behavior. This design freedom is often used in the advantage of the control allocation process, e.g. the priority among the multiple

set of actuator combinations or among the actuators can be determined by optimizing a static performance index. This can also be thought of as affecting the distribution of control effect in magnitude among the actuators. Regardless of the selected method (optimization based allocation [141, 142], daisy chain allocation [143], direct allocation [144] etc.), the resulting mapping from the generalized or virtual control command, v(t), to the upper-level control input, u(t), can be written as a static relationship:

$$u(t) = h\left(v(t)\right) \tag{5.1}$$

A possibility that has been little explored is to also affect the distribution of the control effect in the frequency domain, and use the redundancy to have different actuators operate in different parts of the frequency spectrum. This requires the mapping from $v$ to $u$ to depend also on previous values of $u$ and $v$, hence:

$$u(t) = h\left(v(t), u(t-T), v(t-T), u(t-2T), v(t-2T), ...\right) \tag{5.2}$$

where $T$ is the sampling interval. This equation results in the *dynamic control allocation* procedure. In this study, the method for handling the dynamic control allocation is implemented through the so-called quadratic programming scheme as in the following form:

$$u(t) = \underset{\underline{u}<u<\overline{u}}{\arg\min} \left(J(u(t)) + \gamma^2 \|W_v(Au(t) - v(t))\|^2\right) \tag{5.3}$$

The first term $J(u(t))$ represents a sub-cost for minimal actuator activity while the second term represents the constraint on tracking the virtual control command $v(t)$ computed by the upper level algorithm. In this study, the method is extended by an extra term added to the sub-cost optimization criterion to also penalize the actuator rates as explained above. The derivation for the brake-force allocation application is initiated by stating the relation between the yaw moment generated on the chassis and the wheel brake forces:

$$\begin{aligned} \Delta M_b &= \frac{t_r}{2}\left(F_{x_{fl}} + F_{x_{rl}} - F_{x_{fr}} - F_{x_{rr}}\right) \\ &+ l_f\left(\Delta F_{y_{fl}} + \Delta F_{y_{fr}}\right) - l_r\left(\Delta F_{y_{rl}} + \Delta F_{y_{rr}}\right) \end{aligned} \tag{5.4}$$

where $\Delta$ indicates the change in value. As well known, utilizing longitudinal forces will yield to a change in the lateral force due to the limited force generation capacity of tires which can be explained by the friction circle phenomena. In this study the Dugoff tire model (as

detailed in Ch. 2) is utilized to come up with an expression for the change in the lateral tire forces with respect to the longitudinal tire forces (friction ellipse concept). In what follows, the rate of change in lateral force can be expressed as:

$$\Delta F_{y_i} = \frac{\partial F_{y_i}}{\partial F_{x_i}} F_{x_i} \tag{5.5}$$

where $i = (fr, fl, rr, rl)$. Using this expression the yaw moment can be rewritten as:

$$\begin{aligned} \Delta M_b &= \frac{t_r}{2}\left(F_{x_{fl}} + F_{x_{rl}} - F_{x_{fr}} - F_{x_{rr}}\right) \\ &+ l_f\left(\frac{\partial F_{y_{fl}}}{\partial F_{x_{fl}}} F_{x_{fl}} + \frac{\partial F_{y_{fr}}}{\partial F_{x_{fr}}} F_{x_{fr}}\right) - l_r\left(\frac{\partial F_{y_{rl}}}{\partial F_{x_{rl}}} F_{x_{rl}} + \frac{\partial F_{y_{rr}}}{\partial F_{x_{rr}}} F_{x_{rr}}\right) \end{aligned} \tag{5.6}$$

In addition, the rate of change of the lateral force with respect to longitudinal can be written using the analytical expression of the Dugoff model:

$$\frac{\partial F_{y_i}}{\partial F_{x_i}} = \frac{\partial F_{y_i}}{\partial \lambda_i} / \frac{\partial F_{x_i}}{\partial \lambda_i} \tag{5.7}$$

$$\frac{\partial F_{y_i}}{\partial \lambda_i} = C_\alpha tan(\alpha_i) \frac{\dot{f}(\xi_i)(1-\lambda_i) + f(\xi_i)}{(1-\lambda_i)^2} \tag{5.8}$$

$$\frac{\partial F_{x_i}}{\lambda_i} = C_\lambda \frac{\dot{f}(\xi_i)\lambda + (1+\lambda) f(\xi_i)}{(1-\lambda_i)^2} \tag{5.9}$$

Therefore:

$$\frac{\partial F_{y_i}}{\partial F_{x_i}} = \frac{C_\alpha tan(\alpha_i)(\dot{f}(\xi_i)(1-\lambda_i) + f(\xi_i))}{C_\lambda(\dot{f}(\xi_i)\lambda + (1+\lambda) f(\xi_i))} \tag{5.10}$$

The differentiation of the function $f(\xi)$ with respect to $\lambda$ are given as:

$$\dot{f}(\xi) = \begin{cases} f_1 - f_2 - f_3, & \text{if} - 2 < \dfrac{\mu F_z(\lambda - 1)}{\sqrt{\lambda^2 C_\lambda^2 + C_\alpha^2 \tan(\alpha)^2}} \\ 0, & \text{if} - 2 \geq \dfrac{\mu F_z(\lambda - 1)}{\sqrt{\lambda^2 C_\lambda^2 + C_\alpha^2 \tan(\alpha)^2}} \end{cases} \tag{5.11}$$

where

$$f_1 = \frac{\lambda\mu C_\lambda^2 F_z(\lambda-1)\left(\dfrac{\mu F_z(\lambda-1)}{2\sqrt{\lambda^2C_\lambda^2+C_\alpha^2\tan(\alpha)^2}}+2\right)}{2\left(\lambda^2C_\lambda^2+C_\alpha^2\tan(\alpha)^2\right)^{\frac{3}{2}}} \tag{5.12}$$

$$f_2 = \frac{\mu F_z(\lambda-1)\left(\dfrac{\mu F_z}{2\sqrt{\lambda^2C_\lambda^2+C_\alpha^2\tan(\alpha)^2}}-\dfrac{\mu F_z(\lambda-1)}{2(\lambda^2C_\lambda^2+C_\alpha^2\tan(\alpha)^2)^{\frac{3}{2}}}\right)}{2\sqrt{\lambda^2C_\lambda^2+C_\alpha^2\tan(\alpha)^2}} \tag{5.13}$$

$$f_3 = \frac{\mu F_z\left(\dfrac{\mu F_z(\lambda-1)}{2\sqrt{\lambda^2C_\lambda^2+C_\alpha^2\tan(\alpha)^2}}+2\right)}{2\sqrt{\lambda^2C_\lambda^2+C_\alpha^2\tan(\alpha)^2}} \tag{5.14}$$

Based on the above results, the dynamic control allocation problem is formulated that computes the actuator control signals with minimum possible activation while being subjected to minimal error between the implemented and desired yaw moment. Consequently, the implemented yaw moment value as given in equation 5.6 can be rewritten by the multiplication of a coefficient matrix that includes the above differentiations and the wheel brake forces as the lower level control signals:

$$M_b = B_{lower}u(t) \tag{5.15}$$

where the coefficient matrix $B_{lower}$ is defined as:

$$B_{lower} = \left[\left(\frac{t_r}{2}+l_f\frac{\partial F_{y_{fl}}}{\partial F_{x_{fl}}}\right) \quad \left(-\frac{t_r}{2}+l_f\frac{\partial F_{y_{fr}}}{\partial F_{x_{fr}}}\right) \quad \left(\frac{t_r}{2}-l_r\frac{\partial F_{y_{rl}}}{\partial F_{x_{rl}}}\right) \quad \left(-\frac{t_r}{2}-l_r\frac{\partial F_{y_{rr}}}{\partial F_{x_{rr}}}\right)\right] \tag{5.16}$$

and the control signal vector $u(t)$ is formed by the wheel brake forces:

$$u(t) = \begin{bmatrix}F_{x_{fl}} & F_{x_{fr}} & F_{x_{rl}} & F_{x_{rr}}\end{bmatrix}^T \tag{5.17}$$

This expression provides the constraint for the force allocation problem in terms of the longitudinal tire forces that will successfully implement the desired yaw moment computed by the VSC algorithm. Substituting the above results into the quadratic programming problem in equation 5.3, it can be rewritten as follows:

$$u(t) = \underset{\underline{u}<u<\overline{u}}{\arg\min}\left(\left(\|W_{u_1}u(t)\|^2+\|W_{u_2}u(t-T)\|^2\right)+\gamma^2\|W_v(B_{lower}u-M_b)\|^2\right) \tag{5.18}$$

where $u(t-T)$ stands for the control signal at the previous time step. The weighting coefficient ($W_v$), which becomes a scalar in this case because $M_b \in \mathbb{R}$, scales the upper level control input, and $\underline{u}$ and $\overline{u}$ define the lower and upper bounds respectively for the actuators. The upper bound can be defined using the friction circle phenomena:

$$\overline{u} = \sqrt{\mu^2 F_{z_i}^2 - F_{y_i}^2} \geq F_{x_i} \tag{5.19}$$

As the DYC in this study is based on differential braking action, the lower bound for control can be defined as zero ($\underline{u} = 0 < F_{x_i}$). The sub-cost function $J(u(t))$ is formed by respectively scaling the $\mathcal{L}_2$-norm of the current and previous time step control signals. The last scale factor ($\gamma$) in the proposed cost function defines the emphasis on the minimization of the error in force allocation to meet the requirement from the upper level control.

This linearly-constrained quadratic problem is solved numerically using a weighted-least-square (WLS) approach and computes the optimal wheel brake forces ($F_{x_i}$) at each sample. For computational efficiency the algorithm initializes with a reformulation as in the below form:

$$\begin{aligned} u(t) &= \underset{\underline{u}<u<\overline{u}}{\arg\min} \left\{ \left\| \left[ \begin{pmatrix} \gamma W_v B_{lower} \\ W_u \end{pmatrix} \right] u(t) - \left[ \begin{pmatrix} \gamma W_v M_b \\ W_u u(t-T) \end{pmatrix} \right] \right\|^2 \right\} \\ &= \underset{\underline{u}<u<\overline{u}}{\arg\min} \left\{ \| A_{opt} u(t) - B_{opt} \|^2 \right\} \end{aligned} \tag{5.20}$$

For this reformulation to hold true without losing generality the weighing matrices $W_{u_1}$ and $W_{u_2}$ are to be assumed symmetric and such that:

$$W_u = \left( W_{u_1}^2 + W_{u_2}^2 \right)^{1/2} \tag{5.21}$$

The Active Set Algorithm (ASA) is utilized to numerically solve this problem and implemented in the MATLAB/Simulink environment for evaluation. The active set refers to the set of solutions that satisfies the constraints the optimization problem is subjected to; hence ASA is a widely preferred method in solving problems with equality and/or inequality constraints. The algorithm basically approximates to the optimal solutions by repetitively solving the given equality problems and finalizes at the allowable rate of convergence in the defined active

set [145]. Figure 5.1 details the algorithm implemented in numerical analysis software.

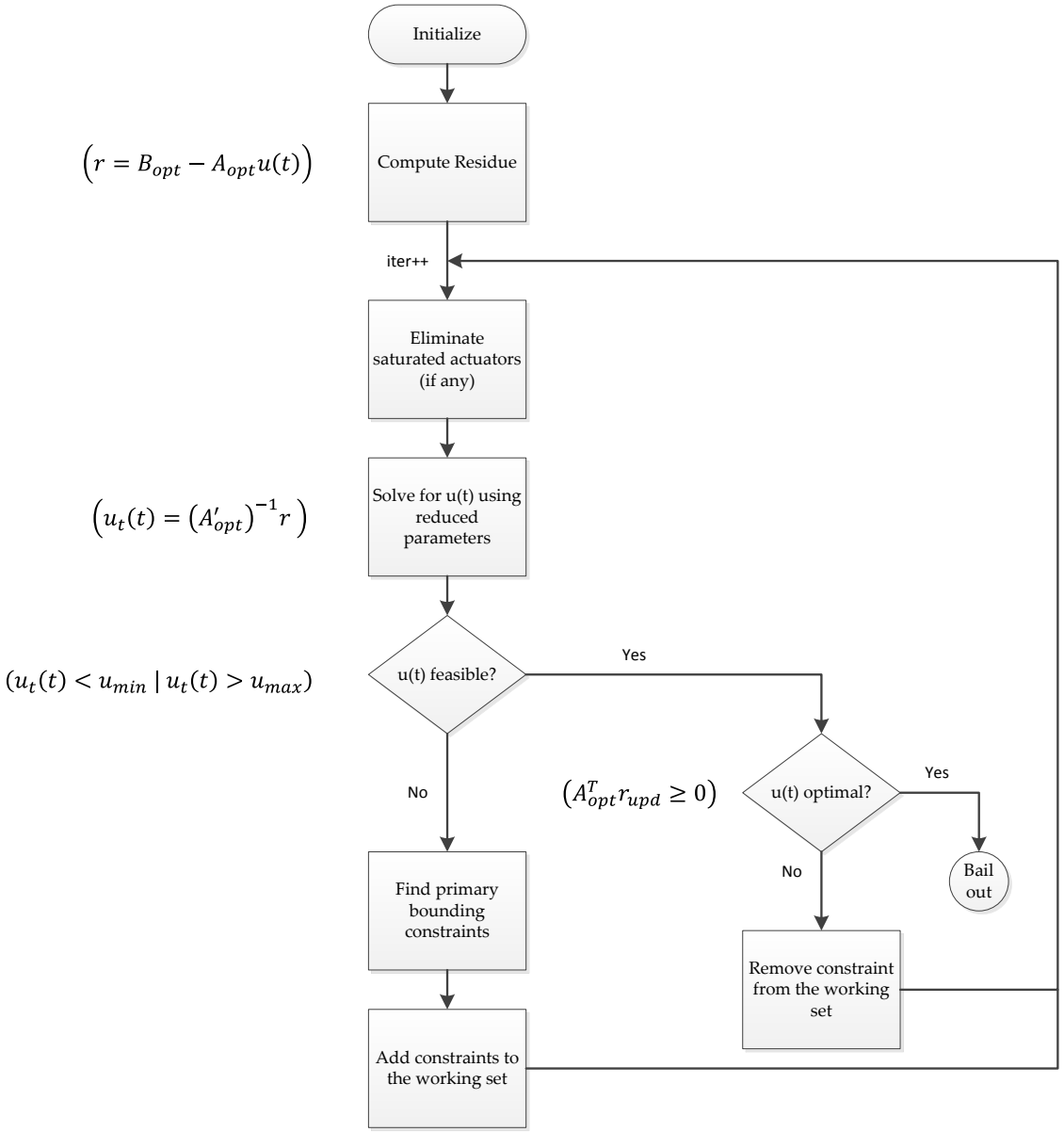


Figure 5.1: The active-set algorithm for numerically solving the control allocation problem using weighted-least squares.

After initializing the problem into the form as given in equation 5.21, the first process becomes computing the residue between desired and current states. The saturated actuators can be provided and accounted for if information is available before entering the iterative loop. Otherwise, the loop starts by reducing any saturated actuators out of the system

dynamics ($A_{opt} \rightarrow A'_{opt}$) if there is any after each iteration. In what follows, the problem is solved for the reduced system ($u_t(t) = (A'_{opt})^{-1} r$) which at the same time removes perturbations due to *active* constraints. The solution in hand is then examined if it remains in the feasible set by comparing to the given upper and lower bounds which are updated with respect to the actuator rates as detailed above. If the solutions are not feasible, the algorithm computes the primary bounding constraints that are at the closest distance to the resulting $u(t)$ and updates the working set by adding the constraints at the minimum distance to the results. Next the algorithm proceeds to the loop for another iteration. Whereas, if the solution turns out feasible, it is examined for optimality ($\left|A^T_{opt} r_{upd}\right| \leq \epsilon$), and affirmative results yield to the termination of the loop. On the other hand, if the optimality condition is not satisfied, the working set is updated by removing the constraints that are at the farthest distance to the results this time, and algorithm proceeds to the loop again. The execution of the algorithm is limited by the number of iterations, and in this study a heuristic limit is assigned for the simulation purposes, which can be further adjusted systemically for the application in hand.

The resulting control signals ($u(t)$) are then implemented through the ABS logic introduced in Chapter 4. The brake signal is determined by means of a proportional regulator that triggers the system according to the current and desired brake torque values. Next section presents the results of the proposed ICC with the control allocation scheme in simulation studies.

### 5.2.2 System Validation using Simulation

The control allocation algorithm detailed in the previous section is implemented in MATLAB/Simulink environment. Figure 5.2 illustrates the block diagram of the complete ICC including the upper level VSC integrated with the dynamic control allocation and lower level ABS algorithms.

The system is evaluated using the same evasive double lane change maneuver as in the VSC study. The resulting corrective yaw-moment is fed into the control allocation algorithm which distributes the wheel brake forces with respect to the actuator rates and saturation while generating the required yaw-moment on the chassis. The following figures summarize the results of the studied simulations. Figure 5.3 compares the control signals assigned by the proposed control allocation theme to the results of the rule-based method to underline some

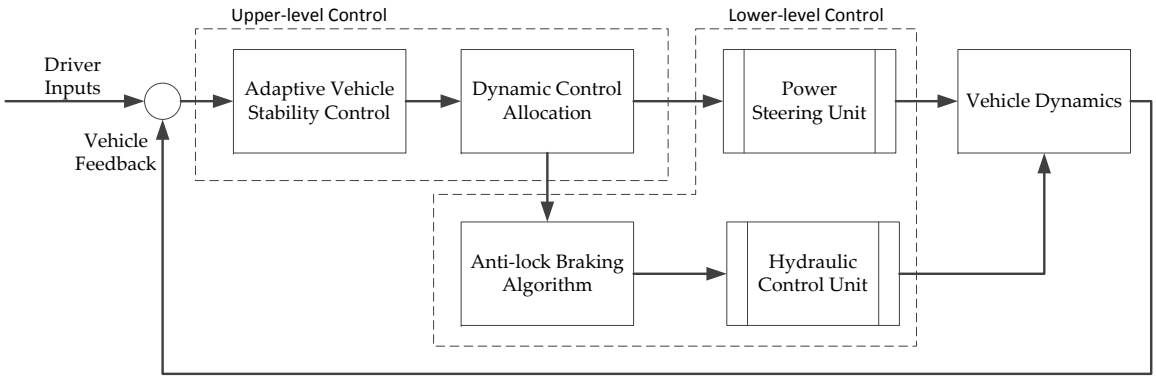


Figure 5.2: Integrated Chassis Control (ICC) system block diagram.

of the advantages of optimal brake distribution. The steering commands (Fig. 5.3a) are also given with respect to the driver's input, which is to be added to the controller signals. In the control allocation algorithm, the sampling rate $T$ for calculating actuator rate is taken as $100Hz$, which is also a common practice in most vehicle controller area network (CAN) applications.

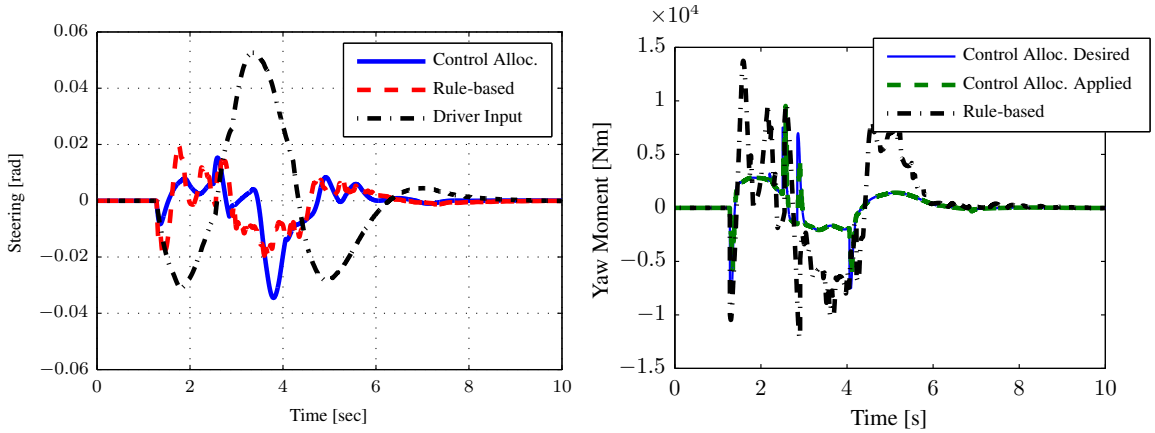


(a) (b)

Figure 5.3: Control signals assigned by the ICC scheme.

Figure 5.4 presents the allocated wheel brake torque values on each wheel using the proposed algorithm in comparison to the rule-based method in Chapter 3. The control allocation algorithm evidently reduces the peaks on each wheel as well as the abrupt precipitations. This, as indicated in Figure 5.5, yields to significantly reduced oscillations in wheel slip simply because of the feasible demand from the braking system rather than instinctive regulation. The upper and lower limits both for saturation and actuator rates set in the control allocation

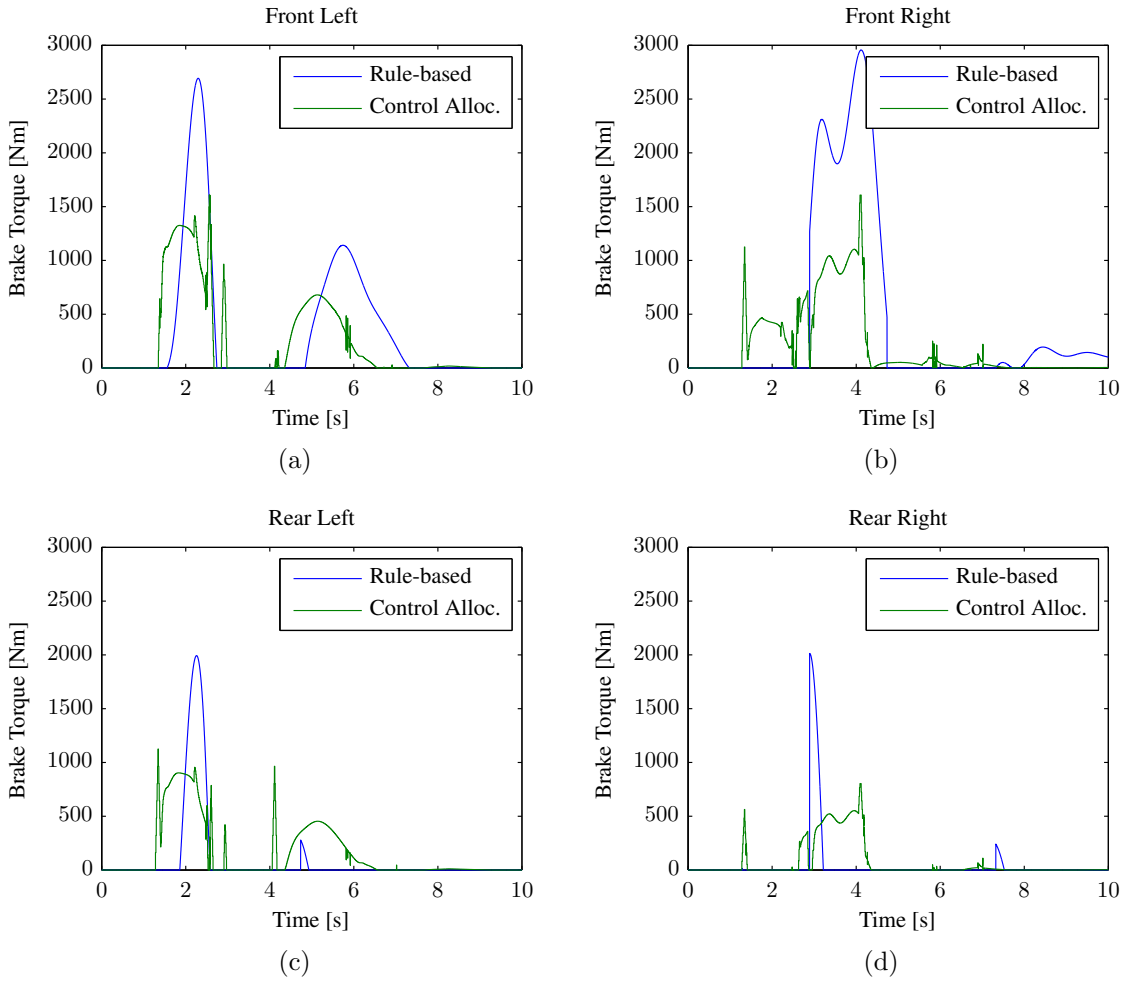


Figure 5.4: Wheel brake forces distribution by dynamic control allocation and rule-based method.

algorithm helps with this smoother control action, which is also apparent in Figure 5.6 which shows the tire force response against the slip variations. As the results indicate, the control allocation algorithm helps with maintaining the tire forces at the possible peak that leads to a significantly more efficient use of tire forces, whereas the rule based algorithm, though does not saturate, but easily drives the tires above the feasible slip values.

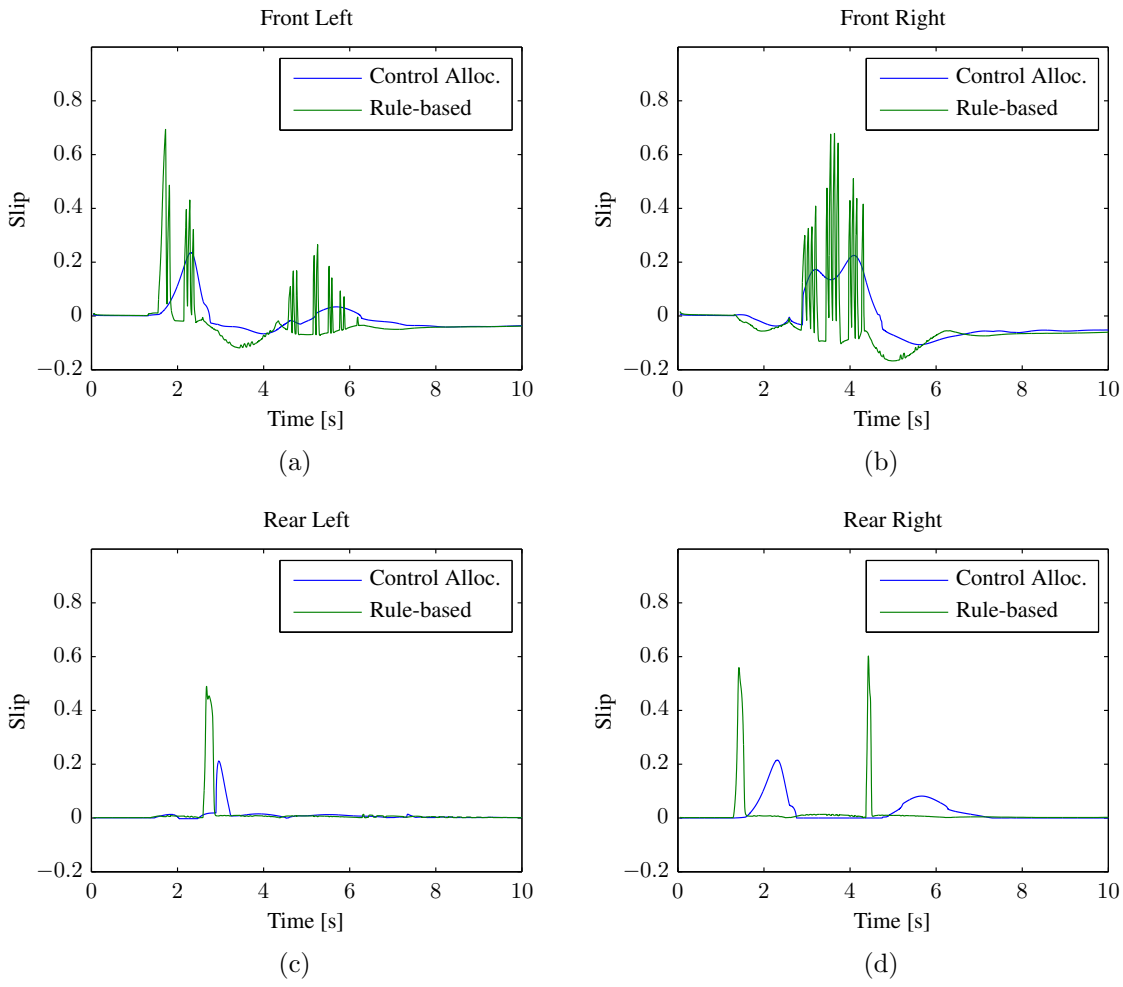


Figure 5.5: Wheel slip variations by dynamic control allocation and rule-based method.

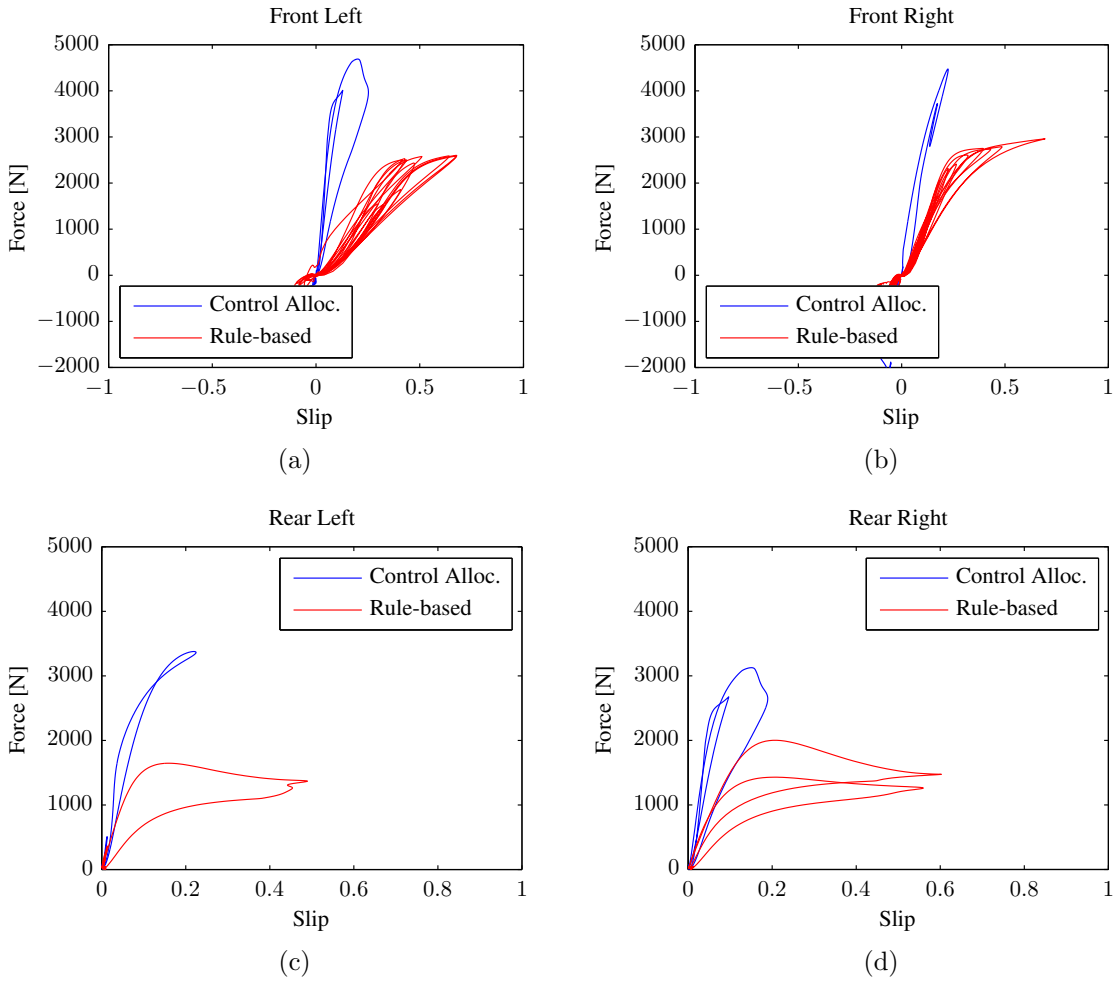


Figure 5.6: Tire force response in ICC with dynamic and rule-based control allocation methods.

## 5.3 $\mathcal{L}_1$ Adaptive Control Method

The trend in adaptive control theory has taken the path of defining larger systems that can be proven asymptotically stable via the well-known Lyapunov methods. Questions such as at which location should the uncertainty appear, what should be the degree of mismatch, how should the adaptive law be modified, etc., to get a negative definite or semidefinite derivative of the associated candidate Lyapunov function for a new class of systems, can be found in almost every study, including this one, addressing the current and next stage of development in the theory of adaptive control. A very compelling archive is available on the efforts for various adaptation techniques utilized over the years, counting from relaxation of the matching conditions in strict-parametric feedback and feedforward systems [146, 147], analysis of robustness of these schemes into unmodeled dynamics [148, 149], extensions to global or semiglobal output feedback stabilization [150], systems with time-varying parameters [151, 152], nonminimum phase systems [153] and finally to relaxation of the relative degree requirement via input-filtering [154].

These fundamental results provide sufficient conditions on the bounds of uncertainties and initial conditions, nevertheless, in practical applications with nonlinear feedback systems boundedness, ultimate boundedness, or asymptotic convergence might fall weak. Such applications require sufficient quantification of unmodeled dynamics, latencies and noise while satisfying performance requirements; and both of these requirements play a cardinal role in the adaptation process. Ideally, an adaptive controller would correctly respond to all the changes in the system's initial conditions, reference inputs, and uncertainties by quickly identifying a set of control parameters that would provide a satisfactory system response, and such satisfactory results are generally achievable with fast estimation schemes that demand high adaptation gains. Although theoretically possible, these high adaptation rates in practice can create high frequencies in the control signals and increased sensitivity to time delays. Therefore, an elementary matter with adaptive controllers is system robustness in the presence of fast adaptation. A considerable number of studies in literature report consistently limited rate of variation of uncertainties, by providing examples of destabilization due to fast adaptation [153]. The $\mathcal{L}_1$ adaptive control method attempts to address this question of robustness with sufficiently fast adaptation by setting a architecture in place for which adaptation is decoupled from robustness. This decoupled architecture allows satisfying transient performance and robustness requirements by avoiding the need of gain scheduling,

persistence of excitation or resorting to unfeasibly high feedback gain. The other equally important advantage of the $\mathcal{L}_1$ method in this application is the extended scope of adaptation with the selected control structure. Rather than the adaptation of selected parameters, the proposed $\mathcal{L}_1$ method allows for adaptation to a nonlinear function of time and system states. Finally these features of $\mathcal{L}_1$ adaptive control theory have been verified in a compelling number of publications and practical applications [155, 156, 157, 158].

The rest of this section facilitates the development of the $\mathcal{L}_1$ adaptive control method and applies it to develop a novel VSC algorithm, which replaces the Lyapunov based algorithm in the previous exercise. The section is concluded by the validation of the algorithm in the same ICC scheme in simulation studies.

### 5.3.1 Derivation of the Control Algorithm

The control architecture developed in this section considers a semi-linear multi-input-multi-output (MIMO) system with uncertain nonlinearities as a function of system states and time. The derivation aims to show that, subject to certain assumptions satisfied, the system can be transformed to a linear system with time varying parameters and disturbances, and the controller objective is to ensure the output of the system to track given reference signals while satisfying semi-global performance criteria. To start with, the modified bicycle model derived in Chapter 3 is reconsidered and extended. First form of extension is by adding second order steering dynamics with the required steering column torque as the input to the system. By this extension, it is aimed to involve actuator dynamics, partially if not entirely, and move a step closer to practical application. Second form of extension is by considering a nonlinear tire model rather than a linear approximation that can capture the saturation

effect of the tire force response. The resulting equations are rewritten as below:

$$\begin{aligned}
\dot{\alpha}_f &= -\left(\frac{2C_f(I_z + l_f^2 m)}{I_z m u} + \frac{u}{l_f + l_r}\right)\alpha_f - \left(\frac{2C_r(I_z - l_f l_r m}{I_z m u} - \frac{u}{l_f + l_r}\right)\alpha_r \\
&\quad + \left(\frac{u}{l_f + l_r}\right)\delta + \dot{\delta} - \frac{l_f}{I_z u} M_b + \theta_1(t, x) \\
\dot{\alpha}_r &= -\left(\frac{2C_f(I_z l_f l_r m)}{m u} + \frac{u}{l_f + l_r}\right)\alpha_f - \left(\frac{2C_r(I_z + l_r^2 m)}{m u} - \frac{u}{l_f + l_r}\right)\alpha_r \\
&\quad + \left(\frac{u}{l_f + l_r}\right)\delta + \frac{l_r}{I_z u} M_b + \theta_2(t, x) \\
\ddot{\delta} &= \left(\frac{b_s}{J_s}\right)\dot{\delta} + \left(\frac{k_s}{J_s}\right)\delta + \tau_c
\end{aligned} \tag{5.22}$$

where

$$\begin{aligned}
\theta(t, x) &= [\theta_1 \quad \theta_2]^T \\
&= \begin{bmatrix} a_{11}x + a_{12}x^2 + \cdots + a_{1n}x^n \\ \\ a_{21}x + a_{22}x^2 + \cdots + a_{2n}x^n \end{bmatrix}
\end{aligned} \tag{5.23}$$

represents the nonlinearities and saturation in tire response by complementing the linear $C_{\alpha_i}\alpha_i$ approximation by a polynomial function. Numerical analysis suggests that one can successfully near to results of a MF tire model by an eight order ($n = 8$) polynomial. The set of equations in 5.22 can be rewritten in state-space form as follows:

$$\dot{x}(t) = Ax(t) + Bu(t) + \Theta(t, x) \tag{5.24}$$

where the coefficient matrices are given as:

$$A = \begin{bmatrix}
-\left(\frac{2C_f(I_z + l_f^2 m)}{I_z m u} + \frac{u}{l_f + l_r}\right) & -\left(\frac{2C_r(I_z - l_f l_r m}{I_z m u} - \frac{u}{l_f + l_r}\right) & -\frac{u}{l_f + l_r} & -1 \\
-\left(\frac{2C_f(I_z - l_f l_r m)}{I_z m u} + \frac{u}{l_f + l_r}\right) & -\left(\frac{2C_r(I_z + l_r^2 m}{I_z m u} - \frac{u}{l_f + l_r}\right) & -\frac{u}{l_f + l_r} & 0 \\
0 & 0 & 0 & 1 \\
0 & 0 & -\frac{k_s}{J_s} & -\frac{c_s}{J_s}
\end{bmatrix}$$

$$B = \begin{bmatrix} 0 & \frac{l_f}{I_z u} \\ 0 & -\frac{l_r}{I_z u} \\ 0 & 0 \\ 1 & 0 \end{bmatrix}, \qquad \Theta(t,x) = \begin{bmatrix} \theta_1(t,x) \\ \theta_2(t,x) \\ 0 \\ 0 \end{bmatrix}$$

In what follows, the system dynamics are re-considered as in the following MIMO system:

$$\begin{aligned} \dot{x} &= Ax(t) + \bar{B}\left(\mu(t)x(t) + \omega u(t)\right) + \xi(t) \\ y &= Cx(t), \qquad x(0) = x_0 \end{aligned} \tag{5.25}$$

where the polynomial approximation functions $\theta_i(t,x)$ are evaluated as the summation $\bar{B}\left(\mu(t)x(t) + \omega u(t)\right) + \xi(t)$, $\omega$ represents an unknown constant input gain and the output $y(t)$ is given only in terms of the states. Provided that the linear part of the system dynamics ($A \in \mathbb{R}^{n\times n}$) is Hurwitz and the input and output coefficients are the same rank ($\bar{B}, C^T \in \mathbb{R}^{n\times m}$), the control objective is to ensure that the outputs $y(t)$ track given bounded reference signals $r(t) \in \mathbb{R}^m$ both in transient and steady state. In the given form of system in equation 5.25, the unknown parameters ($\omega$) and nonlinearities are assumed to be bounded; furthermore the nonlinearities are expected to be differentiable with bounded derivatives. In the subsequent analysis, the terms and their Laplace transforms are used interchangeably where s denotes the Laplace operator, mainly for brevity. The next step in the derivation is to introduce a so-called passive identifier or state predictor with the estimated unknowns:

$$\dot{\hat{x}} = A\hat{x}(t) + \bar{B}\left(\hat{\mu}(t)x(t) + \hat{\omega}u(t)\right) + \hat{\xi}(t), \qquad \hat{x}(0) = 0 \tag{5.26}$$

where the adaptive estimates are given using the Projection operator:

$$\begin{aligned} \dot{\hat{\omega}}(t) &= \Gamma Proj\left(\hat{\omega}(t), -(\tilde{x}^T(t)P\bar{B})^T u^T(t)\right) \\ \dot{\hat{\mu}}(t) &= \Gamma Proj\left(\hat{\theta}(t), -(\tilde{x}^T(t)P\bar{B})^T x^T(t)\right) \\ \dot{\hat{\xi}}(t) &= \Gamma Proj\left(\hat{\xi}(t), -(\tilde{x}^T(t)P)^T\right) \end{aligned} \tag{5.27}$$

The Projection operator augments robustness of the state estimates by enabling a tradeoff with system performance. A major advantage of using this method in estimation is the

guaranteed boundedness of the estimates. In mathematical terminology, Projection operator refers to a linear transformation between a given and a desired vector space. By using a bounded space to project the given parameters, the operator avoids a divergence scenario. Further details on the design of this operator are provided in Appendix A. It is also important to note that the predictor as given above makes use of the system states ($x(t)$) which are assumed to be known and the tracking error is given by $\tilde{x}(t) = \hat{x}(t) - x(t)$. The rest of the parameters are defined as follows: $\Gamma$ stands for the positive definite adaptation gain and $P$ represents the solution of the algebraic Lyapunov equation ($A^T P + PA = -Q < 0$) which guarantees the convergence of the predictor. Having defined the unknown parameters and nonlinearities by the help of the adaptive state predictor, the control signal can be generated by using these estimates, the given reference signal, system states and a low-pass gain filter:

$$u(s) - KC_{LP}(s)\bar{r}(s) \tag{5.28}$$

where $K \in \mathbb{R}^{m \times m}$ is the constant control gain and the regulated reference signal is given as:

$$\bar{r}(t) = \hat{\mu}(t)x(t) + \hat{\omega}u(t) + \xi(t) - K_g r(t) \tag{5.29}$$

The pre-filter gain $K_g$ aims decoupling of the hypothetical reference model dynamics as given below, which leads to trackable reference signals:

$$\begin{aligned} y_r(s) &= C(s\mathbb{I}_{4\times4} - A)^{-1}\bar{B}K_g r(s) \\ &= G_r(s)K_g r(s) \end{aligned}$$

The other regulated signal $\bar{\xi}(t)$ operates on the estimate of the nonlinearities:

$$\begin{aligned} \bar{\xi}(s) &= inv(\bar{B})\hat{\xi}(s) \\ &= (G_r(s))^{-1}\left(C(s\mathbb{I}_{4\times4} - A)^{-1}\right)\hat{\xi}(s) \end{aligned} \tag{5.30}$$

The choice of the low-pass gain $C_{LP}(s)$ and the control gain $K$ are to be made based on the listed criteria being satisfied on the following transfer function:

$$T_f(s) = \omega K(\mathbb{I} + C_{LP}(s)\omega K)^{-1}C_{LP}(s)$$

- $T_f(s)$ is stable with $T_f(0) = \mathbb{I}$ and strictly proper,

- $T_f(s)G_r(s)^{-1}$ is stable and strictly proper,
- The $\mathcal{L}_1$ norm condition should be satisfied, $||\bar{G}(s)||_{\mathcal{L}_1} L < 1$, where $L$ represnets them maximum $\mathcal{L}_1$ norm of $\mu(t)(L = max||\mu(t)||_{\mathcal{L}_1})$ and the transfer function is given by:

$$\bar{G}(s) = (s\mathbb{I} - A)^{-1} B \left(\mathbb{I} - T_f(s)\right)$$

The transfer function $T_f(s)$ is formed by considering the system stability as well as guaranteed boundedness of the system inputs, that is selection of $C_{LP}(s)$ and $K$ satisfying these criteria will prevent any unrestrained increment of states with arbitrary $u(t)$. Let's further detail the procedure to find the gain values satisfying these criteria. A strictly proper selection of the low-pass gain $C_{LP}(s)$ also yields to strictly proper transfer function. The stability of $T_f(s)$ can be addressed by choosing $C_{LP}(s)$ and $K$ to render $-\omega K C_{LP}(s)$ Hurwitz. Similarly, the multiplication $T_f(s)G_r(s)^{-1}$ can be made proper by the choice of the low-pass gain $G_r(s)$, on the other hand its stability follows from the assumption that the poles of $G_r(s)^{-1}$ reside in the left-half plane. Securing the third criterion first requires the stability of $T_f(s)$. Next, based on the description of $\mathcal{L}_1$ norm, the following inequality holds true:

$$||\bar{G}(s)||_{\mathcal{L}_1} \leq ||s\mathbb{I} - A)^{-1}\bar{B}||_{\mathcal{L}_1} ||\mathbb{I} - T_f(s)||_{\mathcal{L}_1}$$

and one can deduce that forming the transfer function $T_f(s)$ with its maximum eigenvalue $(_{max}(T_f))$ arbitrarily small yields to:

$$\lim_{\lambda \to -\infty} ||\mathbb{I} - T_f(s)||_{\mathcal{L}_1} = 0$$

As the eigenvalues of the transfer function $T_f(s)$ are established by the selected gain values, it is shown that the last criterion can always be satisfied by fair choices of $C_{LP}(s)$ and $K$.

The given control architecture in equations 5.26-5.30 yields to satisfactory traction performance provided that the unknown parameters and nonlinearities are successfully predicted to compute the control signal. Therefore the convergence of the predicted values poses an important question of the practicality of the method. Next part summarizes a brief analysis on the convergence of the state estimations and shows that they are strictly bounded, which also indicates that the unknown parameters converge to expected values. Lyapunov analysis allows estimating the bound on the prediction error of the system while proving stability.

The analysis is initiated by employing the following candidate function:

$$\begin{aligned} V(t,\tilde{x},\tilde{\omega},\tilde{\mu},\tilde{\xi}) &= \tilde{x}^T(t)P\tilde{x}(t) \\ &+ \frac{1}{\Gamma}\left(tr(\tilde{\omega}^T(t)\tilde{\omega}(t)) + \sum \tilde{\mu}^T(t)\tilde{\mu}(t) + \tilde{\xi}^T(t)\tilde{\xi}(t)\right) \end{aligned} \tag{5.31}$$

Assuming negligible variation of the input gain ($\dot{\omega} = 0$), the time derivative of this function is found as:

$$\dot{V}(t) = -\tilde{x}^T(t)Q\tilde{x}(t) + \frac{2}{\Gamma}\left(\sum \tilde{\mu}^T(t)\dot{\mu}(t) + \tilde{\xi}^T(t)\dot{\xi}(t)\right) \tag{5.32}$$

Since the unknown parameters and nonlinearities are to be bounded, the Projection operator ensures that:

$$\begin{aligned} \max\left(tr(\tilde{\omega}^T(t)\tilde{\omega}(t)) + \sum \tilde{\mu}^T(t)\tilde{\mu}(t) + \tilde{\xi}^T(t)\tilde{\xi}(t)\right) \\ \leq 4\left(\max(tr(\omega^T\omega)) + M^2 + \Xi^2\right) \end{aligned} \tag{5.33}$$

where $\omega$, $M$ and $\Xi$ represent the bounds of the unknowns. Further assuming the bounds on the time derivatives:

$$||\dot{\mu}(t)||_\infty < d_\mu$$

$$||\dot{\xi}(t)||_\infty < d_\xi$$

yields to the following inequality:

$$\max \sum \tilde{\mu}^T(t)\dot{\mu}(t) + \tilde{\xi}^T(t)\dot{\xi}(t) \leq 2(M^2 d_\mu + \Xi^2 d_\xi) \tag{5.34}$$

Next, consider the operator

$$\gamma = 4\left(\max(tr(\omega^T\omega)) + M^2 + \Xi^2\right) + 4\frac{\lambda_{max}(P)}{\lambda_{min}(Q)}(M^2 d_\mu + \Xi^2 d_\xi) \tag{5.35}$$

The positive definite matrices $P$ and $Q$ satisfy

$$P \leq \lambda_{max}(P)\mathbb{I}, \qquad \lambda_{min}(Q)\mathbb{I} \leq Q$$

which then allows writing

$$\tilde{x}^T Q\tilde{x} \geq \frac{\lambda_{min}(Q)}{\lambda_{max}(P)}\tilde{x}^T(\lambda_{max}(P)\mathbb{I})\tilde{x} \geq \frac{4}{\Gamma}(M^2 d_\mu + \Xi^2 d_\xi) \tag{5.36}$$

Using the inequality 5.34, it concludes that:

$$\dot{V}(t) < 0 \tag{5.37}$$

which restates the stability. In what follows, from the initial conditions $\hat{x}(0) = x(0)$, one can also deduce that:

$$V(0) \leq \frac{1}{\Gamma}\left(tr(\tilde{\omega}^T(t)\tilde{\omega}(t)) + \sum \tilde{\mu}^T(t)\tilde{\mu}(t) + \tilde{\xi}^T(t)\tilde{\xi}(t)\right) < \frac{\gamma}{\Gamma} \tag{5.38}$$

and the continuity of the candidate function dictates the result:

$$V(t) \leq \frac{\gamma}{\Gamma}, \qquad \forall t \geq 0 \tag{5.39}$$

Finally, this result, together with the fact that $\lambda_{min}||\tilde{x}(t)||^2 \leq \tilde{x}^T(t)P\tilde{x}(t) \leq V(t)$ yields to:

$$||\tilde{x}(t)|| \leq \sqrt{\frac{\gamma}{\lambda_{min}(P)\Gamma}} \tag{5.40}$$

The inequality in 5.40 states the bound on the prediction error and together with 5.37 indicates the convergence of it. Proving that the predicted values converge as expected, the control objective reduces to designing the gain values $K$ and $C_{LP}(s)$ for desired performance.

### 5.3.2 System Validation using Simulation

The algorithm as summarized above is implemented in MATLAB/Simulink environment for numerical analysis and validation in simulation studies. Before moving forward with the maneuver experiments, the stability criteria are evaluated so that an estimated set of acceptable control gains is formed. For the initial analysis, a relatively simpler low-pass gain is selected as a symmetric matrix of first order transfer functions as in the below form:

$$C_{LP}(s) = \begin{bmatrix} \frac{a}{s+a} & 0 \\ 0 & \frac{a}{s+a} \end{bmatrix}$$

by which the transfer function $T_f(s)$ is also rendered stable for a similarly symmetric positive definite gain matrix $K$ (e.g. $K \times \mathbb{I}_{2\times 2}$). In what follows, the $\mathcal{L}_1$ norm condition is evaluated

for varying cut-off frequencies on the selected low-pass gain (a). Setting the bound on the uncertainty $\mu(t)$ as 1 (i.e. representing the maximum possible variation on surface friction), numerical values of the norm condition can be computed. Figure 5.7 presents the resulting norm values against the cut-off frequencies.

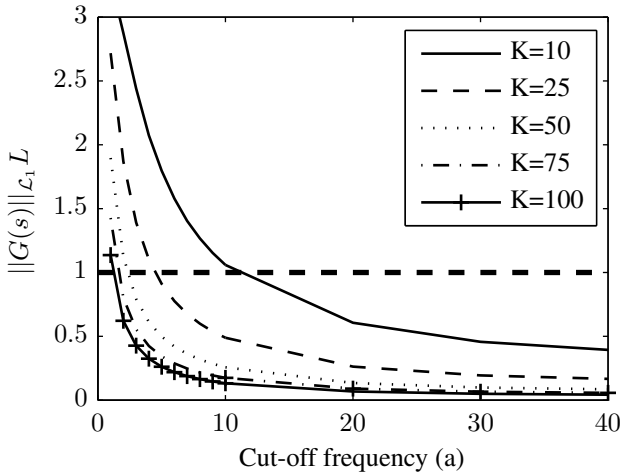


Figure 5.7: The $\mathcal{L}_1$ norm with respect to varying low-pass and control gain.

The results imply that there exists a trade-off between the gain $K$ and the cut-off frequency, however it is possible to find a range of cut-off ($a$) values that renders the system stable irrespective of the selected $K$. On the other hand, simulation results indicate that the cut-off frequency also affects the oscillations on the resulting control signals, and based on the results and on the range found above, one can tune the low-pass gain for desired performance.

A sample study has been conducted by initiating a ramp steer input to the system. The vehicle dynamics are simulated using the 8-degree-of-freedom model as derived in Chapter 2. The system is tested at $60kph$ speed and on high and low friction conditions (0.85 and 0.25 respectively). In what follows, the controller is expected to allow tracking a desired yaw-rate while following the steering input that are taken as the system outputs.

This initial simulation indicates the adaptation capability of the algorithm, specifically to the variations in the tire responses. The open-loop yaw rate variations indicate the difference of the vehicle response due to the changing surface friction and corresponding tire force variations. Yet the system with the control intervention remains in a very reasonable vicinity of the desired yaw-rate signal. Next, the system is put on test with a D-class vehicle model from CarSim software for an evasive double lane change maneuver (DLC) as before. Two

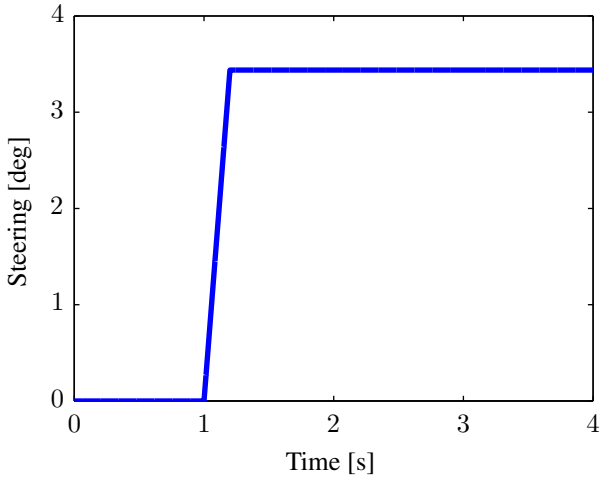


Figure 5.8: Given ramp-steer maneuver.

sets of simulations are carried out for high and low friction conditions at respectively varying speeds. The first test is run on high friction surface to negotiate the given DLC at a speed of $33m/s$ ($120kph$). Following figures summarize the results. The results on the high friction condition indicate promising improvement of the control performance. Comparing the control signal between the two methods, one difference can be seen in the continuity of the steering input. The addition of the second order steering dynamics actually allows computing a steering torque desired at the steering column as a more practical way of implementation, and furthermore yields to the reduced oscillations and peaks on the resulting steering angle degrees. A visible influence as seen on Figure 5.10 and Figure 5.11 is on the utilization of the lateral tire forces, which can be attributed to the change in the adaptation strategy. The proposed $\mathcal{L}_1$ method estimates and adapts to the nonlinearities in the system as a function of states and time rather than to only selected parameters. This provides an advantage to the $\mathcal{L}_1$ method, and furthermore the decoupled structure of adaptation law allows increasing the adaptation gain values, considering a practical bound, to have better estimates of the nonlinearities. Finally, the proposed method yields to a reduction in yaw-rate of the vehicle of almost $0.10rad/s$ (or $5deg/s$) in its peak. The previous section summarizes the variation in the driver/passenger comfort levels with respect to yaw-rate which steps up or down at about $0.12rad/s$ (or $7deg/s$), which therefore indicates that the $\mathcal{L}_1$ method further improves the drive comfort in addition to the control allocation while maintaining satisfactory stability.

Next, the vehicle is tested on the low friction surface ($\mu_{nom} = 0.25$) with the same DLC

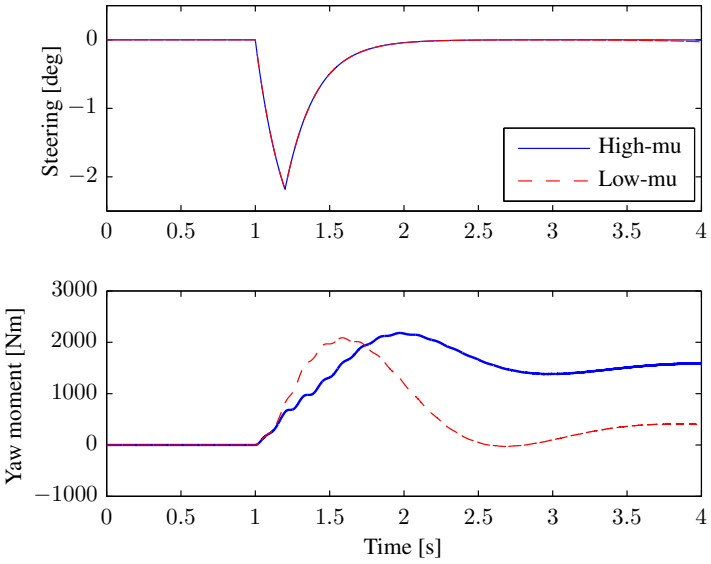


(a)

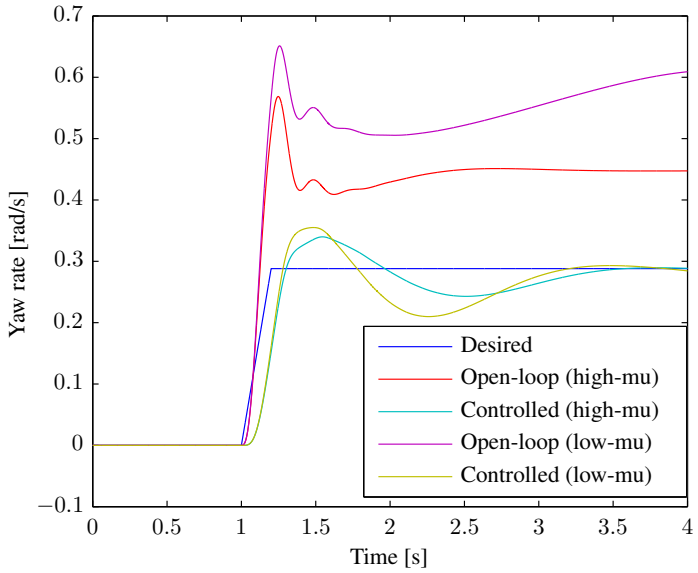


(b)

Figure 5.9: (a) Resulting control signals, and (b) yaw-rate values with and without the control intervention on differing surface friction conditions.

maneuver and at a reduced speed of $22m/s$ (or $80kph$). Following are the simulation results in comparison to the Lyapunov based control algorithm performance.

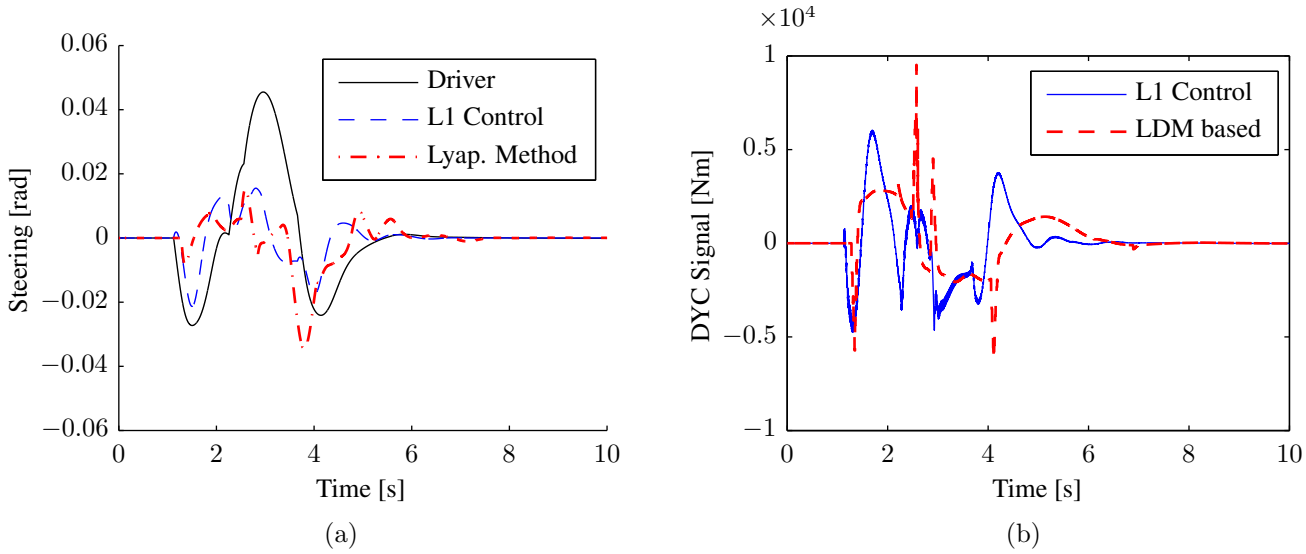


Figure 5.10: Control signals by the $\mathcal{L}_1$ and Lyapunov adaptive methods (a) steering input, and (b) desired yaw-moment on high-mu.

The results indicate that the proposed $\mathcal{L}_1$ method can also satisfactorily adapt to varying surface conditions, and the corresponding change in the system dynamics. Similar to the previous results, the control algorithm yields to extended utilization of the lateral tire forces without leading to any instabilities or saturation conditions (Figure 5.14). The most significant improvement can be seen on the vehicle yaw-rate response (Figure 5.15b). The Lyapunov based algorithm successfully stabilizes the vehicle and allows negotiating the maneuver by avoiding any crash scenario. Nevertheless, the $\mathcal{L}_1$ method allows for further reducing the yaw-rate variations while providing the same level of stability conditions, which provides an increased feeling of safety to the driver and passenger(s).

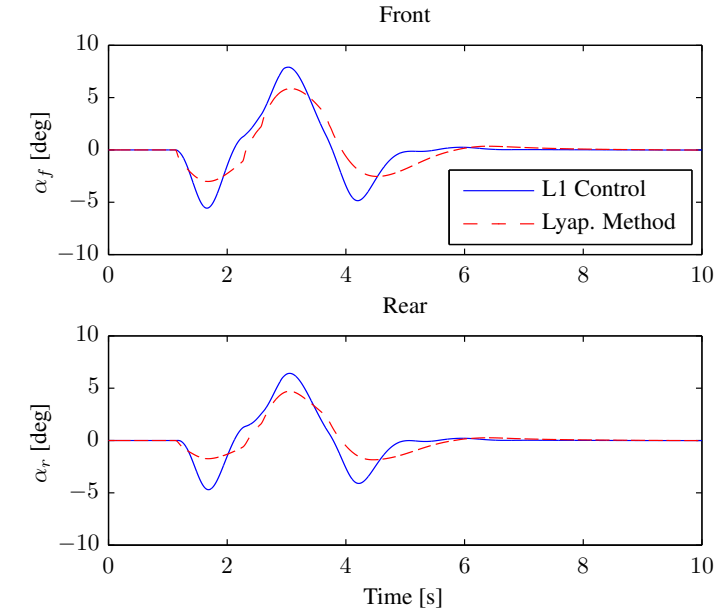


(a)

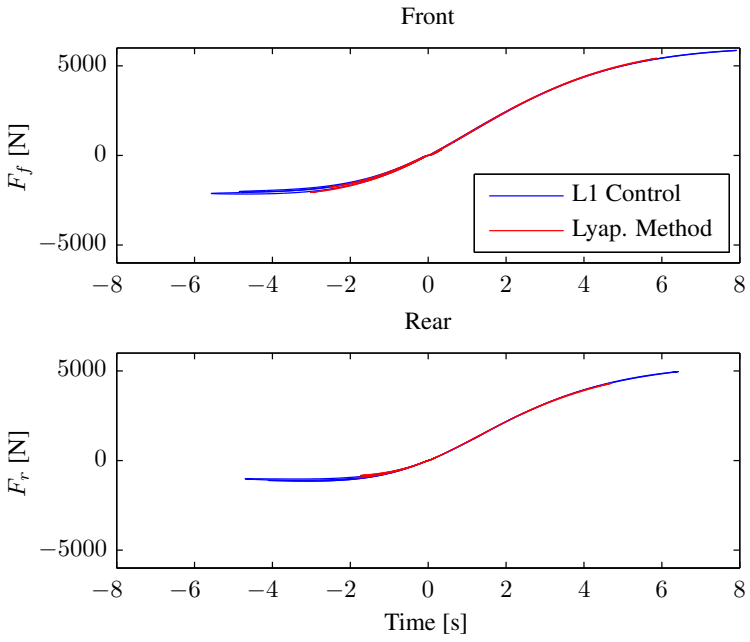


(b)

Figure 5.11: (a) Tire slip-angle variations, and (b) corresponding tire lateral force utilization.

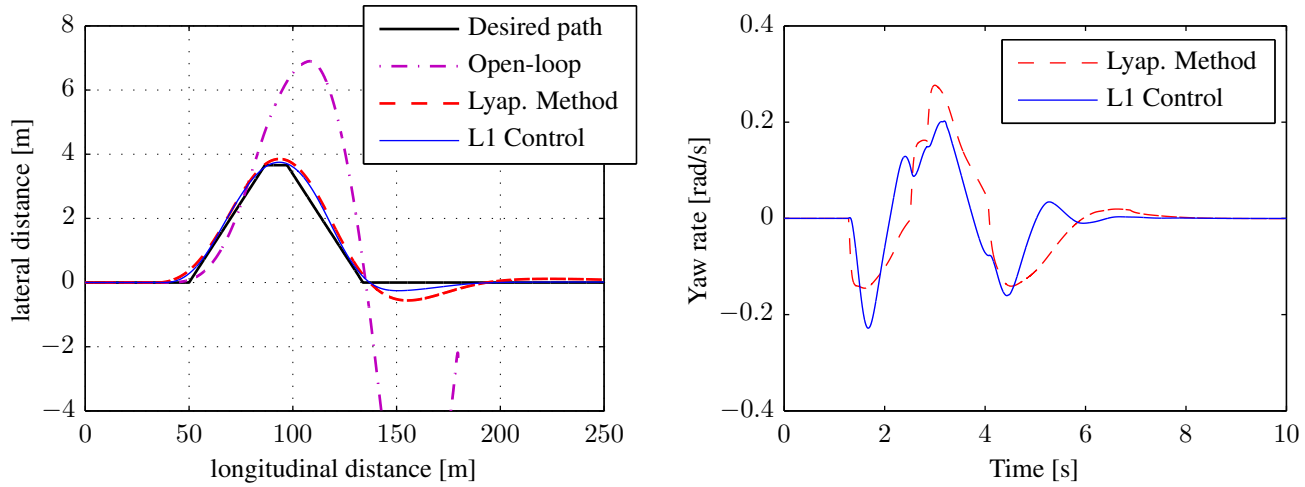


(a) (b)

Figure 5.12: (a) Vehicle CG trajectory in comparison with an open-loop system and with Lyapunov based control method implemented (b) Comparison of vehicle yaw-rate with $\mathcal{L}_1$ control and Lyapunov methods.

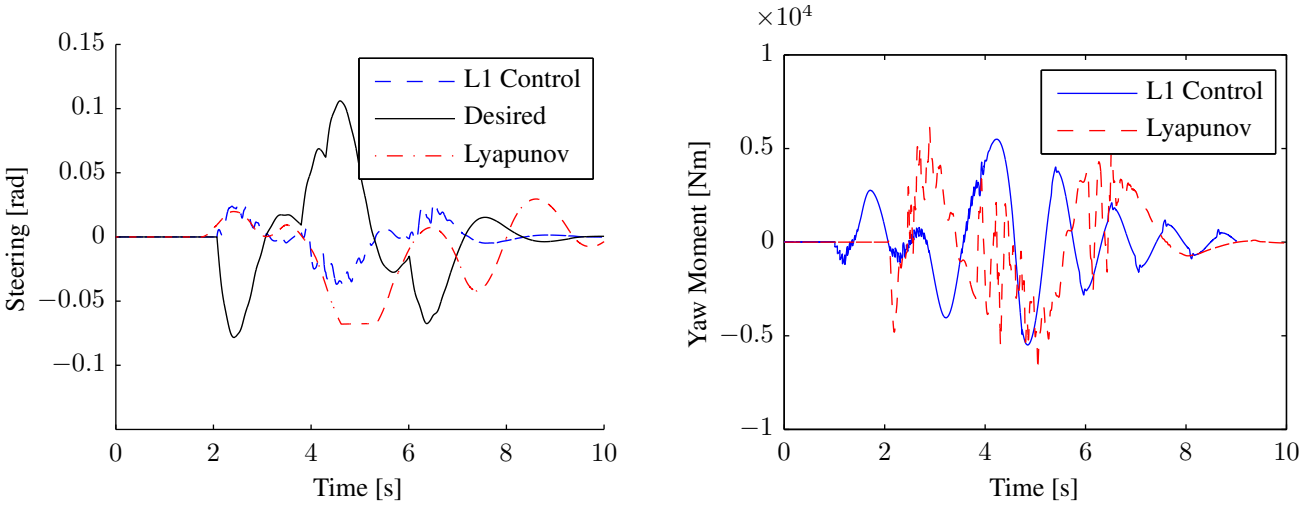


(a) (b)

Figure 5.13: Control signals by the $\mathcal{L}_1$ and Lyapunov adaptive methods (a) steering input, and (b) desired yaw-moment on low-mu.

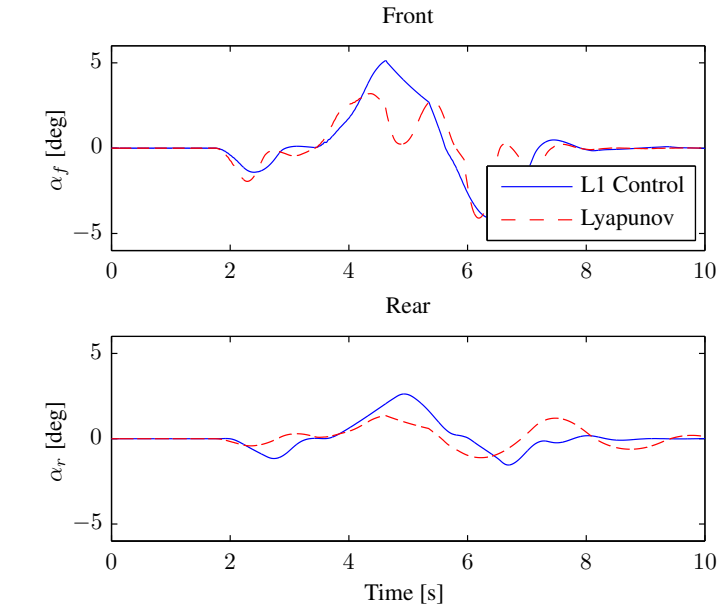


(a)

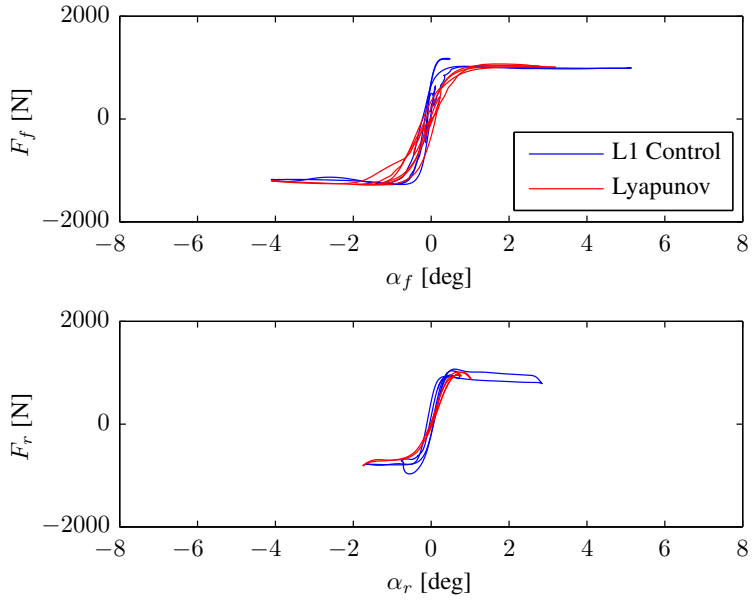


(b)

Figure 5.14: (a) Tire slip-angle variations, and (b) corresponding tire lateral force utilization.

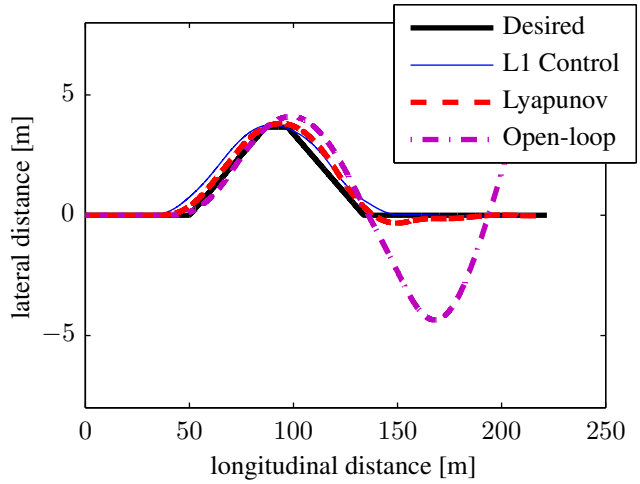


(a)

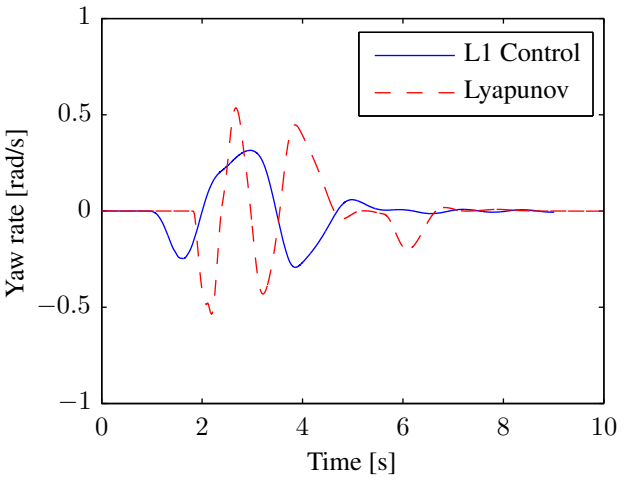


(b)

Figure 5.15: (a) Vehicle CG trajectory in comparison with an open-loop system and with Lyapunov based control method implemented (b) Comparison of vehicle yaw-rate with $\mathcal{L}_1$ control and Lyapunov methods.

## 5.4 Conclusion

This chapter introduces the concept of integrated vehicle control systems (ICC) that structure a centralized control strategy to allow employment of multiple safety systems and actuators focusing on distinct parts of the vehicle without diminishing each other's performances. A dynamic control allocation strategy is presented that is first used to integrate the stability and anti-lock brake algorithms. The control allocation strategy optimally distributes the wheel brake forces while avoiding any saturation or actuator over-rate scenarios. In what follows, a new adaptive control method, the so-called $\mathcal{L}_1$ adaptive control, is introduced and implemented to replace the upper-level control algorithm based Lyapunov's direct method. This new control strategy proposes adaptation to disturbances and nonlinearities in the form of a function of time and states, which are not required to be known a priori. The system dynamics introduced in Chapter 2 are then manipulated to combine the nonlinearities due to the tire force response on a time varying function, and the friction is taken as a time varying disturbance, and this new form is used in the derivation of the control signals.

The new method is evaluated first with an open-loop structure only providing a ramp-steer input on two different friction conditions. This maneuver is expected to drive the tire force into the saturation/nonlinear region and the controller responds satisfactorily both to the nonlinearities in the tire as well as the dynamics variations due to the change in the friction conditions. Next, an evasive double lane change maneuver is executed as in the previous experimentation. The results are presented in comparison with the first adaptive control application. The performance of the new algorithm suggests further improvements over the first method, mainly due to the extended adaptation capability. As a result, the proposed ICC with the $\mathcal{L}_1$ adaptive control and gain-scheduling ABS proposes reliable safety levels while minimizing the compromise in the drive comfort.

# Chapter 6

# Conclusion

## 6.1 Summary and Comments

As summarized in Chapters 1 and 2, the dynamics at the tire road contact have an immense effect on the vehicle's handling and stability characteristics as the majority of the forces and moments acting on the vehicle chassis are generated at the tire contact patch. Sudden changes in the dynamics at this contact patch results in abrupt variations in vehicle characteristics which may lead to lose of control for the inexperienced driver. These types of instabilities underline the importance of monitoring and utilization of the dynamic variations of the tires and tire-road contact for improved vehicle controls and pose it as a novel engineering problem. The active safety systems available today seek to prevent such unintended vehicle behavior by assisting drivers in maintaining control of their vehicles. Nevertheless, the lack of knowledge about the tire-road interactions highly limits their effectiveness. Recent studies in the field introduced the smart tire technology as a solution for dynamic (real-time) tire monitoring. The smart tire technology suggests instrumenting the tire itself for obtaining information on the momentary variations on tire conditions and tire-road interactions.

Motivated by this opportunity and necessity in the field, this study develops tire parameter estimation algorithms and adaptive control strategies to improve vehicle handling and braking performances. The algorithms use the so-called sensor fusion approach that integrates the smart tire technology and model based nonlinear observers to provide information

on tire forces, slip-angle and surface friction conditions. The proposed control and observer algorithms are evaluated using numerical analysis under challenging conditions. To get a better measure of possible improvements in vehicle performance, the tests are executed together with baseline algorithms inspired by conventional systems available today. The results demonstrate that the proposed algorithms can successfully negotiate the given tasks as well as promising considerable improvements over the baseline systems.

The proposed stability algorithm takes advantage of the strong interdependency between the tire slip-angles and the vehicle drive characteristics. Since the algorithm is based on a modified bicycle model that replaces the states with front and rear tire slip-angles, it removes the need for lateral velocity estimation which increases system complexity and introduces intrinsic estimation errors (e.g. integral errors). Furthermore, due to the issues with lateral velocity estimations, a common practice today is to deprive it out of the derivation by assuming zero as desired value. However, depending on the road conditions, especially on bank and graded roads, this might result in undesirable deviations from stable behavior. Another preferable outcome of the tire slip-angle based controller is the reduction in the control load that minimizes the interference with the driver's inputs while maintaining stability as well as lessening the computational power requirements. The algorithm is also finalized with a lower level optimal force distribution algorithm which further improves the performance by minimizing the vehicle velocity variations which is a common issue with differential braking based stability control systems.

The proposed adaptive ABS wheel slip controller utilizes a surface classification method based on the integration of the smart tire technology with a model based observer scheme. Motivated by the initial studies that proved utilization of this information is veritably favorable for enhancing the vehicle's braking performance, this algorithm proposes an adaptation scheme that optimizes a set of threshold values to switch between four phases that basically increases, holds or decreases the applied brake torque/pressure value. The algorithm demonstrates significant improvements in braking distances under different surface conditions over the baseline system. Another advantage of the proposed algorithm is that it follows the same rule-based approach as the conventional ABS algorithms, which makes it easier to implement on currently available brake systems on board.

Finally, an Integrated Chassis Control strategy is introduced by implementing a dynamic

control allocation algorithm that bridges between the stability and brake controllers. Integrated control aims to improve the overall vehicle dynamics performance by derivation of control laws in a unified fashion, based on dynamic models that account for all of the primary directions (e.g. lateral, longitudinal, vertical) of interest for control. The main advantages sought by the use of this approach are as follows.

- To avoid the conflicts and interventions among different subsystems.
- To exploit the potentials of the available processor units at their most feasible by handling the communication and coordination among the sub-controls in the derivation step.

This reduces the computational load on the electronic control unit and yields to the utilization of them only to compute and distribute the control signals. Taking care of the coordination task in the derivation step also assures dispelling of any possible conflicts among the sub-control domains.

To summarize, the conclusions of this study are:

- New tire and vehicle mathematical models were developed based on smart tire technology,
- New Estimation algorithms for processing the smart tire accelerometer signal were developed and used to estimate the tire slip-angle, dynamic wheel load variations and road surface friction condition,
- The estimated parameters were included in the new control algorithms developed for improving vehicle handling and stability and reducing stopping distance,
- New control vehicle control algorithms were developed using a slip angle based model and it was shown that these algorithms can improve vehicle stability in severe driving scenarios,
- A new ABS control algorithm was developed based on adaptation of the brake pressure with respect to surface friction condition, which was shown to significantly improve the vehicle braking performance.

- The stability and braking controllers are integrated by introducing a dynamic control allocation strategy that yields to an Integrated Chassis Control scheme.

All in all, this study provides a very promising first step in the introduction of smart tire technology into the active vehicle safety systems. With the introduction and wider use of smart tire technology on vehicles in near future, these algorithms will be readily implementable. To the author's best knowledge, the technology is expected to be released into the market in recent future starting with high-end sports cars. It is hoped that this study underlines the potential of the integration of this new technology with the vehicle control systems, so that current and future vehicle control systems would benefit from the smart tire technology at its most.

The proposed algorithms provide a substantial base on the grand-scheme of integrating smart tires and vehicle control systems. Regarding this base study, the course of this research is directed to investigate for further idealization and improvement in feasibility of the control strategies and to study their evaluations by including hardware implementations. The following section summarizes possible ideas for improvements and lists respective future studies.

## 6.2 Future Extensions and Impact

The final remarks in terms of the future works of this study are about the implementation of the proposed control algorithms. The studied concepts have been proven primarily through numerical analysis. Although numerical methods are quite viable and widely accepted, they require the system components such as sensor noise or measurement uncertainties to be modeled, which, depending on the physical system in hand might not be a straightforward process. Even with the inclusion of such components, the real world applications might introduce further unexpected and/or unmodeled uncertainties which might yield to unintended performance alterations. In addition, these variations with the real world and simulation implementation of the algorithms might delude with the improvement results in the comparison studies. To avoid these issues, the so-called Hardware-in-the-Loop (HiL) systems are utilized, which relieves the cost of testing by not requiring a complete vehicle in the very cost sensitive research environment; at the same time provides a reliable test-bed to imitate real

world conditions. Therefore, a follow-up step of this study might be taken by implementing and evaluating the proposed algorithms on a HiL system. An initial challenge concerning the practicality of this research is then the adjustment of the algorithms for real-time application. The available coding for numerical analysis, including the optimization procedures, might require further alteration of the selected solution methods specific for the hardware in use. Furthermore, specific real-time strategies (i.e. hard, firm or soft) need to be determined for respective sections of each algorithm.

The successful implementation of the algorithms on hardware will take the study to the next state where they can be migrated to production vehicles for specific tuning and marketing. Based on the analysis as reported in the preceding chapters, these control systems are expected to immensely improve individual vehicle safety as well as the traffic network as a whole. The proposed study also holds a foundation to greatly benefit the Intelligent Transportation Systems (ITS) that are subject to substantial interest today and anticipated to form the future of ground transportation. The smart tire technology will play a central role in binding all members of the transportation network from road surface to the central supervisory offices, which ultimately will yield to an integrated ITS scheme. It will also allow providing extensive information to form databases about various system states such as road condition, congestion, speed limits, etc. which are crucial in the further development of active safety systems but are not available today through any means of sensory equipment in use.

# Bibliography


[1] H. Dugoff, P. Fancher, and L. Segel, "Tire performance characteristics affecting vehicle response to steering and braking control inputs," Tech. Rep., 1969.

[2] J. Dang, "Preliminary results analyzing the effectiveness of electronic stability control (esc) systems," 2004.

[3] C. M. Farmer, "Effect of electronic stability control on automobile crash risk," *Traffic Injury Prevention*, vol. 5, no. 4, pp. 317–325, 2004.

[4] A. Lie, C. Tingvall, M. Krafft, and A. Kullgren, "The effectiveness of electronic stability control (esc) in reducing real life crashes and injuries," *Traffic Injury Prevention*, vol. 7, no. 1, pp. 38–43, 2006.

[5] S. A. Ferguson, "The effectiveness of electronic stability control in reducing real-world crashes: A literature review," *Traffic Injury Prevention*, vol. 8, no. 4, pp. 329–338, 2007.

[6] E. Commission, "Proposal for a regulation of the european parliament and of the council concerning type-approval requirements for the general safety of motor vehicles," 2008.

[7] N. H. T. S. Administration, "Electronic stability control systems controls and displays," 2007.

[8] F. Braghin, F. Cheli, S. Melzi, E. Sabbioni, F. Mancosu, and M. Brusarosco, "Development of a cyber tire to enhance performances of active control systems," September 7-11, 2009 2009.

[9] V. Magori, V. R. Magori, and N. Seitz, "On-line determination of tyre deformation, a novel sensor principle," in *Ultrasonics Symposium, 1998. Proceedings., 1998 IEEE*, vol. 1, pp. 485–488 vol.1.

[10] A. Cyllik, T. Strothjohann, and G. Scholl, "The intelligent tire - applications of the tread sensor der intelligente reifen - anwendunqsmoglichkeiten des reifenprofilsensors," *VDI Berichte*, no. Compendex, pp. 115–124+465, 2001, compilation and indexing terms, Copyright 2011 Elsevier Inc. 2004388359108 Tire pressure Tread sensors Vehicle control systems.

[11] T. Makinen and H. Wunderlich, "Intelligent tyre promoting accident-free traffic," in *The IEEE 5th International Conference on Intelligent Transportation Systems.* IEEE, pp. 606–609.

[12] Z. Zhao, Y. Li, Q. Wang, J. Li, L. Chu, Z. Ma, and D. Liu, "Application of infrared thermometer in testing of temperature field for a rolling tire," in *Proceedings of the IEEE International Vehicle Electronics Conference (IVEC'99), 6-9 Sept. 1999*, ser. Proceedings of the IEEE International Vehicle Electronics Conference (IVEC'99) (Cat. No.99EX257), vol. vol.1. IEEE, pp. 98–101.

[13] D. Snyder, "Piezoelectric reed power supply for use in abnormal tire condition warning systems," April, 9, 1985 1985.

[14] M. Brandt, V. Bachmann, A. Vogt, M. Fach, K. Mayer, B. Breuer, and H. L. Hartnagel, "Highly sensitive algaas/gaas position sensors for measurement of tyre tread deformation," *Electronics Letters*, vol. 34, no. 8, pp. 760–2, 1998.

[15] I. Wagstaff, "Braking new ground," *Automotive Engineer (London)*, vol. 24, no. 4, pp. 61–62, 1999.

[16] "Apollo - final report including technical implementation plan," Tech. Rep. FP5-IST-2001-34372, 2005.

[17] "Friction - final report," Tech. Rep. FP6-IST-2004-027006, 2009.

[18] A. J. Tuononen, "Optical position detection to measure tyre carcass deflections," *Vehicle System Dynamics*, vol. 46, no. 6, pp. 471–481, 2008.

[19] T. Umeno, "Estimation of tire-road friction by tire rotational vibration model," *R&D Review Toyota CRDL*, vol. 37, pp. 53–58, 2002.

[20] X. Zhang, Z. Wang, L. Gai, Y. Ai, and F. Wang, "Design considerations on intelligent tires utilizing wireless passive surface acoustic wave sensors," vol. 4, pp. 3696–3700.

[21] K. Seki, S. Shin, and T. Tabaru, "Analysis of wavelet correlation between tyre sounds and tread patterns," in *Networking, Sensing and Control, 2005. Proceedings. 2005 IEEE*, pp. 241–246.

[22] R. Matsuzaki and A. Todoroki, "Wireless strain monitoring of tires using electrical capacitance changes with an oscillating circuit," *Sensors and Actuators A: Physical*, vol. 119, no. 2, pp. 323–331, 2005.

[23] ——, "Passive wireless strain monitoring of actual tire using capacitanceresistance change and multiple spectral features," *Sensors and Actuators A: Physical*, vol. 126, no. 2, pp. 277–286, 2006.

[24] ——, "Wireless monitoring of automobile tires for intelligent tires," *Sensors*, vol. 8, no. 12, pp. 8123–8138, 2008.

[25] M. Ohori, T. Ishizuka, T. Fujita, N. Masaki, and Y. Suizu, "Fundamental study of smart tire system," in *Intelligent Transportation Systems Conference, 2006. ITSC '06. IEEE*, pp. 1519–1524.

[26] F. Braghin, M. Brusarosco, F. Cheli, A. Cigada, S. Manzoni, and F. Mancosu, "Measurement of contact forces and patch features by means of accelerometers fixed inside the tire to improve future car active control," *Vehicle System Dynamics*, vol. 44, pp. 3–13, 2006.

[27] M. Brusarosco, A. Cigada, and S. Manzoni, "Experimental investigation of tyre dynamics by means of mems accelerometers fixed on the liner," *Vehicle System Dynamics*, vol. 46, no. 11, pp. 1013–1028, 2008.

[28] S. M. Savaresi, M. Tanelli, P. Langthaler, and L. Del Re, "New regressors for the direct identification of tire deformation in road vehicles via in-tire accelerometers," *Control Systems Technology, IEEE Transactions on*, vol. 16, no. 4, pp. 769–780, 2008.

[29] G. Audisio, F. Cheli, S. Melzi, and M. Velardocchia, "Cybertm tyre for vehicle active safety," in *XIX Congress of Italian Association for Theoretical and Applied Mechanics*, pp. 14–17.

[30] S. C. Ergen, A. Sangiovanni-Vincentelli, S. Xuening, R. Tebano, S. Alalusi, G. Audisio, and M. Sabatini, "The tire as an intelligent sensor," *IEEE Transactions on Computer-Aided Design of Integrated Circuits and Systems*, vol. 28, pp. 941–55, 2009.

[31] F. Cheli, E. Leo, S. Melzi, and E. Sabbioni, "On the impact of smart tyres on existing abs/ebd control systems," *Vehicle System Dynamics*, vol. 48, no. sup1, pp. 255–270, 2010.

[32] G. Erdogan, L. Alexander, and R. Rajamani, "Adaptive vibration cancellation for tire-road friction coefficient estimation on winter maintenance vehicles," *IEEE Transactions on Control Systems Technology*, vol. 18, no. 5, pp. 1023–1032, 2010.

[33] F. Cheli, E. Sabbioni, M. Tyre, and S. Melzi, "Enhancement of abs performance through on-board estimation of the tires' response by means of smart tires," 2011.

[34] G. Erdogan, S. Hong, F. Borrelli, and K. Hedrick, "Tire sensors for the measurement of slip angle and friction coefficient and their use in stability control systems," *SAE International Journal of Passenger Cars-Mechanical Systems*, vol. 4, no. 1, pp. 44–58, 2011.

[35] K. B. Singh, "Development of an intelligent tire based tire - vehicle state estimator for application to global chassis control," Ph.D. dissertation, 2012.

[36] K. B. Singh, M. Arat, and S. Taheri, "An intelligent tire based tire-road friction estimation technique and adaptive wheel slip controller for anti-lock brake system," *Journal of Dynamic Systems, Measurement, and Control*, 2012.

[37] M. Abe and W. Manning, *Vehicle handling dynamics: theory and application*. Butterworth-Heinemann, 2009.

[38] H. Pacejka, *Tire and Vehicle Dynamics*. SAE, 2006.

[39] M. W. Sayers, "Symbolic computer language for multibody systems," *Journal of Guidance, Control, and Dynamics*, vol. 14, no. 6, pp. 1153–63, 1991.

[40] T. Kinjawadekar, N. Dixit, G. Heydinger, D. Guenther, and M. Salaani, "Vehicle dynamics modeling and validation of the 2003 ford expedition with esc using carsim," *Society of Automotive Engineers Paper*, pp. 01–0452, 2009.

[41] T. Toyohira, K. Nakamura, and Y. Tanno, "The validity of eps control system development using hils," *SAE Technical Paper*, pp. 01–0008, 2010.

[42] J. Wilkinson, C. Mousseau, and T. Klingler, "Brake response time measurement for a hil vehicle dynamics simulator," 2010.

[43] "Carsim: Math models," 2011.

[44] H. Dugoff, P. Francher, and L. Segel, "An analysis of tire traction properties and their influence on vehicle dynamic performance, sae 700377," *SAE International Journal of Passenger Cars - Mechanical Systems*, 1970.

[45] H. Pacejka and E. Bakker, "The magic formula tyre model," *Vehicle System Dynamics*, vol. 21, no. S1, pp. 1–18, 1992.

[46] E. Herb, H. Krusche, E. Schwartz, and H. Wallentowitz, "Stability-control and traction-control at four-wheel-drive cars," *SAE Technical Paper*, 1988.

[47] N. Rittmannsberger, "Antilock braking system and traction control." IEEE, pp. 195–202.

[48] H. Leffler, R. Auffhammer, R. Heyken, and H. Roth, "New driving stability control system with reduced technical effort for compact-and medium-class passenger cars," *SAE transactions*, vol. 107, no. 6, pp. 416–423, 1998.

[49] K. Jost, "Cadillac stability enhancement," *Automotive Engineering International*, vol. 104, no. 10, pp. 111–113, 1996.

[50] D. Hoffman and M. Rizzo, "Chevrolet c5 corvette vehicle dynamic control system," *SAE transactions*, 1998.

[51] K. Koibuchi, M. Yamamoto, Y. Fukada, and S. Inagaki, "Vehicle stability control in limit cornering by active brake," *SAE transactions*, vol. 105, pp. 555–565, 1996.

[52] T. Pilutti, G. Ulsoy, and D. Hrovat, "Vehicle steering intervention through differential braking," in *American Control Conference*, vol. 3. IEEE, pp. 1667–1671 vol. 3.

[53] Y. A. Ghoneim, W. C. Lin, D. M. Sidlosky, H. H. Chen, Y.-K. Chin, and M. J. Tedrake, "Integrated chassis control system to enhance vehicle stability," *International Journal of Vehicle Design*, vol. 23, pp. 124–144, 2000.

[54] Y. Fukada, "Slip-angle estimation for vehicle stability control," *Vehicle System Dynamics*, vol. 32, pp. 375–388, 1999.

[55] A. Nishio, K. Tozu, H. Yamaguchi, K. Asano, and Y. Amano, "Development of vehicle stability control system based on vehicle sideslip angle estimation," *SAE transactions*, 2001.

[56] G. Baffet, A. Charara, and J. Stphant, "Sideslip angle, lateral tire force and road friction estimation in simulations and experiments," in *IEEE Conference on Control Applications*. IEEE, pp. 903–908.

[57] J. Ackermann, "Robust car steering by yaw rate control," in *IEEE Conference on Decision and Control*. IEEE, pp. 2033–2034 vol. 4.

[58] ——, "Robust decoupling, ideal steering dynamics and yaw stabilization of 4ws cars," *Automatica*, vol. 30, no. 11, pp. 1761–1768, 1994.

[59] J. Ackermann and T. Bnte, "Yaw disturbance attenuation by robust decoupling of car steering," *Control Engineering Practice*, vol. 5, no. 8, pp. 1131–1136, 1997.

[60] J. Ackermann, J. Guldner, W. Sienel, R. Steinhauser, and V. Utkin, "Linear and nonlinear controller design for robust automatic steering," *Control Systems Technology, IEEE Transactions on*, vol. 3, no. 1, pp. 132–143, 1995.

[61] R. Isermann, R. Schwarz, and S. Stolzl, "Fault-tolerant drive-by-wire systems," *Control Systems Magazine, IEEE*, vol. 22, no. 5, pp. 64–81, 2002.

[62] S. Mammar and D. Koenig, "Vehicle handling improvement by active steering," *Vehicle System Dynamics*, vol. 38, no. 3, pp. 211–242, 2002.

[63] S.-S. You, H.-S. Choi, H.-S. Kim, T.-W. Lim, and S.-K. Jeong, "Active steering for intelligent vehicles using advanced control synthesis," *International Journal of Vehicle Design*, vol. 42, pp. 244–262, 2006.

[64] Y. Hsu and J. Gerdes, "Stabilization of a steer-by-wire vehicle at the limits of handling using feedback linearization," in *ASME International Mechanical Engineering Congress and Exposition*.

[65] Y. Ikushima and K. Sawase, "A study on the effects of the active yaw moment control," *SAE transactions*, 1995.

[66] H. Huchtkoetter and T. Gassmann, "Vehicle dynamics and torque management devices," *SAE transactions*, 2004.

[67] R. Osborn and T. Shim, "Independent control of all-wheel-drive torque distribution," *Vehicle System Dynamics*, vol. 44, no. 7, pp. 529–546, 2006.

[68] M. Canale, L. Fagiano, M. Milanese, and P. Borodani, "Robust vehicle yaw control using an active differential and imc techniques," *Control Engineering Practice*, vol. 15, no. 8, pp. 923–941, 2007.

[69] A. Trachtler, "Integrated vehicle dynamics control using active brake, steering and suspension systems," *International Journal of Vehicle Design*, vol. 36, no. 1, pp. 1–12, 2004.

[70] A. Hac and M. Bodie, "Improvements in vehicle handling through integrated control of chassis systems," *International Journal of Vehicle Autonomous Systems*, vol. 1, no. 1, pp. 83–110, 2002.

[71] H. Smakman, "Functional integration of active suspension with slip control for improved lateral vehicle dynamics," in *International Symposium on Advenced Vehicle Control (AVEC) - 5th*.

[72] ——, "Functional integration of active suspension with slip control for improved lateral vehicle dynamics," Ph.D. dissertation, 2000.

[73] H. Duda and S. Berkner, "Integrated chassis control using active suspension and braking," in *7th International Symposium on Advenced Vehicle Control (AVEC)*, vol. 347, p. 352.

[74] T. Hwang, K. Park, S.-J. Heo, and S. Lee, *Integrated Chassis Controller Design of Active Steering and Active Braking Systems Using CL Method*, ser. Communications

in Computer and Information Science. Springer Berlin Heidelberg, 2007, vol. 2, pp. 632–640.

[75] T. Hwang, K. Park, S. Heo, S. Lee, and J. Lee, "Design of integrated chassis control logics for afs and esp," *International Journal of Automotive Technology*, vol. 9, no. 1, pp. 17–27, 2008.

[76] M. Nagai, Y. Hirano, and S. Yamanaka, "Integrated robust control of active rear wheel steering and direct yaw moment control," *Vehicle System Dynamics*, vol. 29, no. S1, pp. 416–421, 1998.

[77] M. Nagai, M. Shino, and F. Gao, "Study on integrated control of active front steer angle and direct yaw moment," *JSAE review*, vol. 23, no. 3, pp. 309–315, 2002.

[78] M. Selby, W. Manning, D. Crolla, and W. Brown, "A comparison of the relative benefits of active front steering and active rear steering when coordinated with direct yaw moment control."

[79] J. He, D. Crolla, M. Levesley, and W. Manning, "Coordination of active steering, driveline, and braking for integrated vehicle dynamics control," *Proceedings of the Institution of Mechanical Engineers, Part D: Journal of Automobile Engineering*, vol. 220, no. 10, p. 1401, 2006.

[80] C. March and T. Shim, "Integrated control of suspension and front steering to enhance vehicle handling," *Proceedings of the Institution of Mechanical Engineers, Part D: Journal of Automobile Engineering*, vol. 221, no. 4, pp. 377–391, 2007.

[81] W. Chen, H. Xiao, L. Liu, and J. Zu, "Integrated control of automotive electrical power steering and active suspension systems based on random sub-optimal control," *International Journal of Vehicle Design*, vol. 42, no. 3, pp. 370–391, 2006.

[82] N. Matsumoto and M. Tomizuka, "Vehicle lateral velocity and yaw rate control with two independent control inputs," *Journal of Dynamic Systems, Measurement, and Control*, vol. 114, no. 4, pp. 606–613, 1992.

[83] M. Salman, Z. Zhang, and N. Boustany, "Coordinated control of four wheel braking and rear steering," in *American Control Conference*. IEEE, pp. 6–10.

[84] M. Shino and M. Nagai, "Independent wheel torque control of small-scale electric vehicle for handling and stability improvement," *JSAE review*, vol. 24, no. 4, pp. 449–456, 2003.

[85] T. Chu and R. Jones, "Integrated four-wheel-steering and direct yaw moment control via robust eigenstructure assignment techniques," in *6th International Symposium on Advenced Vehicle Control (AVEC)*.

[86] E. Ono, K. TaKanami, N. Iwama, Y. Hayashi, Y. Hirano, and Y. Satoh, "Vehicle integrated control for steering and traction systems by [mu]-synthesis," *Automatica*, vol. 30, no. 11, pp. 1639–1647, 1994.

[87] O. Mokhiamar and M. Abe, "Simultaneous optimal distribution of lateral and longitudinal tire forces for the model following control," *Journal of Dynamic Systems, Measurement, and Control*, vol. 126, p. 753, 2004.

[88] Y. Hattori, K. Koibuchi, and T. Yokoyama, "Force and moment control with nonlinear optimum distribution for vehicle dynamics," in *6th International Symposium on Advanced Vehicle Control (AVEC'02)*, pp. 595–600.

[89] X. Shen, D. Li, and F. Yu, "Study on vehicle chassis control integration based on general actuator-plant structure," in *Proc. AVEC06, Taipei, Taiwan*.

[90] X. Shen and F. Yu, "Study on vehicle chassis control integration based on a main-loop-inner-loop design approach," *Proceedings of the Institution of Mechanical Engineers, Part D: Journal of Automobile Engineering*, vol. 220, no. 11, pp. 1491–1502, 2006.

[91] D. Li, X. Shen, and F. Yu, "Integrated vehicle chassis control with a main/servo-loop structure," *International Journal of Automotive Technology*, vol. 7, no. 7, pp. 803–812, 2006.

[92] X. Shen and F. Yu, "Study on vehicle chassis control integration based on vehicle dynamics and separate loop design approach," *International Journal of Vehicle Autonomous Systems*, vol. 5, no. 1, pp. 95–118, 2007.

[93] R. Stengel, *Optimal Control and Estimation*. Dover Publications, 1994.

[94] J. C. Gerdes, C. Wilson, and D. M. Bevly, "The use of gps based velocity measurements for measurement of sideslip and wheel slip," *Vehicle System Dynamics*, vol. 38, no. 2, pp. 127–147, 2003.

[95] R. Daily and D. M. Bevly, "The use of gps for vehicle stability control systems," *IEEE Transactions on Industrial Electronics*, vol. 51, no. 2, pp. 270–277, 2004.

[96] T. Mohan Manubhai, G. Tarak, and M. Joel, "Looking-in and looking-out of a vehicle: Computer-vision-based enhanced vehicle safety," *Intelligent Transportation Systems, IEEE Transactions on*, vol. 8, no. 1, pp. 108–120, 2007.

[97] W. Cheng-Xiang, C. Xiang, and D. I. Laurenson, "Vehicle-to-vehicle channel modeling and measurements: recent advances and future challenges," *Communications Magazine, IEEE*, vol. 47, no. 11, pp. 96–103, 2009.

[98] R. Masmoudi and J. Hedrick, "Estimation of vehicle shaft torque using nonlinear observers," *Journal of Dynamic Systems, Measurement, and Control*, vol. 114, p. 394, 1992.

[99] G. Baffet, A. Charara, and D. Lechner, "Experimental evaluation of a sliding mode observer for tire-road forces and an extended kalman filter for vehicle sideslip angle," in *IEEE Conference on Decision and Control*. IEEE, pp. 3877–3882.

[100] H. Khalil and J. Grizzle, *Nonlinear systems*. Prentice hall Upper Saddle River, NJ, 2002, vol. 122.

[101] S. Tsugawa, "Issues and recent trends in vehicle safety communication systems," *IATSS research*, vol. 29, no. 1, pp. 7–15, 2005.

[102] R. Mangharam, D. Weller, R. Rajkumar, P. Mudalige, and B. Fan, "Groovenet: A hybrid simulator for vehicle-to-vehicle networks," in *Mobile and Ubiquitous Systems: Networking and Services, 2006 Third Annual International Conference on*, pp. 1–8.

[103] T. Day and S. Roberts, "A simulation model for vehicle braking systems fitted with abs," in *SAE World Congress and Exhibition*. SAE.

[104] H. Pacejka, *Tire and vehicle dynamics*. Butterworth Heinemann, 2012.

[105] J. Luo and J.-P. Hubaux, "A survey of intervehicle communication," Tech. Rep., 2004.

[106] D. Reichardt, M. Miglietta, L. Moretti, P. Morsink, and W. Schulz, "Cartalk 2000: safe and comfortable driving based upon inter-vehicle-communication," in *Intelligent Vehicle Symposium, 2002. IEEE*, vol. 2, pp. 545–550 vol.2.

[107] R. Guntur and H. Ouwerkerk, "Adaptive brake control system," *Proceedings of the Institution of Mechanical Engineers 1847-1982 (vols 1-196)*, vol. 186, no. 1972, pp. 855–880, 1972.

[108] H. Ouwerkerk and R. Guntur, "Skid prediction," *Vehicle System Dynamics*, vol. 1, no. 2, pp. 67–88, 1972.

[109] S. Taheri, "A feasibility study of the use of a new nonlinear control law for automobile anti-lock braking systems," *TRANSPORTATION SYSTEMS, 1990*, 1990.

[110] C. Kuo and E. Yeh, "A four-phase control scheme of an anti-skid brake system for all road conditions," *Proceedings of the Institution of Mechanical Engineers, Part D: Journal of Automobile Engineering*, vol. 206, no. 4, pp. 275–283, 1992.

[111] E. Yeh and G. Day, "Parametric study of anti-skid brake systems using poincare map concept," *International Journal of Vehicle Design*, vol. 13, no. 3, pp. 210–32, 1992.

[112] E. Yeh, C. Kuo, and P. Sun, "Conjugate boundary method for control law design of anti-skid brake systems," *International Journal of Vehicle Design*, vol. 11, no. 1, pp. 40–62, 1990.

[113] S. Drakunov, U. Ozguner, P. Dix, and B. Ashrafi, "Abs control using optimum search via sliding modes," *IEEE Transactions on Control Systems Technology*, vol. 3, no. 1, pp. 79–85, 1995.

[114] C. Unsal and P. Kachroo, "Sliding mode measurement feedback control for antilock braking systems," *IEEE Transactions on Control Systems Technology*, vol. 7, pp. 271–281, 1999.

[115] J. Yi, L. Alvarez, R. Horowitz, and C. C. de Wit, "Adaptive emergency braking control using a dynamic tire/road friction model," in *Decision and Control, 2000. Proceedings of the 39th IEEE Conference on*, vol. 1, pp. 456–461 vol.1.

[116] J. Yi, L. Alvarez, X. Claeys, and R. Horowitz, "Emergency braking control with an observer-based dynamic tire/road friction model and wheel angular velocity measurement," *Vehicle System Dynamics*, vol. 39, no. 2, pp. 81–97, 2003.

[117] L. Alvarez, J. Yi, R. Horowitz, and L. Oimos, "Dynamic friction model-based tire-road friction estimation and emergency braking control," *Journal of Dynamic Systems, Measurement and Control, Transactions of the ASME*, vol. 127, no. 1, pp. 22–32, 2005.

[118] R. Keshmiri and A. Shahri, "Intelligent abs fuzzy controller for diverse road surfaces," *World Academy of Science, Engineering and Technology*, vol. 2, no. 2, pp. 62–67, 2007.

[119] M. Habibi and A. Yazdizadeh, "A novel fuzzy-sliding mode controller for antilock braking system," vol. 4, pp. 110–114.

[120] I. Petersen, T. Johansen, J. Kalkkuhl, and J. Ldemann, "Wheel slip control in abs brakes using gain scheduled constrained lqr," in *European Control Conference*, pp. 606–611.

[121] T. A. Johansen, I. Petersen, J. Kalkkuhl, and J. Ludemann, "Gain-scheduled wheel slip control in automotive brake systems," *IEEE Transactions on Control Systems Technology*, vol. 11, no. 6, pp. 799–811, 2003.

[122] S. a. Balamili, . E. Kse, and G. Anla, "Robust control of anti-lock brake system," *Vehicle System Dynamics*, vol. 45, no. 3, pp. 217–232, 2007.

[123] A. Carter, "The status of vehicle-to-vehicle communication as a means of improving crash prevention performance," National Highway Traffic Safety Administration, Tech. Rep., 2005.

[124] "Us dot. national its program plan," US Department of Transportation, Tech. Rep., 2007.

[125] S. Spieckermann, K. Gutenschwager, H. Heinzel, and S. Vo, "Simulation-based optimization in the automotive industry-a case study on body shop design," *SIMULATION*, vol. 75, no. 5/6, pp. 276–286, 2000.

[126] H. Pierreval, R. Bruniaux, and C. Caux, "A continuous simulation approach for supply chains in the automotive industry," *Simulation Modelling Practice and Theory*, vol. 15, no. 2, pp. 185–198, 2007.

[127] U. Kiencke and L. Nielsen, "Automotive control systems: For engine, driveline, and vehicle," *Measurement Science and Technology*, vol. 11, no. 12, p. 1828, 2000.

[128] M. Doumiati, A. Victorino, A. Charara, D. Lechner, and G. Baffet, "An estimation process for vehicle wheel-ground contact normal forces," *IFAC WC*, vol. 8, 2008.

[129] G. G. Wang, "Definition and review of virtual prototyping," *Journal of Computing and Information Science in Engineering(Transactions of the ASME)*, vol. 2, no. 3, pp. 232–236, 2002.

[130] Y. Zhang, A. Tang, T. Palmer, and C. Hazard, "Virtual proving ground - an integrated technology for full vehicle analysis and simulation," *International Journal of Vehicle Design*, vol. 21, no. 4, pp. 450–470, 1999.

[131] S. Sastry and M. Bodson, *Adaptive control: stability, convergence, and robustness*. Prentice-Hall, Inc., 1989.

[132] S. M. Savaresi and M. Tanelli, *Active braking control systems design for vehicles*. London; New York: Springer-Verlag, 2010.

[133] P. Wellstead and N. Pettit, "Analysis and redesign of an antilock brake system controller," in *Control Theory and Applications, IEE Proceedings-*, vol. 144. IET, pp. 413–426.

[134] N. Pettit, *The analysis of piecewise linear dynamical systems*. Springer, 1997, pp. 49–58.

[135] J. M. Gonalves, "Regions of stability for limit cycle oscillations in piecewise linear systems," *Automatic Control, IEEE Transactions on*, vol. 50, no. 11, pp. 1877–1882, 2005.

[136] M. Tanelli, G. Osorio, M. di Bernardo, S. Savaresi, and A. Astolfi, "Limit cycles analysis in hybrid anti-lock braking systems," in *46th IEEE Conference on Decision and Control*. IEEE, pp. 3865–3870.

[137] M. Tanelli, G. Osorio, M. di Bernardo, S. M. Savaresi, and A. Astolfi, "Existence, stability and robustness analysis of limit cycles in hybrid anti-lock braking systems," *International Journal of Control*, vol. 82, no. 4, pp. 659–678, 2009.

[138] J. J. Mor, *The Levenberg-Marquardt algorithm: implementation and theory*. Springer, 1978, pp. 105–116.

[139] M. Arat, "An adaptive vehicle stability control algorithm based on tire slip-angle estimation," in *SAE Commercial Vehicles*, 2012.

[140] L. Petruccelli and M. Velardocchia, "Electro-hydraulic braking system modelling and simulation," 2003.

[141] Y. Ikeda and M. Hood, "An application of l1 optimization to control allocation," in *Proc. AIAA Guidance, Navigation and Control Conference and Exhibit, Denver, CO*.

[142] M. Bodson, "Evaluation of optimization methods for control allocation," *Journal of Guidance, Control, and Dynamics*, vol. 25, no. 4, pp. 703–711, 2002.

[143] W. C. Durham and K. A. Bordignon, "Multiple control effector rate limiting," *Journal of Guidance, control, and Dynamics*, vol. 19, no. 1, pp. 30–37, 1996.

[144] S. P. Berge and T. I. Fossen, "Robust control allocation of overactuated ships; experiments with a model ship," in *Proc. of the 4th IFAC Conference on Manoeuvring and Control of Marine Craft*. Citeseer, pp. 166–171.

[145] J. Nocedal and S. Wright, *Numerical optimization, series in operations research and financial engineering*, ser. Springer, New York, 2006.

[146] M. Krstic, I. Kanellakopoulos, and P. V. Kokotovic, *Nonlinear and adaptive control design*. John Wiley and Sons New York, 1995, vol. 8.

[147] G. Arslan and T. Baar, "Disturbance attenuating controller design for strict-feedback systems with structurally unknown dynamics," *Automatica*, vol. 37, no. 8, pp. 1175–1188, 2001.

[148] Z.-P. Jiang and D. J. Hill, "A robust adaptive backstepping scheme for nonlinear systems with unmodeled dynamics," *Automatic Control, IEEE Transactions on*, vol. 44, no. 9, pp. 1705–1711, 1999.

[149] V. O. Nikiforov and K. V. Voronov, "Nonlinear adaptive controller with integral action," *Automatic Control, IEEE Transactions on*, vol. 46, no. 12, pp. 2035–2037, 2001.

[150] R. Marino and P. Tomei, "Global adaptive output-feedback control of nonlinear systems. i. linear parameterization," *Automatic Control, IEEE Transactions on*, vol. 38, no. 1, pp. 17–32, 1993.

[151] R. Ordez and K. M. Passino, "Adaptive control for a class of nonlinear systems with a time-varying structure," *Automatic Control, IEEE Transactions on*, vol. 46, no. 1, pp. 152–155, 2001.

[152] Y. Zhang, B. Fidan, and P. A. Ioannou, "Backstepping control of linear time-varying systems with known and unknown parameters," *Automatic Control, IEEE Transactions on*, vol. 48, no. 11, pp. 1908–1925, 2003.

[153] P. A. Ioannou and J. Sun, *Robust adaptive control*. DoverPublications. com, 2012.

[154] R. Marino and P. Tomei, "Global adaptive observers for nonlinear systems via filtered transformations," *Automatic Control, IEEE Transactions on*, vol. 37, no. 8, pp. 1239–1245, 1992.

[155] I. M. Gregory, C. Cao, E. Xargay, N. Hovakimyan, and X. Zou, "L1 adaptive control design for nasa airstar flight test vehicle," in *AIAA Guidance, Navigation, and Control Conference*, vol. 5738.

[156] I. Kaminer, O. Yakimenko, V. Dobrokhodov, A. Pascoal, N. Hovakimyan, C. Cao, A. Young, and V. Patel, "Coordinated path following for time-critical missions of multiple uavs via l1 adaptive output feedback controllers," in *AIAA Guidance, Navigation and Control Conference and Exhibit*.

[157] X. Fan and R. Smith, "Model-based l¡ inf¿ 1¡/inf¿ adaptive control of hysteresis in smart materials," in *Decision and Control, 2008. CDC 2008. 47th IEEE Conference on*. IEEE, pp. 3251–3256.

[158] I. Kaminer, A. Pascoal, E. Xargay, N. Hovakimyan, C. Cao, and V. Dobrokhodov, "Path following for small unmanned aerial vehicles using l1 adaptive augmentation of commercial autopilots," *Journal of guidance, control, and dynamics*, vol. 33, no. 2, pp. 550–564, 2010.

# Appendix A

# Projection Operator

As summarized in Chapter 5, the adaptive control strategies are being utilized in an expanding rate. Although being introduced in the midst of the 20th century, the lack of theoretical background suspended the wide-spread of the adaptive techniques until late 1990s. A significant advantage of adaptive controllers is that they can account for system uncertainties without requiring explicit system identification structures, which is particularly noticeable on highly nonlinear systems such as automobile dynamics as addressed in this study. A key assumption that needs to be persuaded though is that the estimates of these uncertainties provided for the control signal computation are to be bounded to be able to guarantee the so-called feedback stabilizability. The Projection Operator is introduced as a remedy in satisfying this condition In the context of the adaptation law, it basically allows transforming the estimated parameters, say $p$, onto a convex and bounded set $\Pi$, which is assumed to define the upper and lower bounds of the expected parameters values, so that the estimations are confined into a known span avoiding parameter drift. This appendix is aimed to provide the formal mathematical description of the operator.

First, the notions of a convex set and convex function need to be defined as they appear extensively through the following definitions.

**Definition** A set $\Omega \subset \mathbb{R}^n$ is *convex* if for all $x, y \in \Omega$ the following holds true:

$$\lambda x + (1 - \lambda)y \in \Omega, \qquad \forall \lambda \in [0 \quad 1]$$

as illustrated below.

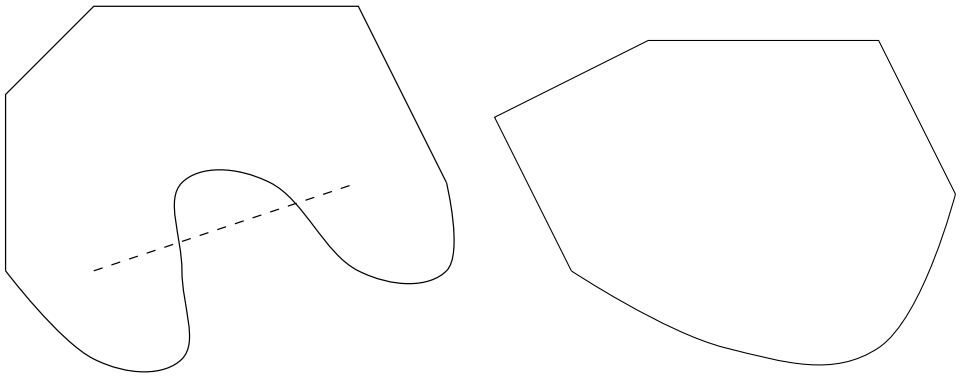

(a) (b)

Figure A.1: (a) Convex (b) non-convex sets.

**Definition** A function $f : \mathbb{R}^n \to \mathbb{R}$ is *convex* if for all $x, y \in \mathbb{R}^n$ the following holds true:

$$f\left(\lambda x_1 + (1-\lambda)x_1\right) \leq \lambda f(x_1) + (1-\lambda) f(x_2), \qquad \forall \lambda \in [0 \quad 1]$$

An illustration is shown below.

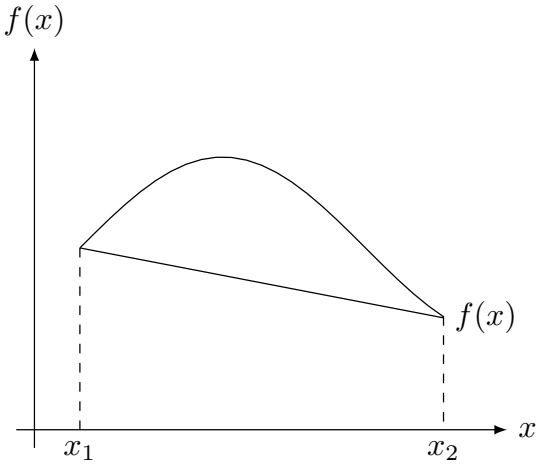


Figure A.2: Convex function $f(x)$.

**Lemma A.0.1.** *Letting $f : \mathbb{R}^n \to \mathbb{R}$ be a convex function, the set (also known as the sublevel set) $\Omega_\delta \triangleq \theta \in \mathbb{R}^n | f(\theta) \leq \delta$ is convex for any arbitrary constant $\delta$.*

The proof can be given as follows. Let $\theta_1, \theta_2 \in \Omega_\delta$, then $f(\theta_1) \leq \delta$ and $f(\theta_2) \leq \delta$. Since $f(x)$ is convex $\forall \lambda \in [0 \quad 1]$, one can find

$$f(\lambda\theta_1 + (1-\lambda)\theta_2) \leq \underbrace{\lambda f(\theta_1)}_{\leq\delta} + (1-\lambda)\underbrace{f(\theta_2)}_{\leq\delta} \leq \lambda\delta + (1-\lambda)\delta = \delta$$

therefore $f(\theta) \leq \delta$, thus $\theta \in \Omega_\delta$.

**Lemma A.0.2.** *Let $f(\theta) : \mathbb{R}^n \to \mathbb{R}$ be a continuously differentiable convex function, choose an arbitrary constant $\delta$ and consider the convex set $\Omega_\delta \triangleq \theta \in \mathbb{R}^n | f(\theta) \leq \delta$. Also let $\theta^*$ be an interior point of $\Omega_\delta$, i.e. $f(\theta^*) < \delta$. Finally choose $\theta_b$ as a boundary point so that $f(\theta_b) = \delta$. Then the following holds true:*

$$(\theta^* - \theta_b)^T \nabla f(\theta_b) \leq 0$$

*where $\nabla f(\theta_b) = \left(\frac{\partial f(\theta)}{\partial \theta_1} \dots \frac{\partial f(\theta)}{\partial \theta_k}\right)^T$ is the gradient vector of $f(.)$ evaluated at $\theta_b$.*

The proof can be given as follows. Since $f(\theta)$ is assumed convex, one can write,

$$f(\lambda\theta^* + (1-\lambda)\theta_b) \leq \lambda f(\theta^*) + (1-\lambda) f(\theta_b)$$

which equivalently leads

$$f(\theta_b + \lambda(\theta^* - \theta_b)) \leq f(\theta_b) + \lambda(f(\theta^*) - f(\theta_b))$$

so for any $0 < \lambda \leq 1$

$$\frac{f(\theta_b) + \lambda(\theta^* - \theta_b)) - f(\theta_b)}{\lambda} \leq f(\theta^*) - f(\theta_b) \leq \delta - \delta = 0$$

and hence taking the limit $\lambda \to 0$ yields to the given lemma.

In what follows the projection operator can be introduced as below.

**Definition** Consider a convex bounded set with smooth boundary given as by

$$\Omega_c \triangleq \{\theta \in \mathbb{R}^n | f(\theta) \leq c\}, \qquad \forall c \in [0 \quad 1]$$

where $f : \mathbb{R}^n \to \mathbb{R}$ is the following smooth convex function

$$f(\theta) = \frac{(\epsilon_\theta + 1)\theta^T\theta - \theta_{max}^2}{\epsilon_\theta \theta_{max}^2}$$

with $\theta_{max}$ being the norm bound imposed on the vector $\theta$, and $\epsilon_\theta > 0$ is the projection tolerance bound of choice. the projection operator is defined as:

$$f(n) = \begin{cases} y, & \text{if } f(\theta) < 0 \\ y, & \text{if } f(\theta) \geq 0 \text{ and } \nabla f^T y \leq 0 \\ y - \dfrac{\nabla f(\theta)(\nabla f(\theta))^T}{||\nabla f(\theta)^2||} y f(\theta), & \text{if } f(\theta) \geq 0 \text{ and } \nabla f^T y > 0. \end{cases}$$

where $\nabla f(\theta)$ is the function gradient evaluated at $\theta$.

A geometrical interpretation of the operator in $\mathbb{R}^2$ can be given as follows to further clarify. Lets define a convex set $\Omega_0$ as:

$$\Omega_0 \triangleq \left\{\theta \in \mathbb{R}^2 | f(\theta) \leq 0\right\}$$

and let $\Omega_1$ represent another convex set such that

$$\Omega_1 \triangleq \left\{\theta \in \mathbb{R}^2 | f(\theta) \leq 1\right\}$$

which also yields to $\Omega_0 \subset \Omega_1$. Finally let $\Omega_A \triangleq \{\theta | 0 < f(\theta) \leq 1\}$ represent an annulus region on $\mathbb{R}^2$. Within $\Omega_A$ the projection algorithm subtracts a scaled component of $y$ that is normal to boundary $\{\theta | f(\theta) = \lambda\}$. When $\lambda = 0$, the scaled normal component us 0, and when $\lambda = 1$, the component of $y$ that is normal to the boundary $\Omega_!$ is entirely subtracted from $y$, so that $Proj(\theta, y)$ is tangent to the boundary $\{| f(\theta) = 1\}$.

Based on this example, a significant property of the projection operator can be given as follows:

$$(\theta - \theta^*)^T (Proj(\theta, y) - y) \leq 0 \tag{A.1}$$

where $\theta^* \in \Omega_0$. The proof starts by noticing

$$(\theta - \theta^*)^T (Proj(\theta, y) - y) = (\theta^* - \theta)^T (y - Proj(\theta, y))$$

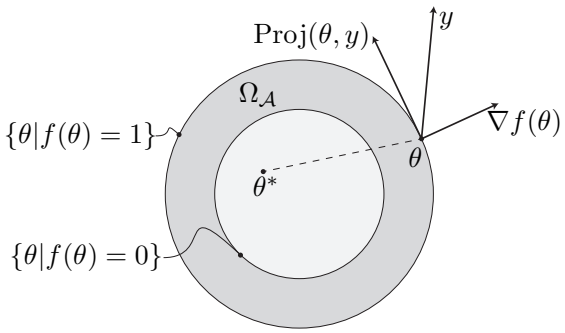


Figure A.3: Graphical illustration of the projection operator in $\mathbb{R}^2$.

which if $f(\theta) > 0$ and $\nabla f(\theta)^T y > 0$, equals to

$$(\theta^* - \theta)^T (y - Proj(\theta, y)) = (\theta^* - \theta)^T \left( y - \left( y - \frac{\nabla f(\theta)(\nabla f(\theta))^T}{||\nabla f(\theta)^2||} y f(\theta) \right) \right)$$

and 0 otherwise. Finally, following the second Lemma yields

$$\frac{\overbrace{(\theta^* - \theta)^T \nabla f(\theta)}^{\leq 0} \overbrace{(\nabla f(\theta))^T y}^{>0} \overbrace{f(\theta)}^{\geq 0}}{||\nabla f(\theta)||^2} \leq 0$$

so in tabular form

$$(\theta^* - \theta)^T (y - Proj(\theta, y)) = \begin{cases} 0, & \text{if } f(\theta) < 0 \\ 0, & \text{if } f(\theta) \geq 0 \text{ and } \nabla f^T y \leq 0 \\ \dfrac{\overbrace{(\theta^* - \theta)^T \nabla f(\theta)}^{\leq 0} \overbrace{(\nabla f(\theta))^T y}^{>0} \overbrace{f(\theta)}^{\geq 0}}{||\nabla f(\theta)||^2}, & \text{if } f(\theta) \geq 0 \text{ and } \nabla f^T y > 0 \end{cases}$$

which leads to the above stated property.

The use of the projection operator can be presented in an example Model Reference Adaptive Control (MRAC) scheme as follows. Consider the first order system

$$\begin{aligned} \dot{x} &= A_p x + B_p u, \qquad x(0) = x_0 \\ y &= Cx \end{aligned}$$

where $A_p$ and $B_p$ are constant plant parameters. The MRAC scheme proposes computing a control input $u$ that allows this system to track the dynamics of a desired reference system drive by a reference signal given as

$$\dot{x}_m = A_m x_m + B_m r$$

where $A_m$ and $B_m$ are constant reference parameters and $r$ is a bounded external reference signal. Attention must be paid to the stability of the reference model (i.e. $A_m$ is a known Hurwitz matrix). The MRAC control law is given by:

$$u = -k_x(t)x + k_g r$$

where $k_x$ and $k_g$ are the feedback gain values. The closed loop dynamics then becomes:

$$\dot{x} = (A_p - B_p k_x)x + B_p k_g r$$

which allows the possibility of perfect reference model matching by the nominal feedback gains:

$$A_p - B_p k_x^* = A_m, \qquad B_p k_g^* = B_m$$

An interesting choice of $k_g$ is as follows which leads to zero steady-state error:

$$k_g = \frac{1}{C A_m^{-1} B_p}$$

However, it is usually the case that the plant parameters $A_p$ and $B_p$ are unknown to us. Therefore an adaptation law is introduced to compute the ideal parameters that is expected to approximate to the nominal gain values as given above:

$$\dot{\hat{k}}(t) = -\Gamma x e^T P B_p, \qquad \hat{k}_x(0) = k_{x_0}$$

where $\Gamma$ is the adaptation gain, $P = P^T > 0$ is the solution for the algebraic Lyapunov equation $A_m^T P + P A_m = -Q$ for arbitrary $Q = Q^T > 0$, and the error signal $e(t)$ proceeds by the following dynamics:

$$\begin{aligned} \dot{e} &= \dot{x} - \dot{x}_m \\ &= -a_m(x - x_m) + (a_m - a_p + b_p \hat{a}_x)x + (b_p \hat{a}_r - b_m)r \end{aligned}$$

The convergence of this error dynamics can be easily proven by Lyapunovs direct method. The following candidate function:

$$V(t) = e^T P e + \frac{1}{\Gamma}(\hat{k}_x - k_x^*)^T(\hat{k}_x - k_x^*)$$

Defining $\tilde{k}_x = \hat{k}_x - k_x^*$ leads to the derivative:

$$\begin{aligned}
\dot{V}(t) &= -e^T Q e + 2ePB_p(\hat{k}_x - k_x^*)^T x + \frac{2}{\Gamma}\tilde{k}_x^T\dot{\tilde{k}}_x \\
&= -e^T Q e + 2\tilde{k}_x^T\left(\frac{1}{\Gamma}\dot{\hat{k}}_x + xe^T PB_p\right) \\
&= -e^T Q e \leq 0
\end{aligned}$$

which proposes stability. As for the asymptotic convergence, one can resort to the Barabalats lemma, which proposes that a differentiable function $V(t)$ has a finite limit as $t \to \infty$ and uniformly continuous, then one can conclude that $\dot{V}(t) \to 0$ as $t \to \infty$. It is clear that the candidate function satisfies the finite limit condition. For uniform continuity, the second derivative can be checked

$$\ddot{V}(t) = -2e^T Q\dot{e}$$

As the given form of the error dynamics $\dot{e}(t)$ is assumed to be bounded, we can conclude that $\dot{V}(e)$ is uniformly continuous and thus its limit converges to zeros as t tends to infinity, which also proves that $e(t) \to 0$ as $t$ tends to infinity. A key assumption in this derivation, as mentioned earlier, is the boundedness of the error signal which is directly dependent on the boundedness of the adaptation law results. Therefore, the projection operator can be utilized to theoretically guarantee this condition. Lets consider the adaptation law above implemented by the projection operator as follows

$$\dot{\hat{k}} = \Gamma Proj(k_x, -xe^T PB_p), \qquad k_x(0) - k_{x_0}$$

and follow the same candidate function by simply replacing the adaptation law which yields to

$$\dot{V}(t) = -e^T Q e + 2\tilde{k}_x\left(Proj(k_x, -xe^T PB_p) + xe^T PB_p\right)$$

Then, from the property B-1 of the projection operator as proven previously, one can write

$$\tilde{k}_x\left(Proj(k_x, -xe^T PB_p) + xe^T PB_p\right) \leq 0$$

which conveniently yields to

$$\dot{V}(t) \leq -e^T Q e \leq 0$$

This, as detailed above, proves the stability of the system and asymptotic convergence of the error signals, while the projection operator ensuring the boundedness of the adaptation law.

# Appendix B

# Case Study - $\mathcal{L}_1$ Adaptive Control of an Active Suspension System

This study investigates the implementation of an adaptive control strategy in active suspension controls. The derivation of the control algorithm and the execution of initial simulations are carried out using a quarter-car model. Road profiles are generated for ISO-D and E grade surface conditions using standard power spectra that served as the system input. To further test the adaptation of the control algorithm and the system response, additional undulations (e.g. bump and ditch) are included on the profile. The dimensions of these additional challenges are adjusted as the physical limitations of the considered suspension system allows. The results of the simulation studies indicate that the adopted control algorithm yields to very promising results in terms of attenuating any excess body acceleration and body travel response that might deteriorate ride comfort. Based on the acceleration margins suggested by the ISO 2631 standards, the proposed control algorithm successfully leads the actuators to isolate the vibrations excited due to the road profile. Finally, the controller is tested using a full-vehicle model of a D-class sedan, implemented in CarSim software. The vehicle is assumed to be equipped with four fully active suspensions. A D-grade rough asphalt with two standard cleats is used as a road profile to excite the system in the frequency range of interest, and the results indicate that the proposed adaptive control strategy significantly improves the isolation capabilities of the suspension system.

## B.1 Introduction

The design of an effective suspension system requires a number of conflicting requirements to be met. The suspension setup has to ensure a comfortable ride while proving good road holding and cornering characteristics. Also, optimal contact between tires and the road surface is needed in various driving conditions in order to maximize braking capacity and thereby safety. The conventional suspension designs in use today come with preset characteristics and aim to achieve vibration isolation through passive means, which might not be able to resolve the trade-off between such conflicting performance requirements.

This study focuses on the application of an adaptive control methodology for an active suspension aiming driver comfort as well as vehicle stability. Specifically, the use of $\mathcal{L}_1$ adaptive control methodology (Hovakimyan and Cao, 2006) is investigated, which proposes to improve robustness of the overall control strategy as well as guaranteeing stability in the case of parameter variations. Analysis on a quarter-car model shows that the proposed adaptive control methodology is superior to a robust $H_\infty$ control algorithm that is most generally used in conventional systems. Further simulations using a full vehicle model using CarSim software shows the proposed method is capable of reducing the sprung mass vibrations below comfort levels (ISO-2631) as well as guaranteeing transverse stability.

## B.2 Mathematical Model and Control Algorithm

Consider a quarter car model of suspension system as shown in Figure B-1. The sprung mass $m_s$ represents the constant mass of the car body, frame, internal components that are supported by the suspension. The sprung mass might vary according to the loading of the car and the adaptive control method is expected to overcome such variations. The unsprung mass $m_{us}$ is the mass of the assembly of the axle and the wheel, $k_s$ and $b_s$ are respectively the spring and damper coefficients of the passive components of the suspension system. The suspension spring constant $k_s$ comprises of a linear stiffness coefficient however the option to combine with nonlinear components is left open. The coefficient $k_s$ and $b_s$ are assumed to have known initial values. The coefficient $k_t$ is the linear tire radial spring constant. The control force generated by the active actuator connected between sprung and unsprung masses is denoted by $f_s$ while $r$ denotes the road disturbance input acting on the unsprung

mass. The vertical displacements of the sprung and unsprung masses with respect to their undeformed suspension positions are denoted by $x_s$ and $x_{us}$ respectively.

Using the above parameters, the dynamic model of the suspension system is given as follows:

$$\begin{aligned} m_s\ddot{x}_s &= -b_s(\dot{x}_s - \dot{x}_{us}) - k_s(x_s - x_{us}) + f_s \\ m_{us}\ddot{x}_{us} &= b_s(\dot{x}_s - \dot{x}_{us}) + k_s(x_s - x_{us}) - k_t(x_{us} - r) - f_s \end{aligned} \tag{B.1}$$

From equation 1 the state space representation is described as follows:

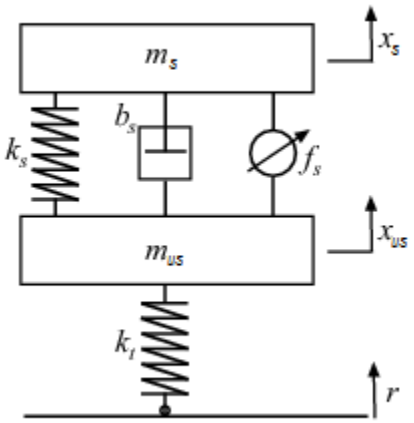


Figure B.1: Quarter car suspension model with single point tire-road contact

$$A = \begin{bmatrix} 0 & 1 & 0 & 0 \\ -\frac{k_s}{m_s} & -\frac{b_s}{m_s} & \frac{k_s}{m_s} & \frac{b_s}{m_s} \\ 0 & 0 & 0 & 1 \\ \frac{k_s}{m_{us}} & \frac{b_s}{m_{us}} & -\frac{(k_s+k_t)}{m_{us}} & -\frac{b_s}{m_{us}} \end{bmatrix}, \quad B_1 = \begin{bmatrix} 0 \\ \frac{1}{m_s} \\ 0 \\ -\frac{1}{m_{us}} \end{bmatrix}, \quad B_2 = \begin{bmatrix} 0 \\ 0 \\ 0 \\ \frac{k_t}{m_{us}} \end{bmatrix}$$

$$\dot{x}(t) = \mathbf{A}x(t) + \mathbf{B_1}u(t) + \mathbf{B_2}r(t)$$

where $x \in \mathbb{R}^4$, $u = f_s \in \mathbb{R}$.

Table B.1: Quarter vehicle parameters

| | | |
|---|---|---|
| Sprung Mass | $m_s$ | $300kg$ |
| Unsprung Mass | $m_{us}$ | $60kg$ |
| Damper Coefficient | $b_s$ | $1,000\frac{N}{m/s}$ |
| Spring Coefficient | $k_s$ | $16,000\frac{N}{m}$ |
| Tire Stiffness | $k_t$ | $190,000\frac{N}{m}$ |

For the control application, the output $y(t)$ is taken as the travel of the sprung mass ($x_b$), hence $C = [1 \quad 0 \quad 0 \quad 0]$, $D = 0$. With this choice of output, the system dynamics can be re-written in the following format:

$$\begin{aligned} \dot{x}(t) &= Ax(t) + b(wu(t) + r(t)) \\ y(t) &= Cx(t), \qquad x(0) = x_0 \end{aligned} \tag{B.2}$$

Furthermore we can assume a symmetric set of upper and lower bounds for the disturbance $r(t)$:

$$|r(t)| \leq \Delta \tag{B.3}$$

where $\Delta$ is a known conservative $\mathcal{L}_\infty$ bound of $r(t)$, which in this application becomes the limits on the road undulations. We further assume that the road disturbance, $r(t)$, is in the form of a continuously differentiable signal with bounded derivatives. The control objective with the $\mathcal{L}_1$ adaptive method is to design a full-state feedback controller to ensure that the system output, $y(t)$, tracks a given bounded reference signal, $r_t(t)$, both in transient and steady state, while all other error signals remain bounded. With this definition in hand, we consider the following state estimator for the quarter-car system dynamics with possible nonlinearities:

$$\begin{aligned} \dot{\hat{x}}(t) &= A\hat{x}(t) + b(wu(t) + \hat{\theta}(t)x(t) + \hat{r}(t)) \\ \hat{y}(t) &= C\hat{x}(t), \qquad \hat{x}(0) = x_0 \end{aligned} \tag{B.4}$$

which replaces the unknown nonlinearities in the form of $\theta(t)x(t)$ with $\theta(t)$ as any nonlinear function of $t$ and unknown disturbances ($r(t)$) with an adaptive estimation governed by the

below equations:

$$\begin{aligned} \dot{\hat{r}}(t) &= \Gamma_r Proj\left(\hat{r}(t), -\tilde{x}^T Pb\right) \\ \dot{\hat{\theta}}(t) &= \Gamma_\theta Proj\left(\hat{\theta}(t), -x(t)\tilde{x}^T Pb\right) \end{aligned} \tag{B.5}$$

In equation B.5, $\tilde{x}$ defines the error signal which is given as $\tilde{x}(t) = \hat{x}(t) - x(t)$. The adaptation gains are given by $[\Gamma_\theta, \Gamma_r] \in \mathbb{R}^+$ and $P$ is the solution of the algebraic Lyapunov equation $A^T P + PA = -Q$, $Q > 0$. After defining the system dynamics and state estimator, the control signal can be generated in the following form:

$$u(s) = C(s)u_{sub}(s) \tag{B.6}$$

where the sub-control $u_{sub}$ is given as:

$$u_{sub} = \frac{k_g r_t(t) - \hat{\theta}^T(t)x(t) - \hat{r}(t)}{w} \tag{B.7}$$

$$k_g = \frac{1}{CA^{-1}b} \tag{B.8}$$

In this definition, $C(s)$ is a strictly proper, stable transfer function with low-pass gain $C(0) = 1$. The stability of the closed loop system is guaranteed if one can design $C(s)$ to satisfy the $\mathcal{L}_1$ gain stability requirement:

$$||G(s)||_{\mathcal{L}_1} L < 1, \tag{B.9}$$

where $G(s) = (s\mathbb{I} - A)^{-1}b(1 - C(s))$. Implementing $C(s)$ with a low-pass filter effect allows the proposed control methodology to modify the loop transfer function such that the phase-margin of the system is expected to improve with increasing adaptation gain [ref]. As well known, with conventional adaptive control methods, increasing adaptation gains actually yields to better tracking performance but at a cost of observing higher gain cross-over frequencies which naturally reduces the phase margin and weakens the relative stability/robustness of the system. Whereas careful selection of the gain transfer function $C(s)$ allows for satisfactory tracking as well as improving/guaranteeing relative stability. A sample case is studied using a linear approximation to the proposed controller implemented on the quarter-car dynamics. The system is trimmed down to a SISO transfer function with control force ($f_s$) as input and body travel ($x_b$) as the output. This linear approximation allows the use of tools from classical controls. Figure 1.2 shows the frequency response of

the plant (quarter-car) and the controller-plant loop transfer functions with increasing adaptation gains, ($\Gamma$). Comparing the results for an adaptive integral control and $\mathcal{L}_1$ methods, one can observe that $\mathcal{L}_1$ method manages to limit the shift of the gain cross-over frequency with increasing $\Gamma$ and consequently allows pulling up the phase margin. The complete $\mathcal{L}_1$

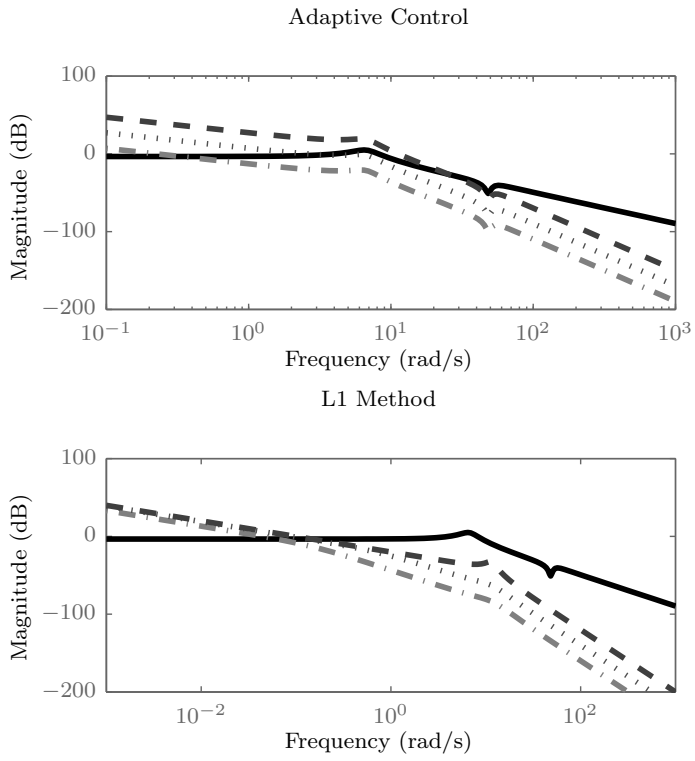


Figure B.2: Frequency response comparison for the linearized QC plant with integral adaptive and $\mathcal{L}_1$ adaptive methods

adaptive controller consists of equations B.4-B.6 subject to $\mathcal{L}_1$ gain stability requirement in equation B.9. The closed loop system is illustrated in Figure B.2.

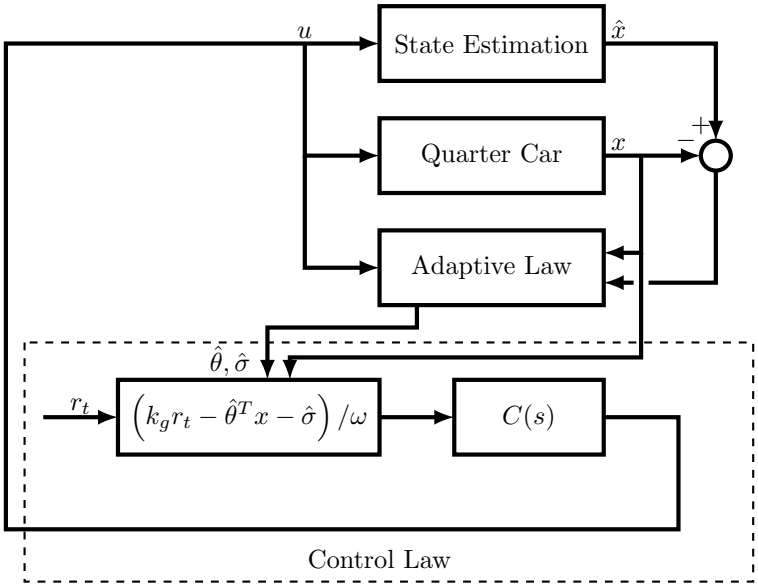


Figure B.3: Closed loop block diagram of the $\mathcal{L}_1$ control scheme

## B.3 System Validation in Simulation

The efficiency of the proposed $\mathcal{L}_1$ control scheme is tested through a series of computer simulations. The road profile is given as a disturbance and the body travel, body acceleration and the suspension deflection are plotted as the outputs. First couple of road profiles are given as simple obstacles to test the controller performance. Figure **??** shows the response of the proposed active suspension system in comparison to a passive counterpart. The results indicate quite satisfactory reduction of sprung mass oscillation within reasonable actuation requirements. Next the proposed controller is compared to a widely used robust control methodology, namely the $H_\infty$ control. The details of the adopted derivation methodology is given by Ezzine and Tedesco [] in further details and skipped here for bravity. In this application, the algorithm is specifically modified to minimize body acceleration ($\ddot{x}_s$) while avoiding resonance at the tire-hop and rattlespace frequencies. The road disturbance is taken from FHWA Long-term Pavement Performance (LTTP) database with max. $0.05m$ undulation. The system is introduced with a nonlinear spring coefficient for the suspension and the tire stiffness in the form of $k(1 - sin(2\pi f_r t))$. Furthermore, for more realistic simulation results, the dynamics for a hydraulic actuator are implemented as an addition to the above described spring nonlinearities. The dynamics are taken as a first order transfer function ($G_a(s) = 45/(s + 45)$) which leads to $\tilde{0}.015s$ time delay in the application of the control

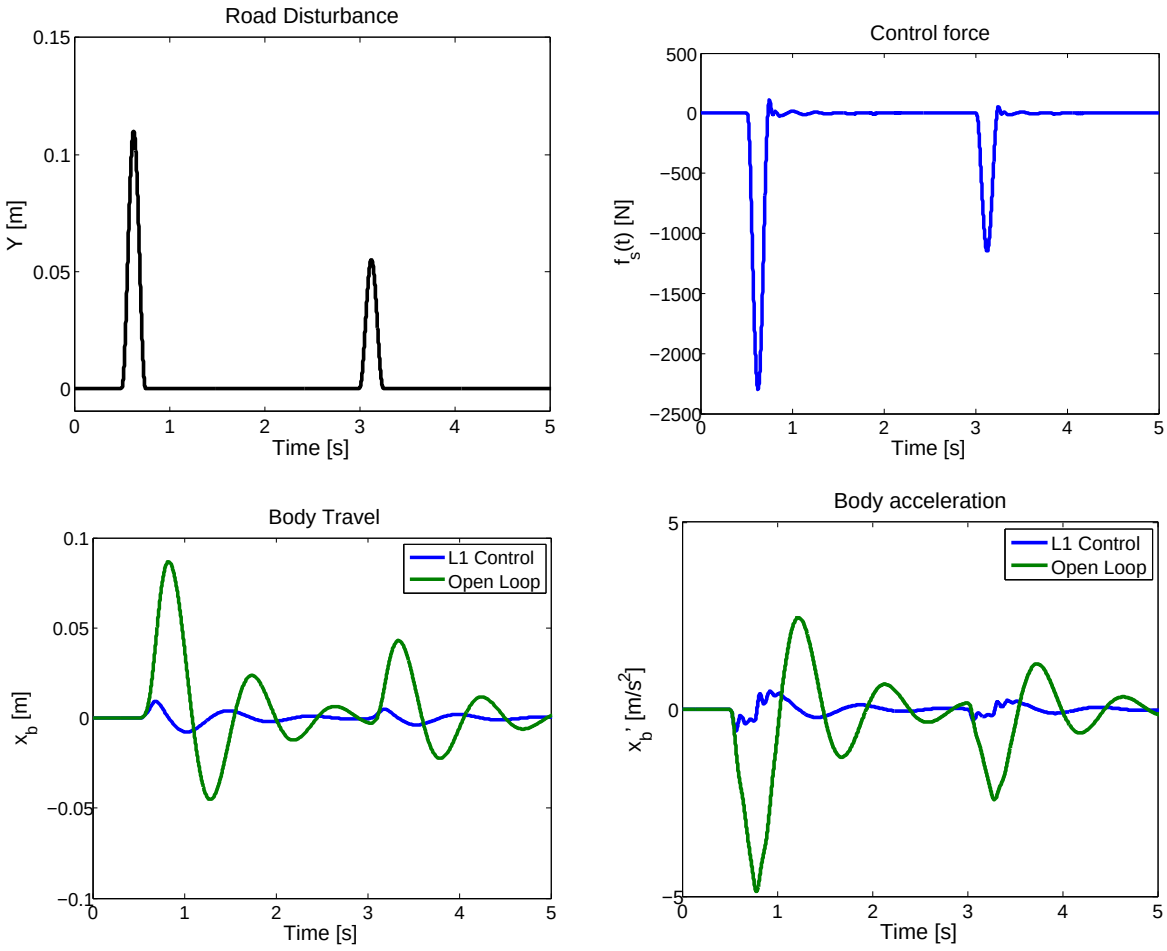


Figure B.4: $\mathcal{L}_1$ controller performance with bump profile.

signal. Figure B.4 summarizes both controller performances for the same road disturbance. The results show that the $H_\infty$ control method successfully rejects any possible resonance response and noticeably reduces oscillations. The body acceleration is effectively reduced as the design objective of the algorithm requires. Nevertheless the $\mathcal{L}_1$ control method yields to superior performance in terms of both selected indicators. Although this improved performance comes at a cost of higher actuator loading by the $\mathcal{L}_1$ method, the peak values still remain in a reasonable range. Finally, Table B.2 shows the root-mean square (RMS) of body acceleration values which is a standard indicator for ride comfort. As the results suggest, both controllers can cope with the nonlinearities and actuator dynamics, and reduce the body accelerations remarkably, but the proposed adaptive method provides exceeding improvements.

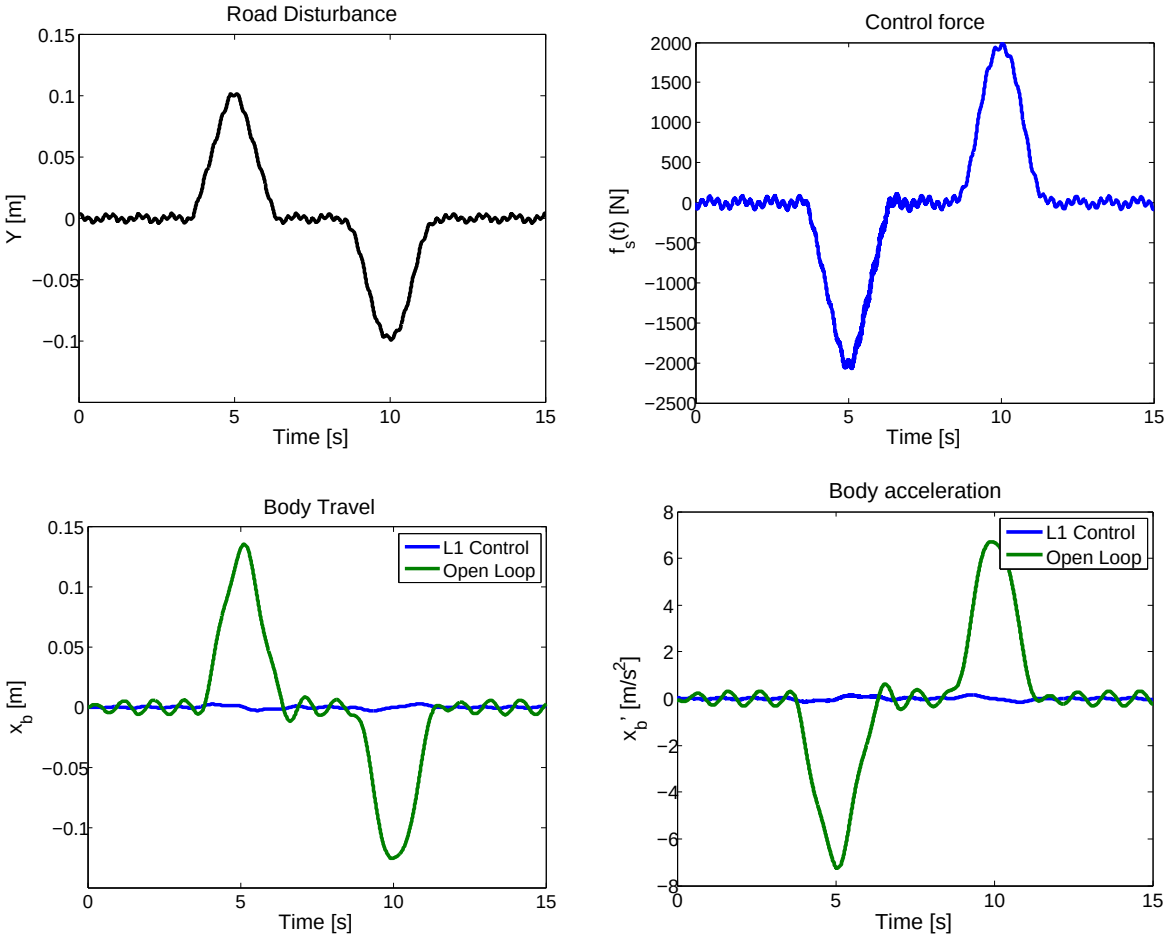


Figure B.5: $\mathcal{L}_1$ controller performance with bump and ditch profiles.

Table B.2: Body Acceleration RMS for $H_\infty$ and $\mathcal{L}_1$ strategies

| | | |
|---|---|---|
| Open-loop | 0.830 | $m/s^2$ |
| $H_\infty$ Control | 0.502 | $m/s^2$ |
| $\mathcal{L}_1$ Control | 0.210 | $m/s^2$ |

In what follows, the control algorithm is implemented on a full vehicle model in CarSim software. The vehicle (Figure B-7a) is assumed to be equipped with active-suspension actuators on the front and rear wheels, and control signal is computed for each actuator as the control force, $f_s$. The vehicle is tested on an ISO-D grade (rough asphalt) road profile on which two standard cleats ($12'' \times 2''$) are placed at $30m$ distance (Figure B-7b). The response for the passive system and the control application are summarized on Figure B-8.

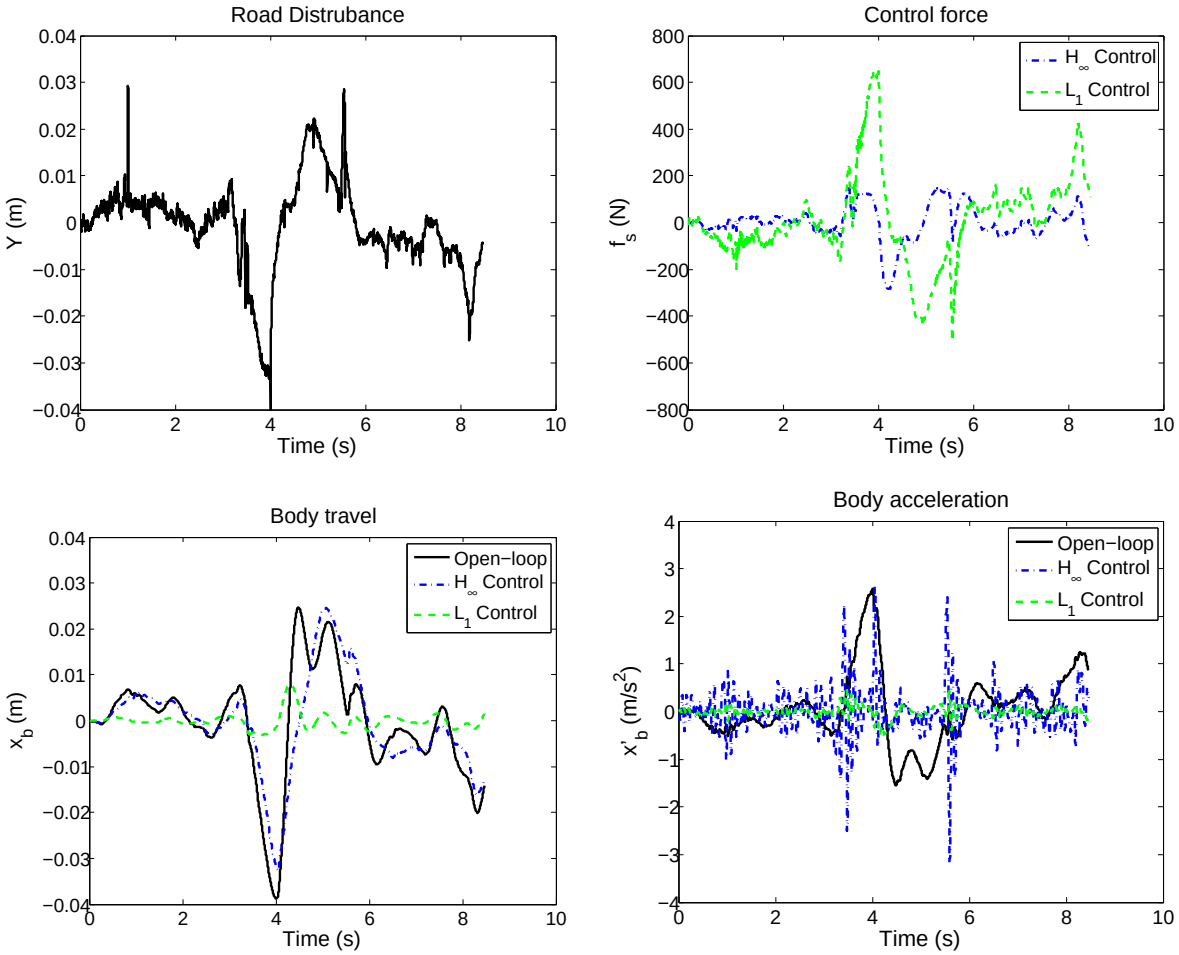


Figure B.6: Comparison of the controller performance for $H_\infty$ and $\mathcal{L}_1$ control methods

The performance of the control algorithm is evaluated based on the thresholds provided by the ISO 2631 standards. Figure B-9 shows weighted acceleration values for the duration of exposure that is suggested by the ISO and the weighing factors for the range of frequencies $(0.5 - 80Hz)$ for which the human body is expected to be most sensitive. ISO-2631 standard suggests that these acceleration thresholds to be increased by $6dB$ (doubled) for fatigue-limited proficiency boundaries and to be decreased by $10dB$ (divide three-fold) for comfort boundaries. The selected road profile excites the vehicle body at lower frequencies ($f_r < 3.5Hz$) which are more often related to comfort/fatigue related problems. The duration of exposure is taken as $8hr.$ in general as given the standard maximum driving period, and based on the thresholds as given in Figure B 9 the fatigue limit for the frequency

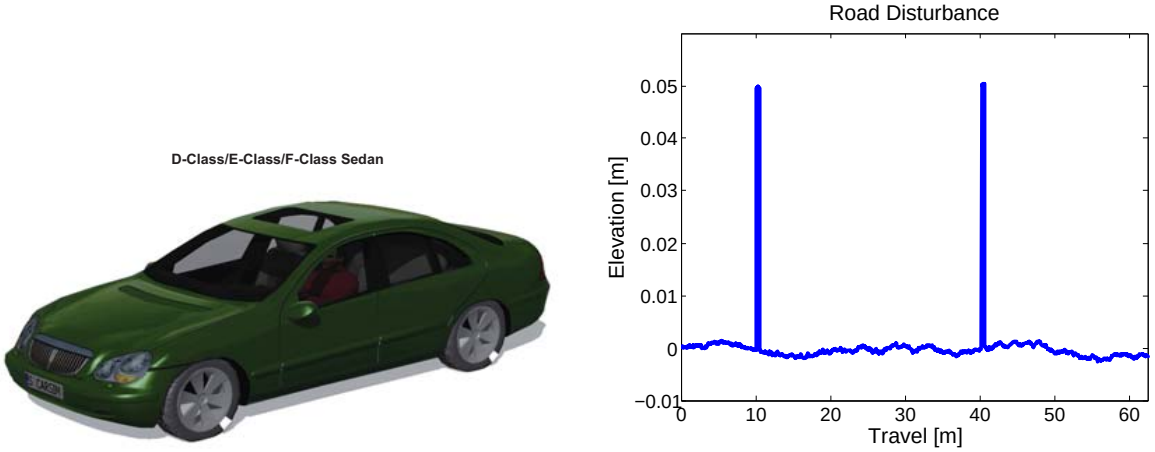


(a) CarSim D-Class Sedan Vehicle (b) Given road profile

Figure B.7: Test bed for the proposed adaptive active suspension control algorithm

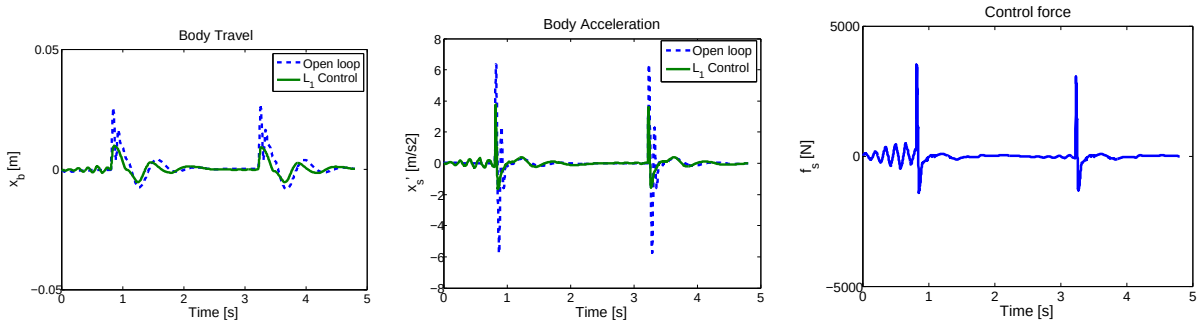


(a) Front

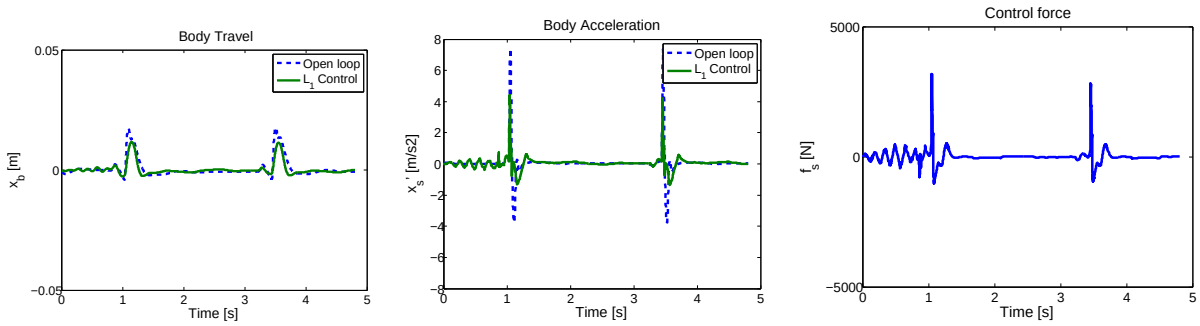


(b) Rear

Figure B.8: Vehicle response to the road profile

range of interest is found as $\tilde{1}.5m/s^2$ and the corresponding comfort limit can be found as $\tilde{0}.37m/s^2$. The resulting weighted accelerations are then evaluated with respect to these

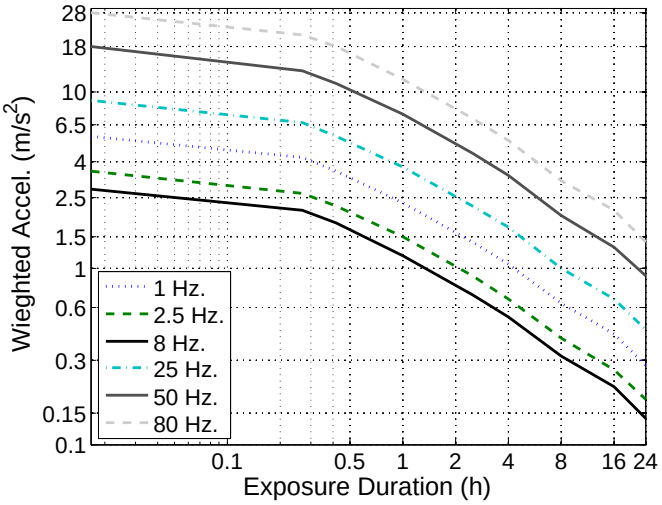


(a) Vibration limits as a function of exposure times

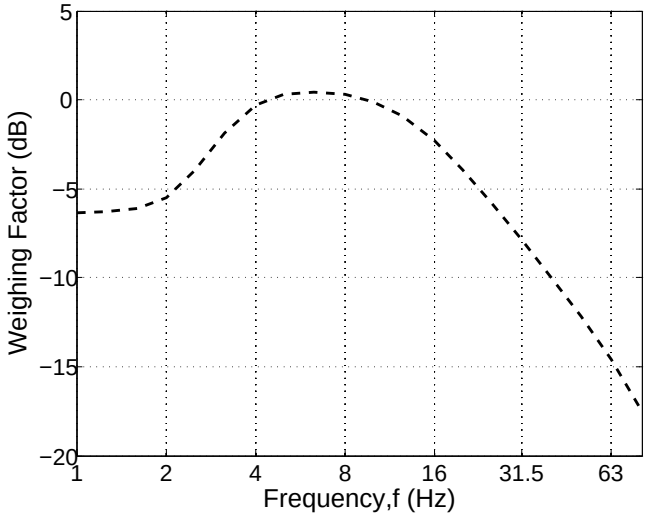


(b) Weighting factors for longitudinal vibrations

Figure B.9: Acceleration thresholds specified by ISO-2631

values as shown in Table B.3. The summarized acceleration values indicate that the passive suspension system is actually a good design that can remain the body inertance vibrations below the specified fatigue level. Adding the actuators with the proposed adaptive control on the other hand takes the vibration levels down to the comfort levels which is especially significant in driving for long durations.

Table B.3: Body Acceleration RMS in CarSim Simulations

| | Passive System | Active System |
|---|---|---|
| Front Suspension | $0.83 m/s^2$ | $0.39 m/s^2$ |
| Rear Suspension | $0.82 m/s^2$ | $0.40 m/s^2$ |

## B.4 Conclusion

Active suspension systems are becoming available and feasible in a considerably increasing rate. They are designed not only to improve the ride quality and comfort but also the safety of the vehicle. As extreme cornering may be required to remain on the road or to avoid an obstacle, implementing the active suspension system are capable of significantly reducing roll-over index. Moreover, as the active part of the suspension would be taking care of realizing good cornering behavior and of static load variations, the primary suspension springs can be tuned purely for optimizing comfort and road holding. Simulations show that the required force and energy for leveling the car even on extreme bounce conditions are reachable, so it can be concluded that the active suspension system is able to reasonably level the car.

The proposed adaptive algorithm is also compared to other commonly utilized controllers in conventional systems. To obtain a better measure of the algorithm's capabilities it is compared to a widely used robust algorithm, namely the $H_\infty$ method. The results indicate that the oscillation levels reduce at a very close rate for both methods, nevertheless the proposed algorithm is capable of better improving the ride comfort by significantly reducing the vehicle body motions, as the algorithm is derived based on that objective. Finally the algorithm is put into examination on a more realistic test-bed by using a vehicle model from the CarSim software. The suspension design for the selected D-class sedan vehicle is taken as the base model for the comparison study. The active system yields to superior performance in both courses of evaluation by reducing the peak body travel and the body acceleration rms almost about half in comparison to the passive suspension. All in all, the performance of the proposed algorithm is found very promising for utilizing in active suspensions and dampers which require high adaptability and robustness at the same time due to the rapidly varying conditions they operate under. The $\mathcal{L}_1$ adaptive control method provides such features by allowing one to modify the controller to both satisfy stability and robustness while providing

adaptability. As a follow-up of this study, further development of trivially selected low-pass gain could be considered which would improve the control response on parts of the given road profile with higher-frequency contents as well as helping with regulating the control efforts.